

CFD Simulation of Spray Drying process using a New Droplet Drying Kinetics

Dissertation

**zur Erlangung des
Doktorgrades der Ingenieurwissenschaften (Dr.-Ing.)**

**des
Zentrums für Ingenieurwissenschaften
Lehrstuhl Mechanische Verfahrenstechnik**

**der
Martin-Luther-Universität
Halle-Wittenberg**

**vorgelegt
von Herrn Ali Darvan
geb. am 10.03.1984 in Amol, Iran**

Gutachter:

- 1. Prof. Dr.-Ing. habil. Martin Sommerfeld**
- 2. Prof. Dr. rer. nat. Amsini Sadiki (TU Darmstadt)**

Tag der öffentlichen Verteidigung: 23.09.2016 in Halle (Saale)

**CFD Simulation of Spray Drying process using a New Droplet Drying
Kinetics**

Acknowledgments

I must start by thanking Professor Martin Sommerfeld who accepted to be my supervisor. He gave me the opportunity to learn what the research is, gave me the great advice professionally as well as the opportunity to experience the new things in my life.

My appreciations are also extended to a number of my colleagues for their technical and moral support during my time in Germany. In particular I need to truly thank Mr. Zeeshan Qadir, Yan Cui, Brian Quintero Arboleda, Dr. Stefan Horender, Dr. Santiago Iain, Mathias Dietzel, Martin Ernst, Silvio Schmalfuß, Lars Pasternak, Philipp Malli, and Matthias Kuschel who helped me in the different aspects of my education.

Last, but not least, I would like to thank my wife Aram for having much patience and constant faith in me.

Ali Darvan

November 2016, Halle (Saale), Germany

1 Abstract

The main objective of this work was the developing of a reliable CFD model of spray drying process for describing the drying of suspension or solution droplets under the conditions relevant for the spray dryers and moreover, overcome some of the drawbacks recognized in the previous drying models existed in the literature.

A more detailed droplet drying model which considers not only the rate of moisture loss, but also enables having a better understanding regarding the morphological evolution of the droplets throughout the drying process. In comparison to the previous introduced models, in the present model the diffusion equation for the solid phase within the droplet is solved in order to consider the concentration profiles inside the droplet.

Moreover, the experiments proved that due to the growing concentration of solid content at the droplet surface during the constant drying rate period, the droplet temperature increases continuously and therefore contrary to the previous models which supposed the droplet temperature to be constant in this period, the change of droplet temperature is considered during this period by taking the heat balance equation into account in the present model. Besides, by calculation of the crust thickness, it was possible to consider its role in reduction of the mass transfer rate in the present drying model as well.

Successful applications of the introduced drying model for simulation of the different kind of droplets in the different drying conditions are required to prove the ability and capability of this model for estimation of the drying behavior of different single droplets throughout the drying process both in the constant and falling drying rate periods. Hence in the first step of this work, the application of the present drying model for prediction of the behavior of different single droplets during the drying process is accomplished.

Finally, after successful applications of this model for simulation of the single droplets drying, the developed droplet drying model is implemented into the Euler-Lagrange approach for 2-way coupled simulation of a pilot-plant co-current spray dryer to evaluate the ability and capability of this model for prediction of the performance of these kinds of spray dryers and thus assess its applicability for the spray drying simulation in the large scale. Comparison of the experimental measurements and the predicted results for this case is done to confirm the ability of the developed model to approximate the

experimental results. As a conclusion, the analysis of the results provided by the developed model showed there are good agreements between the predicted results and the experimental data both for the single droplet cases and the case of pilot-plant spray dryer; therefore it can be said that the present model has the potential and ability in order to be incorporated as a sub-model in the CFD simulation of the spray dryers.

Contents

1	Abstract	6
2	Introduction	11
2.1	Introduction	11
2.3	Literature review	13
2.3	Thesis Objective and Structure	18
3	Modelling	20
3.1	Drying kinetics	20
3.2	Methodology	22
3.3	Modelling Procedure	24
3.3.1	Modelling Assumptions	24
3.3.1.1	Assumptions in Constant Rate Period;.....	24
3.3.1.2	Assumptions in Falling Rate Period;.....	25
3.3.2	Modelling Approach	26
3.3.3	Numerical procedure	32
3.3.4	Application to the single droplet drying simulation.....	34
3.3.5	Grid independence study	36
3.3.6	Colloidal silica droplets.....	38
3.3.7	Skimmed milk droplets	40
3.3.8	Sodium sulphate decahydrate droplets	43
3.4	Comparison with other models	47
3.5	Conclusion of the chapter.....	49
4	Calculation approaches for spray dryers	51
4.1	Calculation approaches for the spray drying process.....	51
4.1.1	Heat and Mass balances methods.....	51
4.1.2	Equilibrium based methods.....	51
4.1.3	Rate-based models.....	52

4.1.4	Models based on the application of Computational Fluid Dynamics (CFD):.....	52
4.1.4.1	STEP ONE: PRE-PROCESSING	53
4.1.4.2	STEP TWO: SOLVER.....	54
4.1.4.2.1	Finite difference approach:.....	54
4.1.4.2.2	Finite Element approach:	54
4.1.4.2.3	Spectral approach	55
4.1.4.2.4	The finite volume approach.....	55
4.1.4.3	STEP THREE: POST-PROCESSING	57
4.2	Previous studies about CFD modelling of spray drying	57
5.	Modelling Procedure	62
5.1	Basics of the turbulent reacting multiphase flows	62
5.1.1	PDF approach.....	62
5.1.2	Eulerian-Eulerian (two-fluid) approach	63
5.1.3	Eulerian-Lagrangian approach	64
5.2	Euler-Lagrange Approach: An Extended Model for Spray Dryer Simulation.....	65
5.2.1	Fluid Phase Modelling	65
5.2.2	Dispersed Phase Modelling.....	71
5.3	Particle Tracking	74
5.4	Dispersion modelling	75
5.5	Turbulence modulation modelling	76
5.6	Two-way Coupling Procedure	77
5.7	Numerical methodology	79
5.7.1	Numerical method for gas phase.....	79
5.7.2	Features of numerical solution	80
5.7.3	Numerical method for dispersed phase	81
5.7.4	Averaging technique	82
6	CFD Modelling of spray drying process	84

6.1	Measuring procedure.....	84
6.2	Geometry and numerical procedure	85
6.2.1	Injection procedure.....	91
6.2.2	Characteristics of the dispersed phase.....	92
6.3	Grid independence study	94
6.4	Simulation results and discussion	96
6.4.1	Results for the Fluid Phase.....	96
6.4.2	Results for the Dispersed Phase	101
6.4.2.1	Droplets velocity	105
6.4.2.2	Droplets temperature	107
6.4.2.3	Material solid content.....	109
6.4.2.4	Particle size distribution	112
6.5	Comparison with other models	114
6.6	Summary of the chapter:	116
7	Conclusion.....	118
7.1	Conclusion.....	118
7.2	Outlook.....	120
	Nomenclature	122
	Curriculum Vitae.....	133

2 Introduction

2.1 Introduction

Among the many industrial drying technologies, the spray drying has a particular role in the industry, because it involves the drying of solid included droplets (e.g. solution, suspension) to the dry powders with control over the final particle morphology and practical powder properties. Spray drying can also fulfill the environmental standards in aspects of emission and safety.

Due to the high demand for the productions which are produced by the spray drying method in the market, the needs of the industrial application of spray drying stayed on the high level in the last decades. Hence many researchers in the companies and universities have focused on this field to develop and improve this technology numerically and experimentally (e.g. ‘International Drying Symposium 2014’).

Nevertheless, there are still many things about spray drying which should be understood to achieve the best drying conditions and to obtain the desired product quality. One of the most important phenomena, not yet fully understood, is the mechanism of the solid particle formation in the condition of simultaneous heat and mass transfer process existed in the drying chambers.

In spite of the great achievements in the field of numerical methods, because of the complex hydrodynamics and mutual interaction of the transport processes in the two-phase gas-particles system the scaling-up of a spray drying process is still a problematic issue for the researchers.

Generally speaking, the main errors in the scaling-up of a spray drying process are caused by an incorrect determination of the drying kinetics, difficulties in the modelling of the gas flow turbulence (Oakley 1994) and an improper definition of some initial parameters particularly the atomization parameters which contrary to the experiment observations it is usually supposed that all the particle fractions have the same initial velocity and spraying angle (Zbicinski and Li 2006). The experimental results attained so far showed that each particle fraction is characterized by distribution of both the velocity and the spraying angle, which is important for the understanding of spray drying mechanism and for establishing a confident model for the scaling-up of a spray drying process (Li 2006).

The flexibility and effectiveness made the Computational Fluid Dynamics (CFD) technique to be widely applied in the designing and scaling-up of the spray drying process. Especially Since 1977 when Crowe developed the Particle Source in Cell (PSI-Cell) method (Crowe 1977), the CFD modelling of the transport process between the dispersed phase (particles) and continuous phase (drying gas) in the spray dryers has been continuously improved. However, despite of the great progress in the CFD technique, due to the complication of the hydrodynamics as well as the complexity of mutual interaction of the transport processes in the two-phase gas- particles system existed in spray drying process, the CFD spray drying models still are not able to describe the spray drying process correctly and their application in the simulation of spray dryers performance is still limited.

In order to utilize the advantages of CFD techniques for design of the spray dryers and modelling of the spray drying process, development of a new drying model which agrees with the experimental observations in order to overcome some weaknesses existed in the previous commonly used models (such as considering the constant temperature distribution within the droplet or neglecting the solids diffusion transport within the droplet) and moreover, having the potential for being used as a sub-model within the CFD simulation of the spray dryers is the main purpose of the present work.

The application of a drying model enables the consideration of mass and heat exchange between the continuous and dispersed phase in this process (drying process). In addition, the evaporation of solvent leads to the significant changes of material properties and hence the change of the collision behavior of drying particles (i.e. particle-particle collision, agglomeration and particle-wall collision) (Blei 2005). Due to these reasons, an appropriate drying model which is able to properly describe the heat and mass transfer between droplets and drying gas is essential for the correct prediction of the product characteristics by modelling.

But so far a comprehensive model for the numerical predictions of drying process is not available. Hence, the main emphasis of this work is introducing a reliable model for describing the drying of suspension or solution droplets under conditions relevant for the spray dryers. A more detailed droplet drying model which considers not only the rate of moisture loss, but also enables having a better understanding regarding the morphological evolution of the droplet throughout the drying process. In comparison to the previously

introduced models, in the present model the diffusion equation for the solid phase within the droplet is solved in order to consider the concentration profiles inside the droplet. Moreover, the experiments proved that due to the growing concentration of solid content at the droplet surface during the constant drying rate period, the droplet temperature increases continuously and therefore, contrary to the previous models which supposed the droplet temperature to be constant in this period, the change of droplet temperature is considered during this period by taking the heat balance equation into account in this developed model. Besides, by calculation of the crust thickness, it is possible to consider its role in the reduction of mass transfer rate in the present drying model. Application of the developed model for the simulation of three different systems: colloidal silica, aqueous sodium sulphate and skimmed milk droplets has been done to evaluate the ability and capability of this model for estimation of the drying behavior of different single droplets throughout the drying process.

Finally, the developed droplet drying model is implemented into the Euler-Lagrange approach for 2-way coupled simulation of a pilot-plant co-current spray dryer to assess the ability of this model for giving the relevant information about the drying process in the drying chamber as well as some product properties which help us to have a better understanding about the spray drying process.

2.3 Literature review

This chapter includes the literature review of the different drying models which has been used for modelling of the drying kinetics of single droplets during the drying process.

Many investigators studied the drying kinetics of single droplets and developed different drying models based on the experimental observations for describing the drying process of single droplets. The assumption of a proper moisture migration mechanism, derivation of the governing equations for the heat and mass transfer mechanisms and solving the derived equations based on the numerical methods are the basis of the most of drying models for the single droplets.

Using the principles of irreversible thermodynamics, Luikov (1975) developed a drying model for the porous materials in which the drying material is divided into the dry and wet regions separated by a receding evaporation front which moves toward the material center as the drying proceeds. The advantage of this model is that there is no requirement for the assumption of any controlling mechanism for the internal moisture movement, but the

requirement of diffusion and thermal conduction coefficients which have to be determined experimentally made the application of this drying model limited.

Two different drying models named as ‘solid sphere’ and ‘hollow sphere’ drying model were developed by Wijlhuizen *et al.* (1979). In the ‘solid sphere’ drying model, it is supposed that the moisture diffuses through the droplet and the evaporation occurs at the droplet surface. The diffusion mechanism is described by applying a binary diffusion coefficient which is a function of droplet temperature and moisture content. In the ‘hollow sphere’ drying model, it is assumed that an initial gas bubble with uniform vapor concentration exists within the droplet and the movement of water due to the gas bubble expansion is included in the diffusion equation. In the both models, the temperature distribution inside the droplets is ignored and moreover, neglecting the consideration of crust formation caused the overestimation of predicted results by these models in comparison with the experimental data.

Sano and Key (1982) developed a drying model to describe the evaporation of moisture from the single droplets which contain colloidal particles. In this model, it was supposed that when the equilibrium vapor pressure of moisture within the droplet exceeds the ambient pressure, the droplet inflates and ruptures, so that a hollow sphere will form. Either by the increase of void radius and keeping the outer radius constant or by the decrease of outer radius and keeping the void radius constant, the deformation of hollow sphere is described and the diffusion of moisture within the droplet is calculated by a Fickian transport equation. Although this model is a more realistic model but some disadvantages such as the neglecting of heat transfer resistance, ignoring the temperature distribution inside the droplet and also the determination of the inflation ratio and diffusion coefficient which are based on the experiments made the applicability of this model limited

A receding interface model for drying of the single droplets was developed by Cheong *et al.* (1986). In this model, it is supposed that an evaporation interface which recedes towards the center of droplet (as the drying proceeds) divides the droplet into the dry and wet region. This model describes the diffusion of water vapor in the dry region by a

Fickian transport equation with an effective diffusion coefficient. The main weakness of this model is the assumption of linear temperature distribution in the dry region. Because this assumption underestimates the resistance to the heat transferred to the interface and thus causes the higher drying rate than the actual case. Moreover, contrary to the experimental observations which proved the existence of the apparent constant drying rate period, the falling drying rate conditions prevail for the whole drying process in this model.

Abramzon and Sirignano (1989) developed a simple but sufficiently accurate model for the vaporization of a moving fuel droplet which can be used in the spray combustion calculations. This model represents the extension of the classical droplet vaporization model and takes into account some effects such as the variable physical properties, non-unitary Lewis number in the gas film, effect of the Stefan flow (blowing) on the heat and mass transfer between the droplet and gas as well as the effect of the transient liquid heating inside the internally circulating droplet. The transient liquid heating inside the droplet is calculated using a spherically symmetric 'effective conductivity model'. The effective thermal conductivity of the liquid fuel is introduced to account for the heat enhancement due to the internal liquid circulation. This model can be used in the wide range of droplet sizes and Reynolds numbers and due to its simplicity is suitable for the spray combustion calculations. Nevertheless, the presence of solid within the droplets completely changes the heat and mass transfer process so that the presence of solid introduces a new resistance for the heat and especially mass transfer and totally changes the nature of these processes which existed between the droplet and its environment.

The main disadvantage of this model is that this model was developed to simulate the evaporation of pure droplets (e.g. fuel droplets) and is not able to predict the evaporation of droplets containing solids. Generally speaking, the models which are suitable for the combustion calculations due to the lack of consideration of solid content within the droplet are not good options for the simulation of drying process.

Nesic and Vodnik (1991) studied the drying of different droplets experimentally and also developed a model illustrating the heat and mass transfer mechanisms during the evaporation of droplets containing dissolved or dispersed solids. In their model, the drying

of a single droplet is divided into some stages including the constant and falling drying rate periods. This model covers all stages of droplet evaporation with a single set of differential equations and the stage transition criteria have been proposed as well. Mixing and/or diffusion can control the initial period of evaporation and the presence of crust introduces a new resistance for the heat and especially mass transfer. It is suggested that the reduction of the surface partial pressure can be modelled with an exponential law and by using the concentration-dependent diffusivity the diffusion of water vapor through the solid crust was modelled. Although there is an acceptable agreement between the results obtained by this model and the experimental data but some drawbacks existed in this model such as the ignoring of heat transfer resistance of the wet core region, neglecting the effect of diffusing water vapor through the crust to the heat transfer, neglecting the temperature distribution within the droplet as well as the determination of diffusion coefficients for the different materials based on the experiments made restriction on the applicability of this model.

Farid (2003) developed a model to predict the change of droplet mass and temperature when it is exposed to the hot gas, as in the spray drying process of the droplets containing solids occurs. In this model, the droplet was assumed to experience some shrinkage, with no temperature change but rapid mass losses in the constant drying rate period followed by the significant change in the droplet mass and temperature in the falling rate period. This approach supposed that both the internal and the external heat transfer resistance control the drying process and that the thermal conductivity of the crust mainly controls the drying procedure, while the other physical properties have very small effects on this process. The model considers the droplet shrinkage and unlike the other models includes the temperature distribution within the droplet and also showed that the temperature distribution within the droplet cannot be ignored even for very small droplets. The model predicted reasonably well both the measured temperature and the mass of different single droplets. But the neglecting of mass transfer resistance of the crust region, ignoring the heating effect of water vapor diffusing through the pores of the crust and not having any equation for the calculation of moisture/solid concentration within the droplet are the main drawbacks of this model which puts a limitation on the applicability of this model.

The main advantages and disadvantages of the previous most famous drying models are summarized in Table 2.1.

Table 2.1: Summarizing the main advantages and disadvantages of the previous most famous drying models

Model	Advantages	Disadvantages
Abramzon & Sirignano	Simplicity, Accurate prediction of pure liquid droplets evaporation, usable for combustion calculations	Give no information about the solid and temperature distribution within the droplet, Unsuitable for the spray drying calculations
Sano & Keey	Providing information about the moisture distribution within the droplet, Simple equation for the temperature calculation	Give no information about the temperature distribution within the droplet, No consideration of drying stages when calculating the temperature
Nesic & vodnik	Providing information About solid distribution within droplet, Cover the whole drying process with a single set of differential equations	Give no information about the temperature distribution within the droplet, Neglecting the heat transfer resistance of wet core.
Farid	Providing information about the temperature distribution within the droplet, Consideration of the droplet shrinkage	Give no information about the solid distribution within the droplet, Assuming constant temperature in the constant drying rate period

2.3 Thesis Objective and Structure

As it was mentioned before, the main focus of this work is the consideration of a trustable model for describing the drying of droplets containing solids (e.g. suspension or solution) under the conditions relevant for the spray dryers in order to overcome some of the drawbacks recognized in the previous models. A more detailed droplet drying model which considers not only the rate of moisture loss, but also enables having a better understanding regarding the morphological evolution of the droplets throughout the drying process. Then, the introduced model has to be applied for the simulation of different kinds of droplets in the different drying conditions in order to prove the ability and capability of this model for the estimation of drying behavior of different single droplets.

Finally, the developed drying model has to be implemented into the Euler-Lagrange approach for 2-way coupled simulation of a pilot-plant co-current spray dryer to evaluate the ability of this model for the prediction of the performance of these kinds of spray dryers and also its capability for providing the relevant information about the drying process as well as some product properties by which we can have a better understanding about the spray drying technology. Besides, the outline of this thesis can be represented as following:

The previous section focused on the reviewing of the important previous works relating to the numerical simulation of single droplet drying process and the advantages and disadvantages of the previous models were discussed as well.

Chapter 3 describes the drying kinetics, the different approaches existed for drying modelling and the detail of modelling procedure applied in this work for developing the introduced drying model. Furthermore, in this chapter the developed drying model is applied for the simulation of three different systems of single droplets and the validation of the present model has been done using the experimental data, and at the end of this chapter the results obtained by the present model were compared with the results of other drying models.

Chapter 4 discusses the different calculation approaches for the modelling of typical spray dryers and focuses on the models which are based on the application of Computational Fluid Dynamics (CFD). Additionally, the previous works relating to the application of the CFD techniques for modelling of the spray dryers are reviewed.

Chapter 5 contains the describing of the different modelling approaches applied for the turbulent reacting multiphase flows. The main emphasis of this chapter is on the Euler-Lagrange Approach as used in the present work and includes the description of the fluid phase modelling, dispersed phase modelling, dispersion modelling, turbulence modulation modelling as well as two-way coupling procedure. Moreover, the numerical methodology applied for the continuous (gas) phase, dispersed (droplet) phase, as well as the averaging technique, are explained in this chapter.

In chapter 6, after a discussion about the measuring procedure which was done at the Technical university of Lodz in Poland, the CFD Modelling of a pilot-plant co-current spray dryer using the developed drying model is carried out in order to evaluate the ability of this developed drying model for the prediction of the performance of these kinds of dryers and thus assess its applicability for the spray drying simulation in the large scale. The validation of the present drying model is done using the experimental data and additionally the results achieved by the present model are compared with the results of other drying models.

Finally, in chapter 7, the conclusions of this work are presented.

3 Modelling

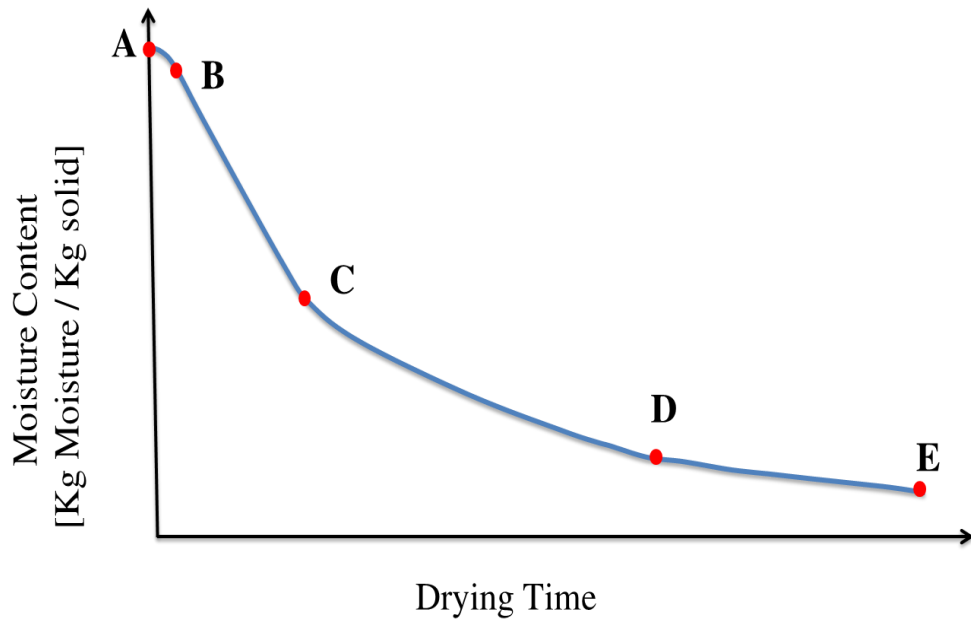
3.1 Drying kinetics

The experimental observations of the drying of single droplets containing solids (e.g. solutions and suspensions) showed the different rates of the moisture content reduction for the single droplets in the drying process as time proceeds (Fig. 3.1(a)) and accordingly due to the various processes affecting the moisture loss, the drying rate profile also showed the different trend during the drying as shown in Figure 3.1(b).

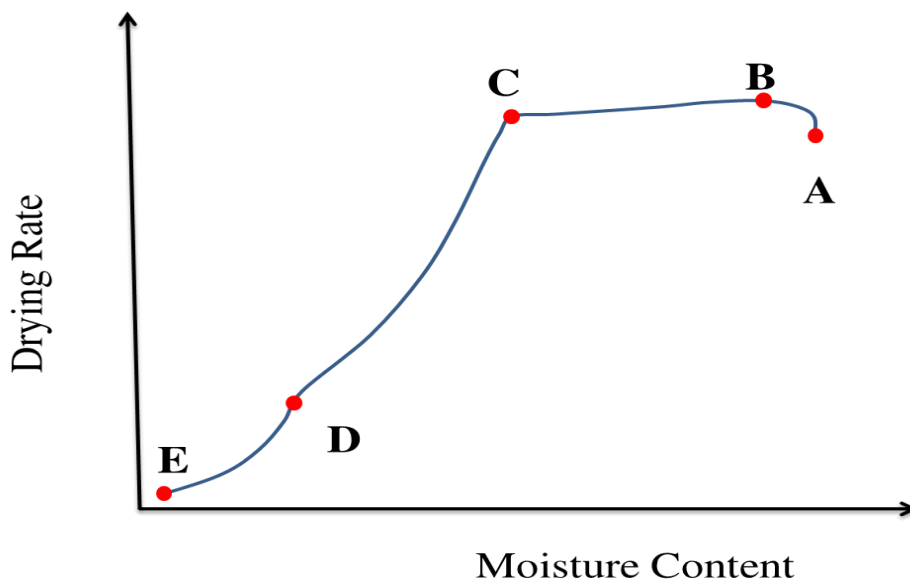
Dividing the drying process to a number of different drying periods has been done firstly by Sherwood (1929a, b). As it can be seen in Figure 3.1, when the drying is started, there is a short period (line A-B in Fig. 3.1(b)) in which the droplet heats and the drying rate increases.

As soon as the thermal equilibrium between the droplet and its surroundings is achieved (i.e. when the droplet's surface temperature reaches the equilibrium temperature which is usually almost equal to the wet-bulb temperature of drying gas); almost all heat energy transferred to the droplet results in the evaporation of moisture. This is the constant drying rate period in which the rate of removal of the moisture remains nearly constant (line B-C in Fig. 3.1(b)) and the droplet surface is at the wet bulb temperature.

The constant drying rate period continues until the surface solids concentration reaches the saturation concentration and after that the drying rate starts to decrease gradually (line C-D in Fig. 3.1(b)) due to the solid crust formation and its growth which create a new resistance for the mass transfer process. This is the falling drying rate period in which the drying gas flows within the pores and the drying interface moves toward the center of droplet. Line D-E in Figure 3.1(b) displays the second falling drying rate period during which the moisture is removed only by the vapor diffusion, the drying rate decreases further and the particle temperature reaches to the drying gas temperature (Handscomb 2008).



(a)



(b)

Figure 3.1: Schematic drying rate curves displaying, (a) moisture content against time; and (b) drying rate against moisture content.

3.2 Methodology

Many single droplet drying models can be found in the literature. These drying models can be categorized mainly in:

1) Those which only provide the information about the average temperature and moisture content of the droplet but are not able to give any insights to the morphological evolution of the droplet during the drying process. This category includes:

1a) characteristic drying curve approach:

Using the characteristic drying curves obtained in the experiments is the simplest way for the modelling of droplet drying (Langrish and Kockel 2001). The low computational expense is the main advantage of this model which makes it suitable for the CFD applications. Nevertheless, providing no information about the morphology of droplet is the main drawback of this model which makes it inappropriate when the detailed information about the droplet is required.

1b) Reaction engineering approach:

The reaction engineering approach for the droplet drying modelling is introduced firstly by Chen and Xie (1997). The method considers the drying as a competitive process between an activation type ‘evaporation’ reaction and a ‘condensation’ reaction. A normalized curve of the evaporation activation energy against the moisture content is considered to be characteristic of a given material (Handscomb 2008).

Giving no information about the morphological changes of the droplet and the experimental effort which is necessary for providing the activation energy curve and sorption isotherm put a limitation on the applicability of this model.

2) The mechanistic models; which provide some information about the morphological changes of droplet during the drying process such as the information about the moisture/solid distribution within the droplet and the size of dried particle .This category includes:

2a) effective diffusion coefficient models:

This approach is one of the most commonly used methods when getting information about the moisture distribution within the droplet is the main aim of the modelling. Diffusion of

moisture within the droplet is calculated by a Fickian transport equation and there is no assumption about the formation of the crust region in such models. The effective diffusion coefficient which is a function of temperature and moisture content controls the mass transfer rate in these models (e.g. drying model of Sano & Keey 1982). These models provide little information about the morphological evolution of droplet and hence, many researchers tried to combine their model with such models to achieve more morphological information (Verdurmen *et al.* 2004).

2b) Shrinking core models:

The shrinking core models divided the drying process into two main stages including the constant drying rate period (first stage) and the falling drying rate period (second stage). In the first stage, it is supposed that the droplet heats, evaporation of free water existed on the surface of the droplet commences, the droplet size starts to reduce (shrinkage) and the solid crust forms and grows on the surface of the droplet. While in the second stage, it is assumed that the solid concentration on the droplet surface reaches and exceeds the critical value, the shrinkage of droplet stops, a core-crust interface divides the droplet into two zones, the evaporation takes place at this receding interface and the crust thickness is the factor of mass transfer resistance. In such models which have been developed so far, in order to simplify the model, either the temperature distribution or the moisture distribution within the droplet was neglected (e.g. drying model of Farid 2003 and Nestic & vodnik 1991).

2c) Models with a Bubble:

This class of drying models consists of the models which consider the formation of a bubble within the droplet when the equilibrium vapor pressure of moisture within the droplets exceeds the ambient pressure (e.g. drying model of Wijnhuizen *et al.* 1979, Sano & Keey 1982). Such dried-particle morphology is common in the drying process but only if the drying gas temperature is higher than the boiling point of moisture (water). Determination of the inflation ratio based on the experiment for each case and validation of such models just in the high temperature drying conditions put a restriction on the applicability of these kinds of models (Handscorn 2008).

3.3 Modelling Procedure

The drying model developed in this study is a mechanistic model based on the receding evaporation front approach which divides the drying process to the different stages. Dividing of the drying process to the different stages agrees with the experimental observations as well. The present model is a shrinking core model which is combined with an effective diffusion approach to provide the spatial information about the droplet moisture/solid content as well as the temperature distribution within the droplet. The governing heat and mass transfer equations, which consider the heat transfer resistance and the mass transfer resistance of the dry crust region, are derived for all stages of drying as described in the following section.

3.3.1 Modelling Assumptions

3.3.1.1 Assumptions in Constant Rate Period;

In the constant drying rate period (line B-C in Fig. 3.1(b)), heat is transferred by the convection from the drying air to the droplet surface and leads to the evaporation of free water. This stage of drying continues until the whole free water is evaporated (see Fig. 3.3). The following modelling assumptions are considered in this stage of drying:

1. Droplet has and keeps the spherical shape as well as the spherical symmetry.
2. Conduction is considered to be the mechanism of heat transfer inside the droplet.
3. The radius of droplet is shrinking.
4. Heat is transferred by the convection from the drying air to the droplet surface.
5. Removing of free moisture at the droplet surface is considered by the receding of the radius of the droplet.
6. Constant drying conditions are supposed in which the temperature, humidity and velocity of the drying air are constant.
7. There are no chemical and physical interaction between the solids and moisture.
8. Temperature and solid concentration change only in radial direction.
9. This stage of drying lasts until there is no free moisture on the droplet surface.

10. Moisture vapor will be removed by the convection from the droplet surface.
11. Thermal and concentration equilibrium condition are supposed at the evaporation interface.
12. Capillary effects and internal circulation within the droplet are neglected.

3.3.1.2 Assumptions in Falling Rate Period;

In the falling drying rate period (line C-D in Fig. 3.1(b)), the partially dried particle is assumed to be divided by a moving core-crust interface into two distinct zones including the inner wet core and the outer dry crust. Evaporation is supposed to take place at this receding interface which recedes toward the center of droplet so that the crust thickness creates a new resistance for the heat and mass transfer process (see Fig. 3.4). The following modelling assumptions are considered in this stage of drying:

1. Droplet has and keeps the spherical shape as well as the spherical symmetry.
2. Conduction is considered to be the mechanism of heat transfer inside the droplet.
3. Heat is transferred by the convection from the drying air to the droplet surface.
4. A receding evaporation interface is supposed to exist which divides the droplet into the inner wet core and the outer dry crust region.
5. Removing of the moisture in the pores of the droplet is considered by the receding of core-crust (evaporation) interface.
6. Droplet radius does not change during this stage of drying.
7. Constant drying conditions are supposed in which the temperature, humidity and velocity of the drying air are constant.
8. Pores of the solid crust region are filled with air, and the moisture vapor diffuses within these pores and will be removed by convection from the droplet surface
9. Temperature and solid concentration change only in the radial direction.
10. There are no chemical and physical interaction between the solids and moisture.

11. Thermal and concentration equilibrium condition are supposed at the evaporation interface.
12. Capillary effects and internal circulation within the droplet are neglected.

3.3.2 Modelling Approach

The model presented in this work supposed that the drying of a spherical solid-included droplet can be divided into four distinct stages, as displayed in Figure 3.2.

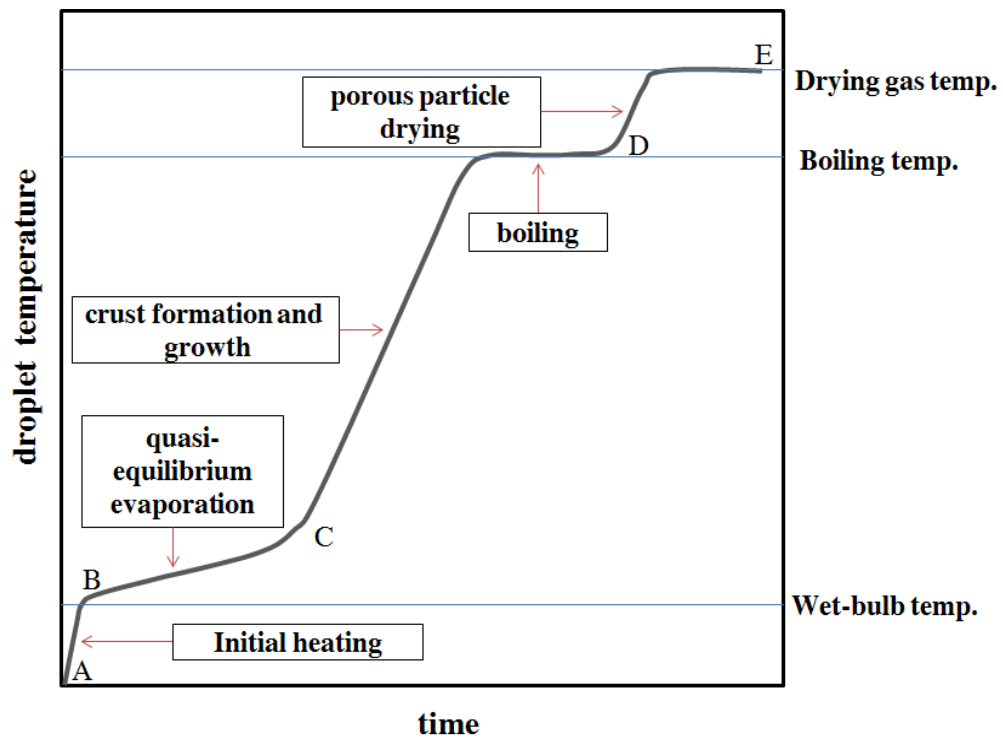


Figure 3.2: Stages of a single droplet drying process.

First stage: Initial warm-up period (path: A–B in Fig. 3.2), the first stage considers the sensible heating of the droplet in which the droplet’s surface temperature reaches the equilibrium temperature, which is usually almost equal to the wet-bulb temperature of the drying gas. During this stage most of the heat transferred to the droplet from the drying gas is used for the droplet heating, and hence the evaporation process is very slow.

The heat conduction equation (Eq. (3.1)) is solved using the boundary conditions (Eq. (3.2) and (3.3)) to estimate the temperature distribution inside the droplet throughout this period.

$$\frac{\partial T}{\partial t} = \frac{\alpha}{r^2} \left[\frac{\partial}{\partial r} \left(r^2 \frac{\partial T}{\partial r} \right) \right] \quad (3.1)$$

$$\frac{dT}{dr} = 0 \quad \text{at } r = 0 \quad (3.2)$$

$$-k \frac{dT}{dr} = h (T_s - T_\infty) \quad \text{at } r = R. \quad (3.3)$$

Here T_s and T_∞ represent the droplet surface temperature and air temperature respectively.

In order to determine the surface concentration, the diffusion equation formulated in terms of mass fraction for the solid phase within the droplet is solved:

$$\frac{\partial C}{\partial t} = \frac{1}{r^2} \frac{\partial}{\partial r} \left(r^2 D_{AB} \frac{\partial C}{\partial r} \right) \quad (3.4)$$

With the boundary conditions at the droplet surface:

$$4\pi R^2 D_{AB} \frac{\partial C}{\partial r} = \frac{4}{3} \pi C_s \left(\frac{dR}{dt} \right)^3 \quad (3.5)$$

And at the center of droplet:

$$\frac{\partial C}{\partial r} = 0. \quad (3.6)$$

The diffusion equation is solved not only for this stage but also for all other stages of drying to provide the solid mass fraction within the droplet in the whole drying process.

Second stage: Quasi-equilibrium evaporation (path: B–C in Fig. 3.2), in this stage, similar to what occurs in the evaporation process of a pure liquid droplet, it is assumed that the evaporation of free water existed on the surface of the droplet commences and the droplet size starts to reduce (shrinkage). Heat transferred to the droplet from the surroundings is mainly used for the evaporation and moreover, the growing solid concentration at the droplet surface causes the droplet temperature to increase gradually during this stage.

The change of droplet temperature can be obtained by solving the heat balance equation:

$$2\pi R \text{Nu} \lambda_{\text{air}} (T_\infty - T_s) = m C_v \frac{dT}{dt} + L \frac{dm}{dt}. \quad (3.7)$$

The boundary layer surrounding the droplet is the only resistance for the mass transfer (i.e. diffusion of vapor) throughout this stage and hence, the rate of evaporation can be determined using the equation of mass transfer for a pure liquid droplet as:

$$\frac{dm}{dt} = 2\pi R \text{ Sh } D_{\text{air}} (\gamma_s - \gamma_\infty) \quad (3.8)$$

The heat and mass transfer correlation for spheres is given by the Ranz-Marshall correlations (Ranz & Marshall 1952):

$$\text{Nu} = 2 + .6 \text{ Re}^{.5} \text{ Pr}^{.33} \quad (3.9)$$

$$\text{Sh} = 2 + .6 \text{ Re}^{.5} \text{ Sc}^{.33} \quad (3.10)$$

The change of droplet radius can be calculated as:

$$\frac{dR}{dt} = - \frac{1}{\rho_d 4 \pi R^2} \frac{dm}{dt} \quad (3.11)$$

Schematic illustration of this stage is displayed in Figure 3.3.

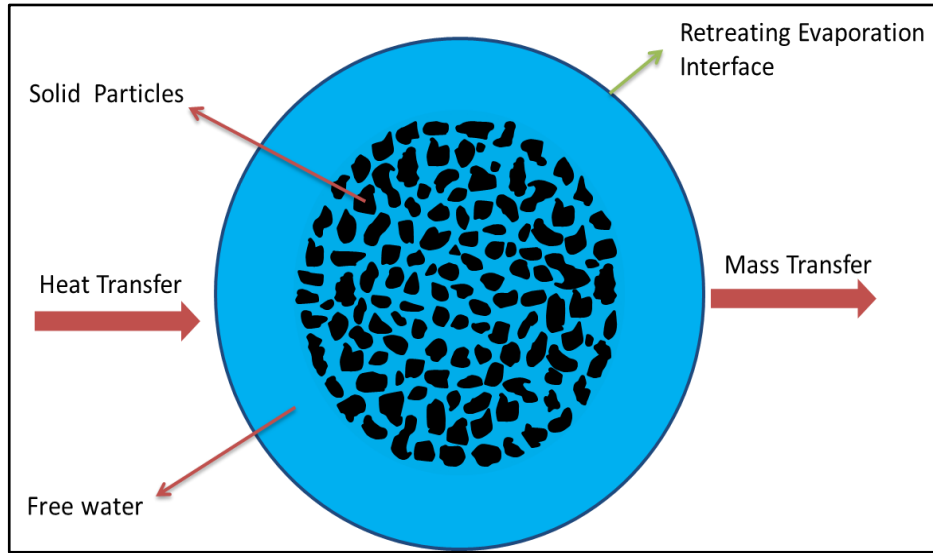


Figure 3.3: Schematic illustration of the constant rate period of drying process.

Third stage: Crust formation period and boiling (path: C–D in Fig. 3.2), this stage begins when the surface solids concentration reaches the saturation concentration. During this stage, solid segregation in the form of agglomeration or crystallization commences, which establish a solid crust on the droplet surface and hence the shrinkage is assumed to be stopped.

The partially dried particle is assumed to be divided by a moving core-crust interface into two distinct zones including the inner wet core and the outer dry crust. Evaporation is supposed to take place at this receding interface which retreats toward the center of droplet. The crust thickness creates a new resistance for the mass transfer and thus the

drying rate decreases significantly. The dry crust is supposed to have constant “bound” moisture that cannot be removed anymore, whereas the receding interface and the wet core are assumed to be fully saturated with the water. Furthermore, when the drying gas temperature is higher than the boiling temperature and the droplet temperature reaches the boiling temperature, a huge volume of vapor will be produced under the crust which cannot diffuse out at the rate at which it is generated. This causes the internal pressure of particle to increase and thus based on the mechanical characteristics of the solid crust the crack or inflation of the particle may occur which lead to the escape of vapor and relieving of the pressure difference, or even particle may explode and to be completely disintegrated.

For the analysis of this stage, a one dimensional spherical finite difference framework is used in which the numbers of nodes in the core and in the crust region is constant but in each time step with the movement of the receding interface the distance between the grids varies with time as the drying proceeds.

For the purpose of grid generation in both the wet core and the dry crust region for the starting of numerical calculation in this stage of drying (falling rate period), an initial crust thickness is needed which is considered to be 10 % of the critical droplet radius (i.e. the droplet radius at the end of the constant drying rate period). The interface tracking continues until the wet core radius reaches to 10 % of the critical droplet radius. Due to numerical difficulties it is not possible to perform the numerical calculation until the interface location reaches to the center of droplet ($r=0$).

In order to account for the core-crust interface, Eq. (3.1) is rewritten for both the core and the crust zone in terms of the total derivative of temperature with respect to time as:

$$\frac{dT}{dt} = \frac{r}{R_v} \frac{dR_v}{dt} \frac{\partial T}{\partial r} + \frac{\alpha}{r^2} \left[\frac{\partial}{\partial r} \left(r^2 \frac{\partial T}{\partial r} \right) \right] \quad (3.12)$$

With following the boundary conditions:

$$\frac{dT}{dr} = 0 \quad \text{at } r = 0 \quad (3.13)$$

$$-k \frac{dT}{dr} = h (T_s - T_\infty) \quad \text{at } r = R. \quad (3.14)$$

$$-k_{\text{crust}} \frac{\partial T_{\text{crust}}}{\partial r} + k_{\text{core}} \frac{\partial T_{\text{core}}}{\partial r} = \varepsilon \rho_{\text{water}} \lambda_{\text{water}} \frac{dR_v}{dt} \quad \text{at interface position} \quad (3.15)$$

Where R_v , ε and λ are the position of the core-crust interface within the droplet, porosity and the latent heat of evaporation of water respectively.

In order to capture the movement of the core-crust interface through the radial direction of droplet the heat balance equation at the interface is solved (Farid 2003):

$$(\omega_0 - \omega_b) L \rho_{av} \frac{dR_v}{dt} = - \left(k_{cru} \frac{\partial T}{\partial r} \Big|_{r=R_v} \right) - \left(k_{co} \frac{\partial T}{\partial r} \Big|_{r=R_v} \right). \quad (3.16)$$

In fact, this equation is resulted from the application of the heat balance at the core-crust interface (i.e. evaporation interface), at which the difference between the heat transferred from the solid crust to the evaporation interface and the heat transferred to the core region from this interface is used to evaporate some of the moisture (water) existing in the pores of the core region.

The rate of mass transfer is specified by the diffusion of vapor through the boundary layer surrounding the droplet liquid core and through the solid crust as follows:

$$\frac{dm}{dt} = \frac{2\pi (\gamma_s - \gamma_\infty)}{\frac{1}{R_{cri} Sh D_{air}} + \frac{\delta}{2D_{cru} R_{cri} (R_{cri} - \delta)}} \quad (3.17)$$

This equation is actually derived from this fact that the increase of solid concentration at the droplet surface leads to the reduction of partial pressure of water vapor at the droplet surface and additionally the growing solid crust thickness introduces a new resistance to the mass transfer process as well.

There are two distinct terms in the denominator of Eq. (3.17). The first term represents the resistance for the diffusion of vapor through the boundary layer while the second term indicates the resistance generated by the solid crust. The diffusion coefficient of the solid crust “ D_{cru} ” is usually significantly bigger than the convection-diffusion coefficient of the boundary layer around the liquid core “ $Sh D_{air}$ ”, and hence, the formation and growth of the solid crust ($\delta > 0$) create a considerable new resistance for the diffusion of vapor and therefore change the mass transfer procedure as well as the heat balance (Nesic and Vodnik 1991). Schematic illustration of this stage is displayed in Figure 3.4.

In order to provide ‘‘the second to third stage transition criterion’’ or in other words, in order to determine the end of the constant rate period and the beginning of the falling rate period of drying, it should be specified at what point the surface concentration C_s , approaches the saturation point C_{sat} . This purpose is achieved by solving the diffusion equation formulated in terms of mass fraction for the solid phase within the droplet (Eq. (3.4) – (3.6)). This stage of drying begins when the surface solid concentration reaches or exceeds the saturation concentration which is most often equal to the saturation solubility of the solute (solid) in the solvent (water) and is determined by the experiment.

Besides, Werner (2005) suggested another transition criterion for this stage of drying based on a relation between the droplet surface temperature and its glass transition temperature. He proposed at some point defined by a critical $X = (T_s - T_g)$ value a rigid surface will develop so that the surface skin is mechanically strong enough to resist against the volume change and fix the droplet radius for the remaining time of the drying process. The critical values of X from 0-40°C were considered to represent a reasonable temperature range at which a rigid skin can form (Werner 2005, Werner *et al.* 2008).

Forth stage: porous particle drying (path: D–E in Fig. 3.2), in this stage the droplet is considered as an almost dried porous particle in which the evaporation of bound liquid with a decreasing rate occurs and the particle temperature asymptotically reaches the drying gas temperature. During this final stage, the temperature distribution within the dried particle was estimated using Eq. (3.1) – (3.3) by taking into account only the crust thermo-physical properties.

Aside from the estimation of temperature distribution within the droplet, the average temperature of the droplet is calculated by using the numerical integration of the temperature distribution in the radial direction of droplet as:

$$T_{ave} = \frac{3}{r^3} \int_0^r r^2 T(r) dr \quad (3.18)$$

In the following sections in all graphs which show the droplet temperature versus the time, the calculated temperatures represent the averaged values of temperature.

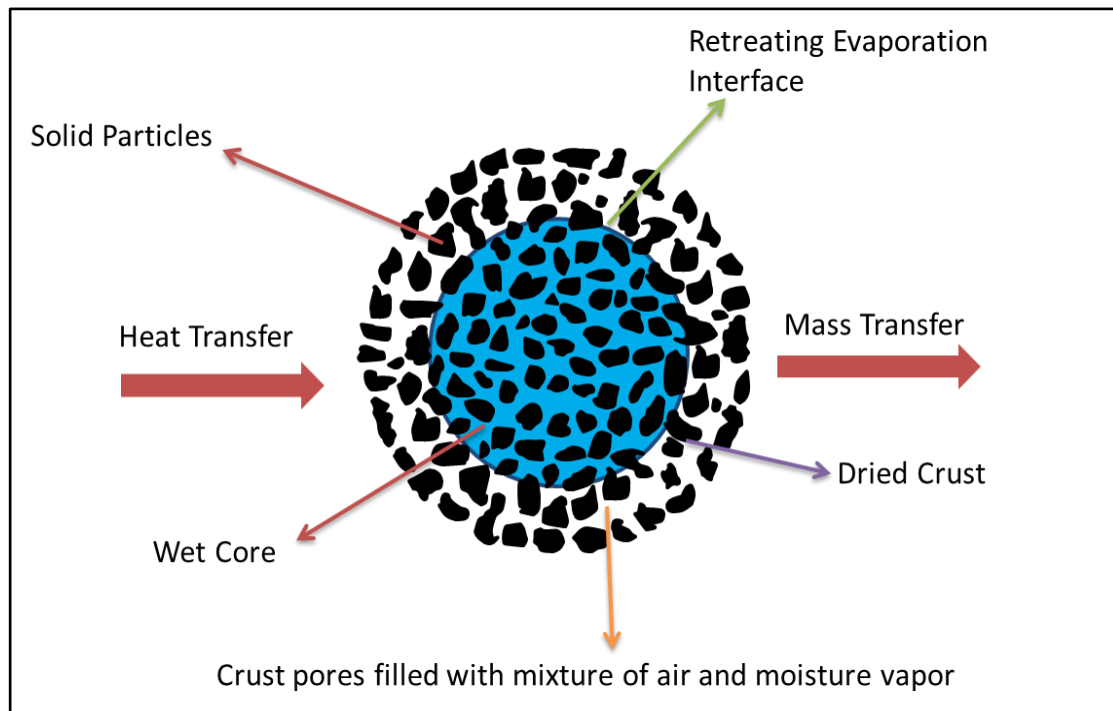


Figure 3.4: Schematic illustration of the falling rate period of drying process.

3.3.3 Numerical procedure

Nowadays the numerical methods are widely used in order to solve the heat and mass balance equations. In the numerical techniques, the computational domain is divided into the small regions called meshes and it is supposed that the system of differential equations is valid over the finite domain. Using some approaches such as the finite difference or finite volume the system of differential equations is transformed into a system of algebraic equations and then is solved over the domain at each of the finite meshes (AL-Hafidh 2008).

At the present work, the explicit finite difference technique is used for solving the mass and heat balance equations within the droplet. For this purpose, a one dimensional spherical finite difference framework, in which the droplet is discretized into the 50 number of shells with equal thickness, has been developed in order to model the heat and mass transfer during the drying process.

The spatial derivatives were discretized using the forward, backward or central difference schemes where appropriate, while the forward time difference approximation was used for the discretization of time derivatives as follows:

$$\frac{d\phi}{dr}(t_i, r_j) = \frac{\phi(t_i, r_{j+1}) - \phi(t_i, r_j)}{\Delta r} \quad (3.19)$$

$$\frac{d\phi}{dr}(t_i, r_j) = \frac{\phi(t_i, r_j) - \phi(t_i, r_{j-1})}{\Delta r} \quad (3.20)$$

$$\frac{d\phi}{dr}(t_i, r_j) = \frac{\phi(t_i, r_{j+1}) - \phi(t_i, r_{j-1})}{2\Delta r} \quad (3.21)$$

$$\frac{d\phi}{dt}(t_i, r_j) = \frac{\phi(t_{i+1}, r_j) - \phi(t_i, r_j)}{\Delta t} \quad (3.22)$$

Mesh in the constant drying rate period is based on the moving boundary which means in each time step the boundary conditions will have a new location according to the reduction of droplet radius due to the shrinkage. Figure 3.5 displays the mesh in the constant drying rate period as applied in the simulation.

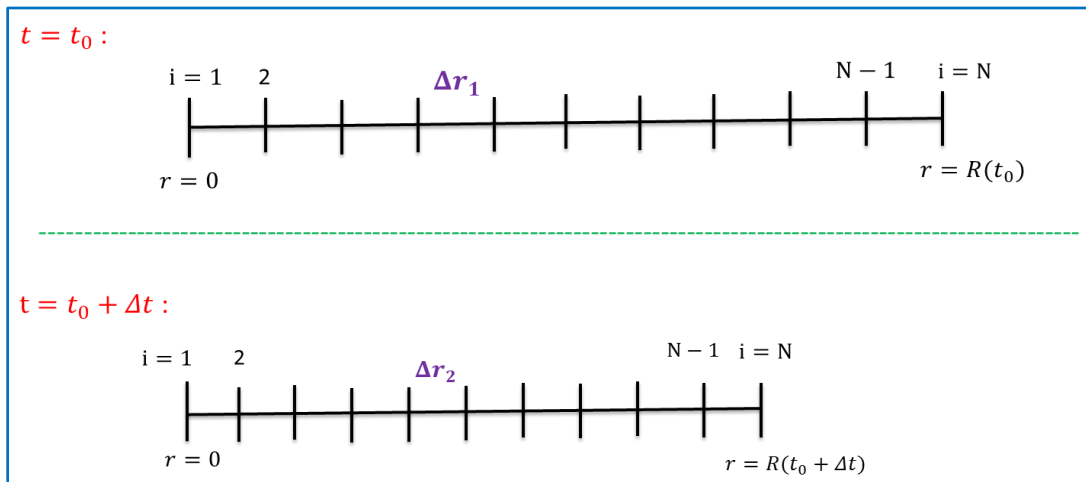


Figure 3.5: Mesh arrangement in the constant drying rate period.

Mesh in the falling drying rate period is a kind of dynamic mesh named variable space network method in which the numbers of nodes in the core and crust region are constant but in each time step with the movement of interface the distance between the grids varies with time. Figure 3.6 shows the mesh in the falling drying rate period as applied in the simulation.

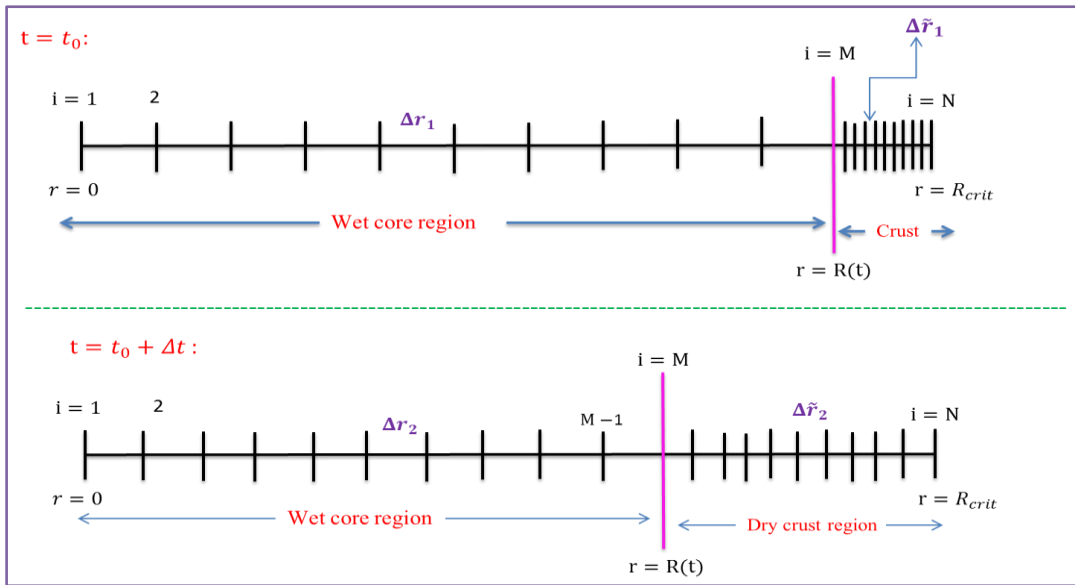


Figure 3.6: Mesh arrangement in the falling drying rate period.

3.3.4 Application to the single droplet drying simulation

In the next step, this developed model is applied to simulate three different systems: colloidal silica, aqueous sodium sulphate and skimmed milk droplets in order to evaluate the accuracy and ability of this model for predicting the drying behavior of these different single droplets both in the constant and in the falling rate period.

These three different systems are selected due to the availability of their experimental data for validation of our simulations, as well as their different characteristics (i.e. having the porous and fragile crust or dense and low porous structure) which caused the different behavior of these droplets during the drying process.

After successful validation of the modelling results against the experimental data, it can be used as a sub-model for predicting the performance of different spray drying towers as well. In the model calculations, the following initial conditions are being used. As the surrounding humidity was not provided in the experimental publications, it was assumed to be zero. The initial droplet temperature was assumed to be uniform with a value according to the specifications in the experimental papers. Table 3.1 shows the different systems and their drying conditions as were used in the simulation and in Table 3.2 the physical properties of different systems can be found. Besides, in the following sections in all graphs which show the droplet temperature versus the time, the calculated temperatures represent the averaged values of temperature (see Eq. (3.18)).

Table 3.1: Different systems and their drying condition

Case	Test case	W _s [wt%]	D _d [mm]	T _{air} [K]	T _d [K]	V _{air} [m/s]	ρ [kg/m ³]	C _{sat} Kg solid/kg solution
1	Skim Milk	20	1.9	343	281	1.3	1249	0.34
2	Skim Milk	20	1.6	363	289	1.0	1234	0.50
3	Skim Milk	30	1.94	373	294	1.0	1249	0.40
4	Skim Milk	30	1.90	423	301	1.0	1249	0.40
5	Colloidal Silica	30	2.06	374	290	1.73	1004	0.64
6	Colloidal Silica	30	2.0	451	293	1.40	1027	0.64
7	Sodium Sulphate	14	1.46	363	301	1.0	1952	0.40
8	Sodium Sulphate	14	1.85	383	293	1.0	991	0.40

Table 3.2: Physical properties of different systems

Test case	D _{cru} [m ² /s]	k _{core} [W/(m·K)]	k _{crust} [W/(m·K)]	D _{AB} [m ² /s]
Colloidal Silica	1.0×10^{-6}	0.6	0.55	See Eq. (3.21)
Skim milk	1.5×10^{-6}	0.4	0.07	See Eq. (3.22)
Sodium Sulphate	1.5×10^{-7}	0.95	0.9	See Eq. (3.23)

3.3.5 Grid independence study

The figures 3.7 and 3.8(a) depict the grid study for the droplet mass and temperature calculation of the skimmed milk droplet respectively at the drying condition mentioned in the case 2 of Table 3.1.

The grid resolution study is performed using 3 different grids including the coarse, fine and dense grid consisting of 15, 25 and 50 numbers of shells respectively.

As it was expected the results provided by the calculations with the fine and dense grid have better agreement with the experimental data and moreover, the difference between the results for these two grids are not considerable. Hence the fine grid is selected for the final spray dryer calculation.

Figure 3.8(b) shows the grid study for the temperature distribution within the colloidal silica droplet. As shown in this Figure, as well as Figure 3.8(a), using the coarse grid resulted in an under-prediction of droplet temperature while such under-prediction is not observed for the fine and dense grid and the difference between the results for fine and dense grid is negligible as well.

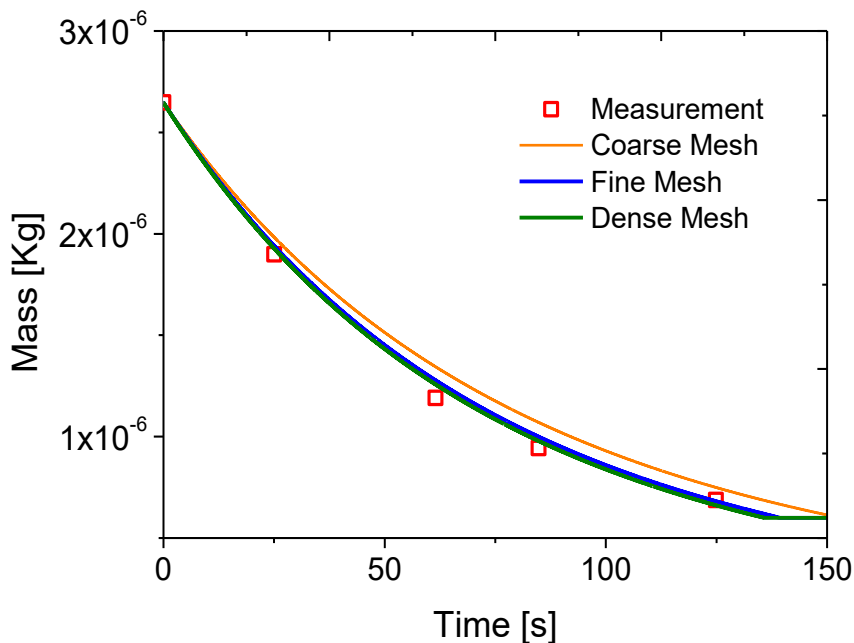


Fig. 3.7: Grid Study for Simulated drying of a 20 wt% skimmed milk droplet (lines) compared with experimental results from Nescic (1989) (symbols) at: $T_{\text{air}} = 363^{\circ}\text{K}$, $V_{\text{air}} = 1.0$ m/s, $D_d = 1.60$ mm and $T_d = 289$ K (**Case 2**).

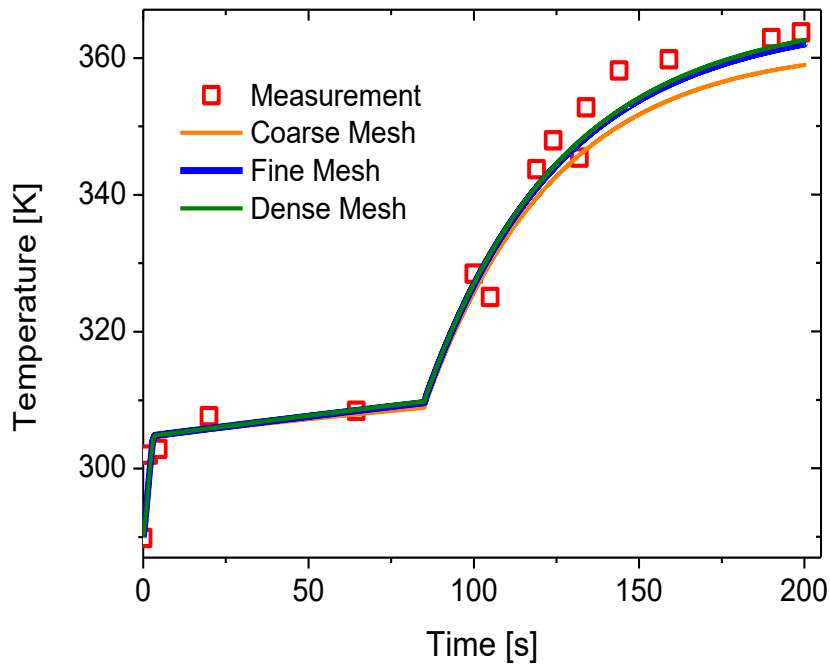


Fig. 3.8(a): Grid Study for Simulated drying of a 20 wt% skimmed milk droplet (lines) compared with experimental results from Nestic (1989) (symbols) at: $T_{\text{air}} = 363^{\circ}\text{K}$, $V_{\text{air}} = 1.0$ m/s, $D_d = 1.60$ mm and $T_d = 289$ K (**Case 2**).

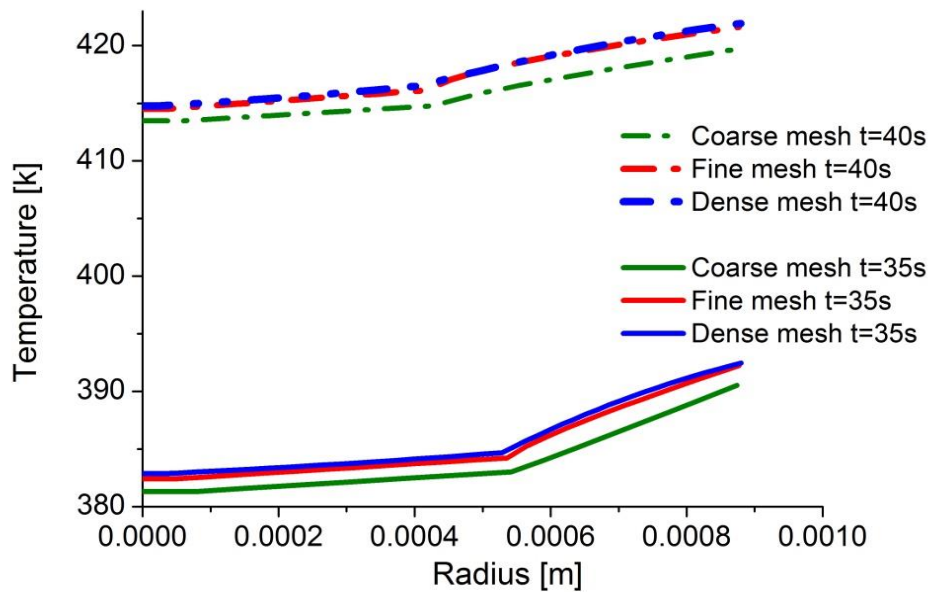


Fig. 3.8(b): Grid Study for temperature distribution within droplet for drying of 30 wt% colloidal silica at: $T_{\text{air}} = 451^{\circ}\text{K}$, $V_{\text{air}} = 1.40$ m/s, $D_0 = 2.00$ mm and $T_d = 293\text{K}$; for two different instants of time.

3.3.6 Colloidal silica droplets

The first test case simulated is the drying of a droplet containing 16 nm colloidal silica particles suspended in the water. Nestic and Vodnic (1991) identified the colloidal silica as a material which has a very porous and fragile crust that does not represent a considerable resistance to the heat and mass transfer; and hence the temperature levels and the evaporation rates are very close to those of pure liquid droplets.

Based on their experiment, the gel formation was observed when the SiO₂ bulk concentration reached the 40% or slightly higher. Before the formation of gel structure, there is a strong internal circulation inside the droplet which is induced by the air drag force so that the concentration and temperature profiles are almost flat. As the gel structure is formed, the internal circulation stops and the internal diffusion mechanism controls the process. Thereupon, a solid crust gradually appears at the droplet surface and the growth of this crust accelerates the increase of droplet temperature; so that the droplet temperature rapidly reaches the drying air temperature after all unbound water is evaporated. The model parameters used to predict the drying process are:

The internal diffusion coefficient:

$$D_{AB} = \exp\left(-\frac{28.1+282\omega_A}{1+15.47\omega_A}\right) \quad (3.23)$$

The crust diffusion coefficient, $D_{\text{cru}} = 10^{-6} \text{ m}^2/\text{s}$ and the thermal conductivity of the crust, $k_{\text{cru}} = 0.55 \text{ W}/(\text{m}\cdot\text{K})$.

With these parameters, it is possible to simulate the drying process regarding the mass and temperature of droplet as shown in the figures 3.9 and 3.10. Due to the formation of a porous and fragile crust there is no considerable change in the drying rate throughout the drying process except for the final stage of drying which can be due to the further increase of the heat and mass transfer resistance caused by the growing thickness of the solid crust. As it can be seen, the model calculations are in good agreement with the experimentally measured values.

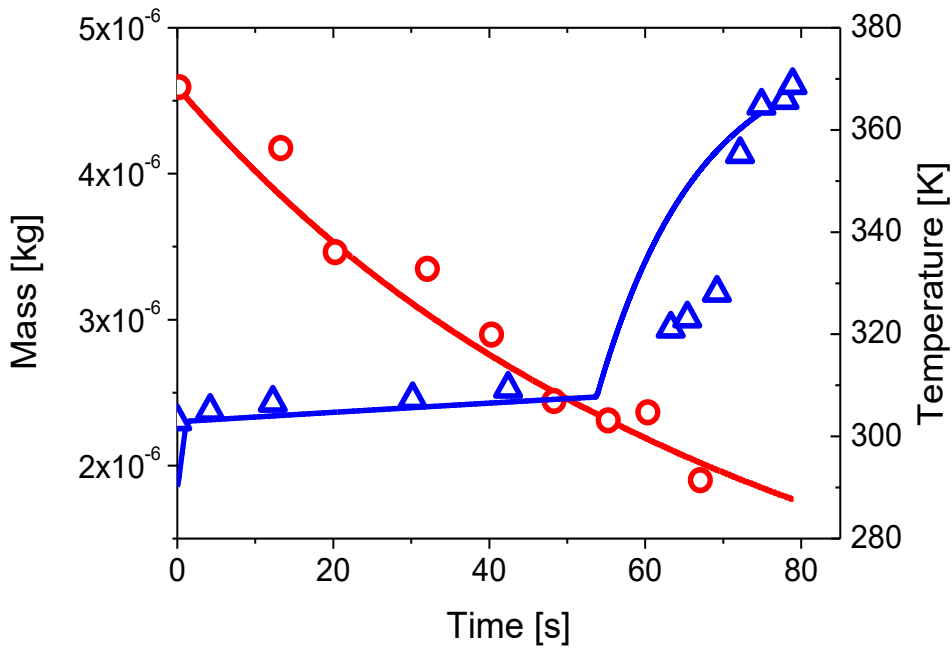


Fig. 3.9: Simulated drying of a 30 wt% colloidal silica droplet (lines) compared with experimental results from Nescic & Vodnik (1991) (symbols) at: $T_{\text{air}} = 374^{\circ}\text{K}$, $V_{\text{air}} = 1.73 \text{ m/s}$, $D_d = 2.06 \text{ mm}$ and $T_d = 290 \text{ K}$ (Case 5).

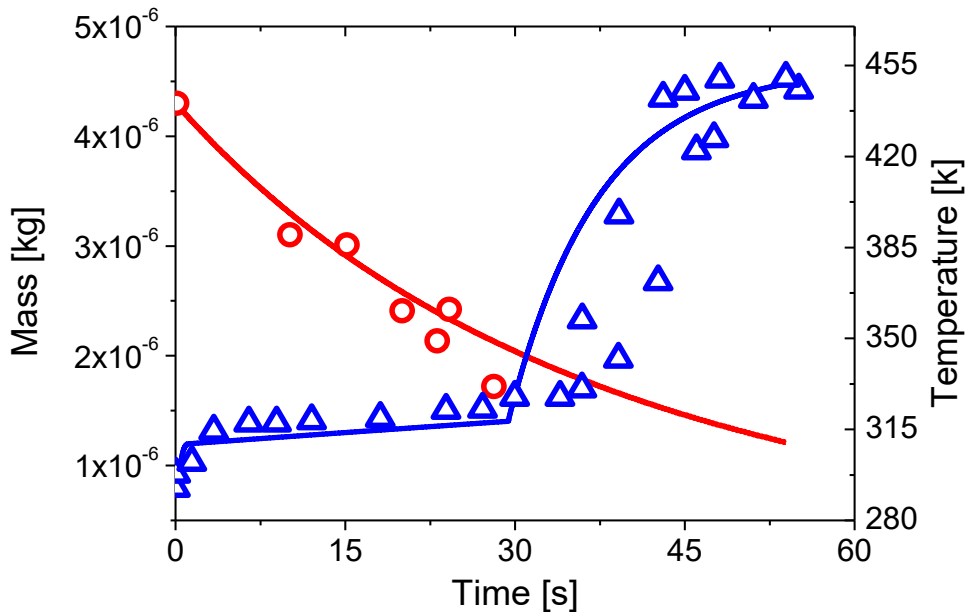


Fig. 3.10: Simulated drying of a 30 wt% colloidal silica droplet (lines) compared with experimental results from Nescic & Vodnik (1991) (symbols) at: $T_{\text{air}} = 451^{\circ}\text{K}$, $V_{\text{air}} = 1.40 \text{ m/s}$, $D_0 = 2.00 \text{ mm}$ and $T_d = 293\text{K}$ (Case 6).

3.3.7 Skimmed milk droplets

Skimmed milk is one of the most commonly spray dried biological materials. As the experiments of Nesic and Vodnic (1991) showed the behavior of skimmed milk droplets during the drying process is very similar to the behavior of colloidal silica droplets. There was no boiling stage even for the high drying air temperatures and no intense internal circulation was observed which can be explained by the higher viscosity of milk.

In the figures 3.11, 3.12, 3.13 and 3.14 the measured temperature, mass and moisture content of the skimmed milk droplets are compared with the results calculated from the present model. In the temperature profiles the same trends as were noticed in the drying of colloidal silica are identified for the skimmed milk droplets as well, and moreover, they are very well predicted by the model calculations. As shown, the droplet temperature increases rapidly during the initial warm-up period followed by a slight variation in the constant drying rate period as well as a gradual increase throughout the falling drying rate period. Contrary to what was observed in the drying of colloidal silica, the drying rates in the constant and falling rate periods are quite different from each other for the drying of skimmed milk droplets. The decreasing drying rate in the falling rate period could be resulted from the growing resistances for the heat and mass transfer generated by the solid crust as it forms and grows during this period of the drying.

Model parameters used to predict the evaporation process are:

The internal diffusion coefficient:

$$D_{AB} = \left\{ \frac{(38.912 + 323.39 \omega_A)}{(1 + 15.8 \omega_A)} - \frac{\Delta H}{R} \left(\frac{1}{T} - \frac{1}{303} \right) \right\} \quad (3.24)$$

The crust diffusion coefficient, $D_{\text{cru}} = 1.5 \times 10^{-6} \text{ m}^2/\text{s}$ and the thermal conductivity of the crust, $k_{\text{cru}} = 0.07 \text{ W}/(\text{m}\cdot\text{K})$. Using these parameters the predicted temperature, mass and moisture content history for the skimmed milk droplets agreed very well with the experimentally observed values. Furthermore, contrary to the fast rise in the temperature of colloidal silica droplets, in the temperature of skimmed milk droplets such a fast rise is not observed. The main reason of such a different behavior is the different values of crust thermal conductivity which these droplets (i.e. colloidal silica and skimmed milk) have. This property (i.e. the crust thermal conductivity), which mainly controls the heat transfer in the falling drying rate period, for the colloidal silica is about

eight times bigger than that of skimmed milk droplets. This is expected because of the much higher thermal conductivity of colloidal silica particles in comparison with the powdered milk.

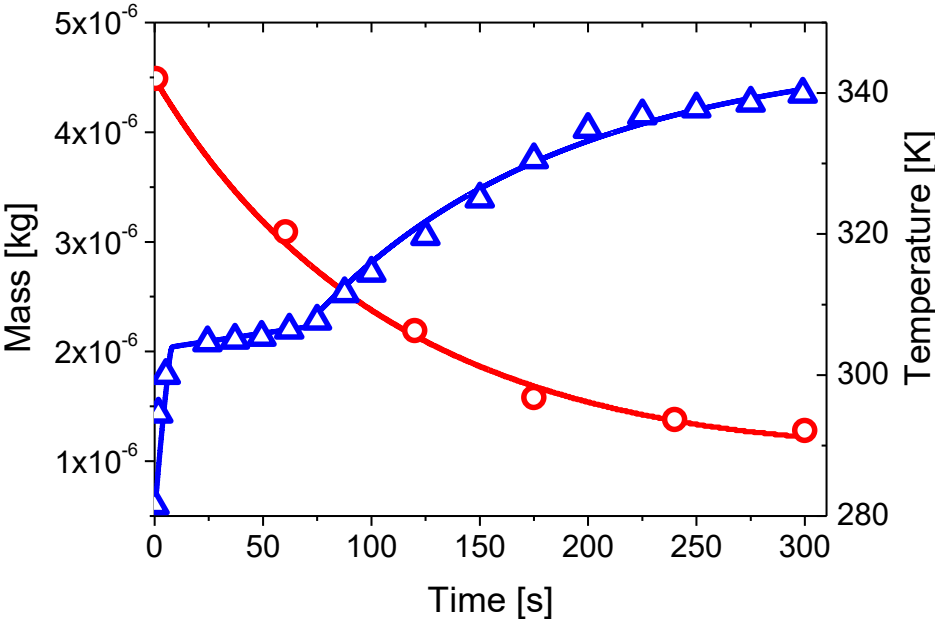


Fig. 3.11: Simulated drying of a 20 wt% skimmed milk droplet (lines) compared with experimental results from Chen *et al.* [1999] (symbols) at: $T_{\text{air}} = 343^{\circ}\text{K}$, $V_{\text{air}} = 1.3 \text{ m/s}$ $D_d=1.90 \text{ mm}$ and $T_d = 281\text{K}$ (**Case 1**).

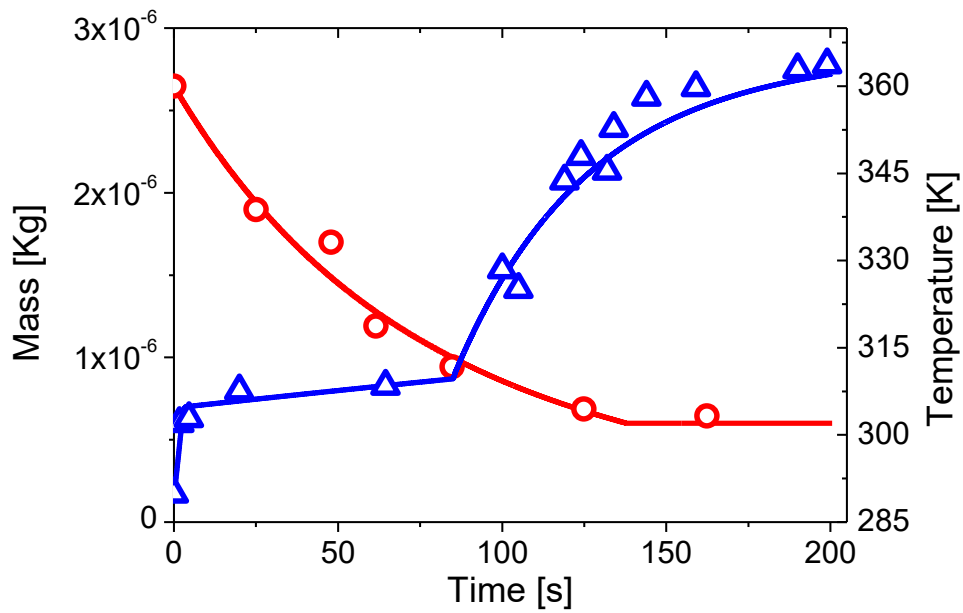


Fig. 3.12: Simulated drying of a 20 wt% skimmed milk droplet (lines) compared with experimental results from Nestic (1989) (symbols) at: $T_{\text{air}} = 363^{\circ}\text{K}$, $V_{\text{air}} = 1.0 \text{ m/s}$, $D_d = 1.60 \text{ mm}$ and $T_d = 289 \text{ K}$ (Case 2).

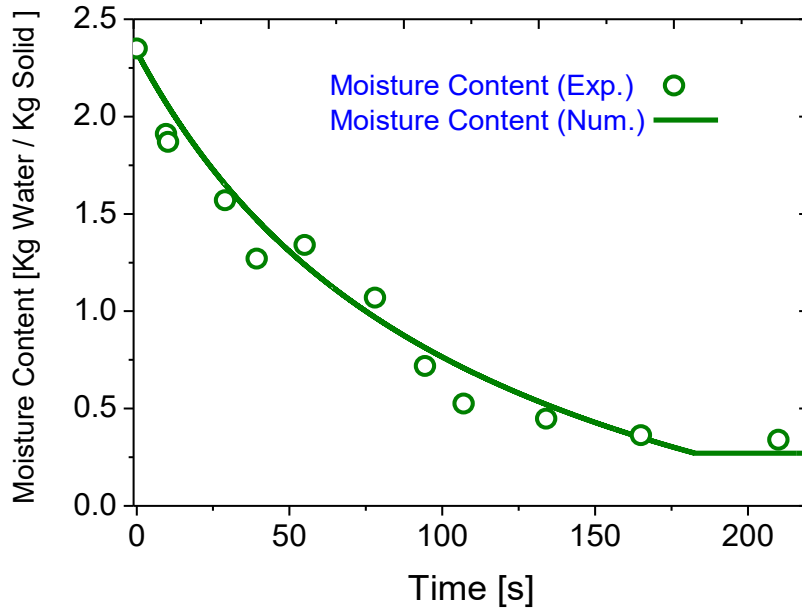


Fig. 3.13: Variation of moisture content of a 30 wt% skimmed milk droplet (line) compared with experimental results from Sano & Keey (1982) (symbol) at: $T_{\text{air}} = 373^{\circ}\text{K}$, $V_{\text{air}} = 1.0 \text{ m/s}$, $D_d = 1.94 \text{ mm}$ and $T_d = 294 \text{ K}$ (Case 3).

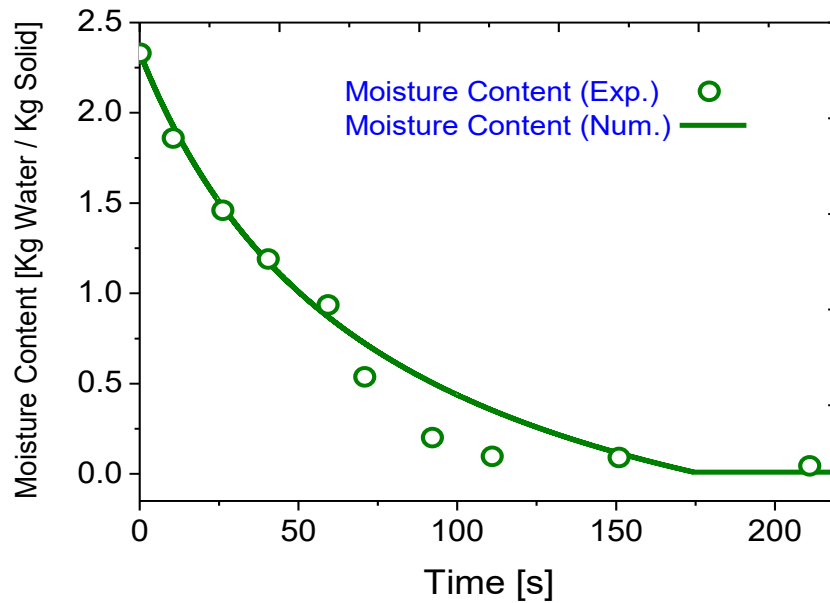


Fig. 3.14: Variation of moisture content of a 30 wt% skimmed milk droplet (line) compared with experimental results from Sano and Keey (1982) (symbol) at: $T_{\text{air}} = 423^{\circ}\text{K}$, $V_{\text{air}} = 1.0$ m/s and $D_d = 1.9$ mm and $T_d = 301$ K (**Case 4**).

3.3.8 Sodium sulphate decahydrate droplets

Sodium sulphate is selected as a model material for those kinds of solutions which form an impermeable crust during the drying process. The experiments on the drying of sodium sulphate droplets (Nesic and Vodnik 1991) showed that the solid crust established and thickened in these droplets during the falling rate period has a dense and relatively low porous structure which generates a further resistance to the diffusion of water vapor, and thus causes the rate of drying to reduce significantly during this period of drying.

From the figures 3.15 and 3.16, it can be recognized that during the constant rate period the evaporation rate is under-predicted in comparison to the experimental measurements. This disagreement is perhaps caused by the inaccurate determination of the reduction of partial vapor pressure at the droplet surface. As seen in these figures, the droplet temperature gradually increases in the constant rate period while due to the formation and growth of the rigid dry crust it (i.e. droplet temperature) increases sharply during the falling rate period. According to the experiments (Cheong 1983), decahydrate crystals melt at 34°C and form anhydrous sulphate solution. When the evaporation of water begins, the droplet temperature drops and decahydrate crystals will be reformed. This ‘‘melting & re-crystallization process’’ leads to the formation of different hydrates which

perhaps changes the density of the solid concentration within the droplet (Dalmaz 2005). This particular characteristic of the decahydrate crystals may also be the reason of deviation of predicted values from the experimental data.

Model parameters used to predict the evaporation process are:

The internal diffusion coefficient:

$$D_{AB} = \left\{ (.4444\omega_A - 1.4497\omega_A^{.5} + 1.1475) \left(\frac{T}{298} \right) \times 10^{-9} \right\} \quad (3.25)$$

The crust diffusion coefficient, $D_{cru} = 1.5 \times 10^{-7} \text{ m}^2/\text{s}$ and the thermal conductivity of the crust, $k_{cru} = 0.9 \text{ W}/(\text{m}\cdot\text{K})$.

In General, although the model predictions deviate slightly from the experimental results but the overall ability of the model to approximate the experimental measurements for this test case is satisfactory.

The figures 3.17 and 3.18 show the temperature distribution inside the droplet at the different time steps of calculation for the sodium sulphate droplet in two different drying conditions.

In the constant drying rate period, the variation of temperature inside the droplet is negligibly small because most of the heat transferred to the droplet from surrounding is mainly used for the evaporation but in the falling rate period as the solid crust thickens, the heat transfer resistance will be increased and thus the difference between the droplet surface temperature and the wet core temperature increases and therefore the higher temperature gradients within the droplet are observed at this period of drying.

Furthermore, in the core region, the temperature gradient is smaller than that of the crust region which is due to the higher thermal conductivity of this (core) region. As the resistance to the heat transfer is inversely proportional to the thermal conductivity, in the cases /regions which have higher thermal conductivity the heat can flow better within the droplet and therefore less temperature gradient is observed.

Besides, the higher drying gas temperature in the second case yields the higher temperature gradients within the droplet in comparison with the first case.

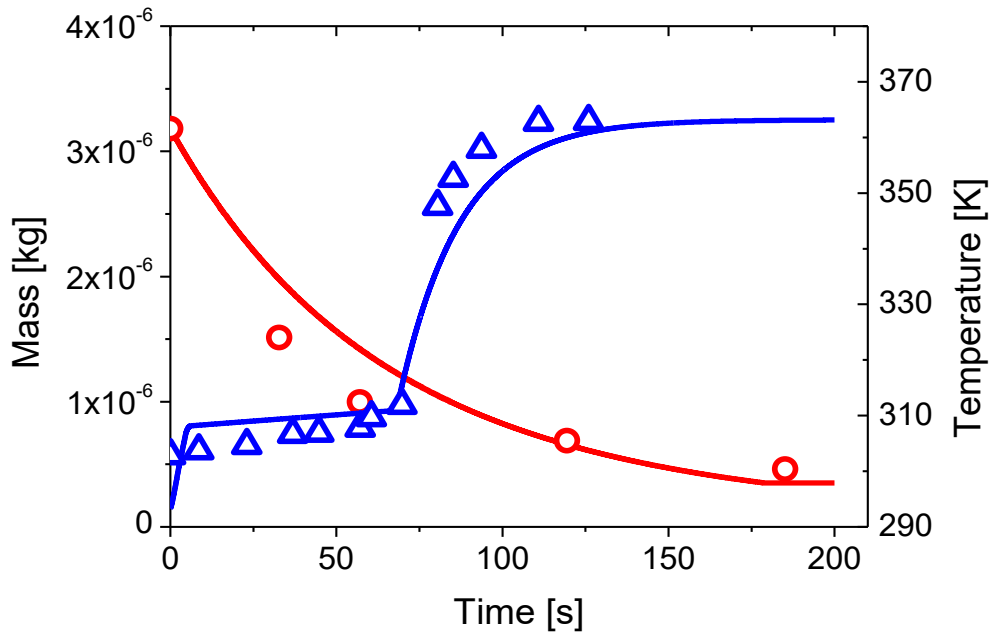


Fig. 3.15: Simulated drying of a 14 wt% sodium sulphate in water droplet (lines) compared with experimental results from Nestic & Vodnik (1991) (symbols) at: $T_{\text{air}} = 363^{\circ}\text{K}$, $V_{\text{air}} = 1.0 \text{ m/s}$, $D_d = 1.46 \text{ mm}$ and $T_d = 301\text{K}$ (**Case 7**).

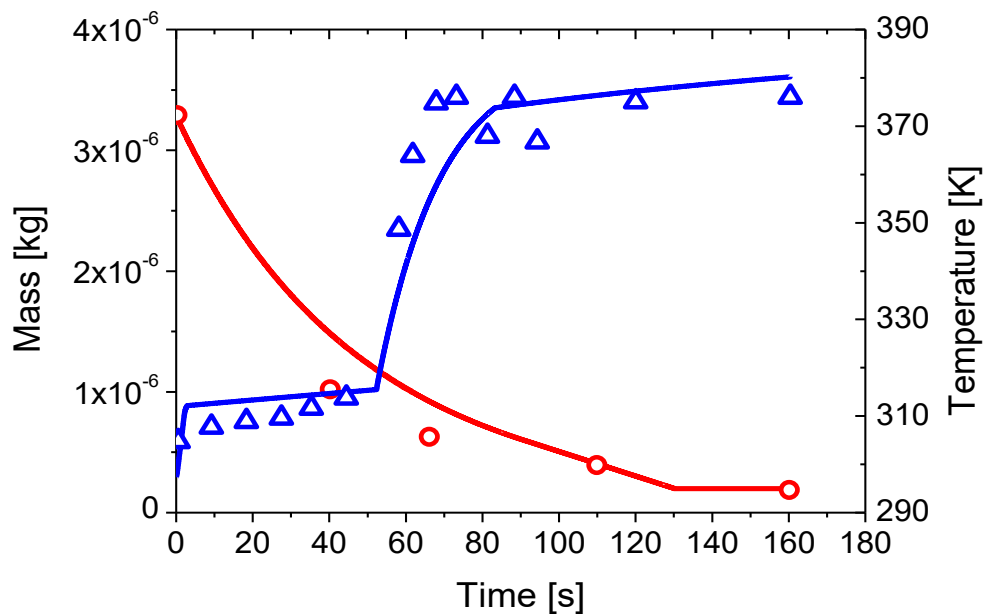


Fig. 3.16: Simulated drying of a 14 wt% sodium sulphate in water droplet (lines) compared with experimental results from Nestic & Vodnik (1991) (symbols) at: $T_{\text{air}} = 383^{\circ}\text{K}$, $V_{\text{air}} = 1.0 \text{ m/s}$ and $D_d = 1.85 \text{ mm}$ and $T_d = 293\text{K}$ (**Case 8**).

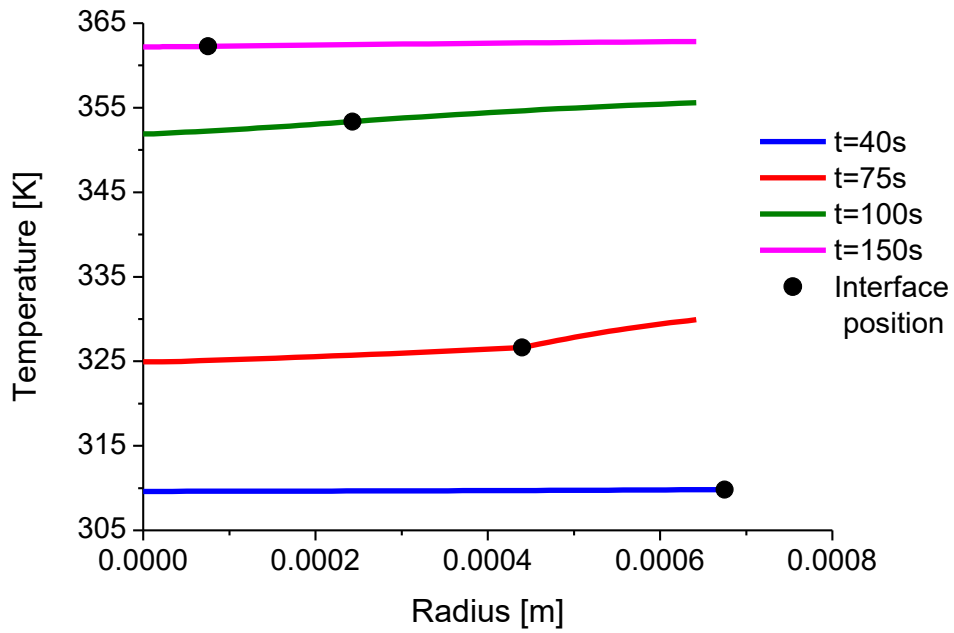


Fig. 3.17: Temperature distribution within the droplet at different time steps of calculation for 14 wt% sodium sulphate in water droplet at: $T_{\text{air}} = 363^{\circ}\text{K}$, $V_{\text{air}} = 1.0 \text{ m/s}$, $D_d = 1.46 \text{ mm}$ and $T_d = 301\text{K}$ (Case 7).

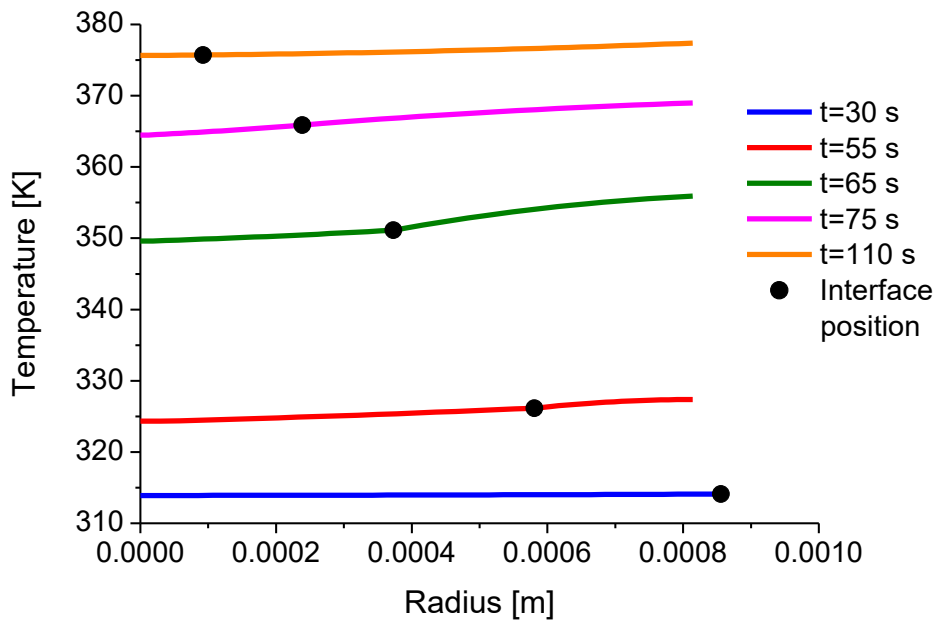


Fig. 3.18: Temperature distribution within the droplet at different time steps of calculation for 14 wt% sodium sulphate in water droplet at: $T_{\text{air}} = 383^{\circ}\text{K}$, $V_{\text{air}} = 1.0 \text{ m/s}$ and $D_d = 1.85 \text{ mm}$ and $T_d = 293\text{K}$ (Case 8).

3.4 Comparison with other models

The present model is compared with the other models which are available in the literature, e.g. Sano & Keey (1982), Nestic & Vodnic (1991), and Farid (2003) model. The figures 3.19, 3.20, 3.21 and 3.22 show the droplet temperature and mass profiles as a function of time for the different models in the different drying conditions. As shown in these figures; the results produced by the new model which considers the temperature and moisture distribution within the droplet in the most cases fit better with the experimental data than the other models. Especially the transition of the temperature from the ‘‘quasi-equilibrium stage’’ to the ‘‘crust formation & its growing stage’’ in the most cases are captured correctly.

The reason of no clear indication of ‘‘the constant and falling rate period transition’’ in the Sano & Keey model can be the lack of consideration of the drying stages when calculating the temperature of droplet which resulted in the continuous increase of droplet temperature and the reason in the Farid model can be the lack of clear transition criteria for the different stages of drying. In the Nestic & Vodnik model, although in the temperature profiles the indication of transition is clear but using a single equation for the temperature calculation in the whole drying process may lead to the unclear indication of ‘‘the constant and falling rate period transition’’ in the temperature profiles .

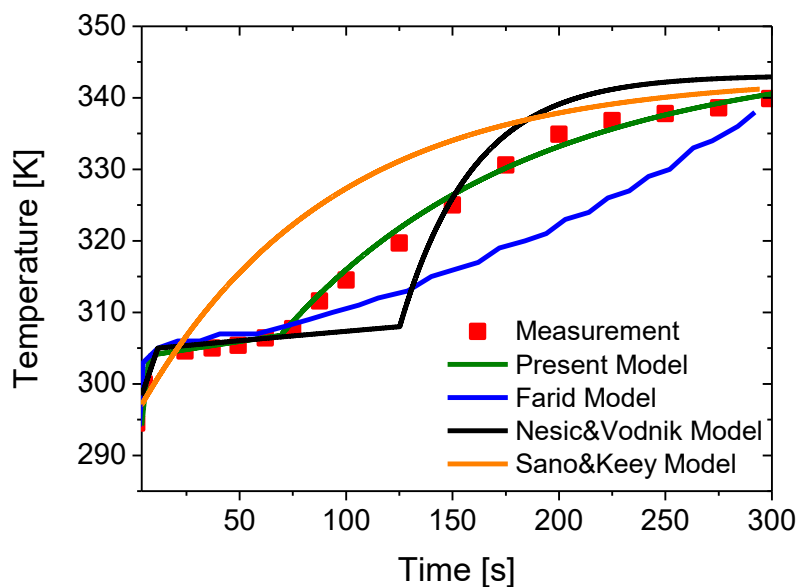


Fig. 3.19: Comparison of average temperature as a function of time for different models (droplet of 20 wt% (solid content) skim milk during drying at: $T_{\text{air}} = 343^{\circ}\text{K}$, $V_{\text{air}} = 1.3 \text{ m/s}$, $D_d = 1.90 \text{ mm}$ (case 1).

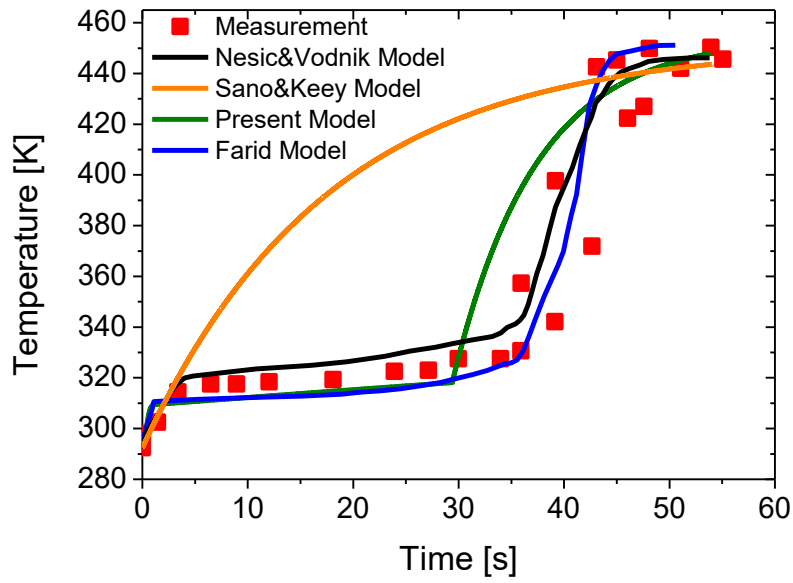


Fig. 3.20: Comparison of average temperature as a function of time for different models (droplet of 30 wt% (solid content) colloidal silica during drying at: $T_{\text{air}} = 451^{\circ}\text{K}$, $V_{\text{air}} = 1.40 \text{ m/s}$ and $D_d = 2.00 \text{ mm}$ (**case 6**).

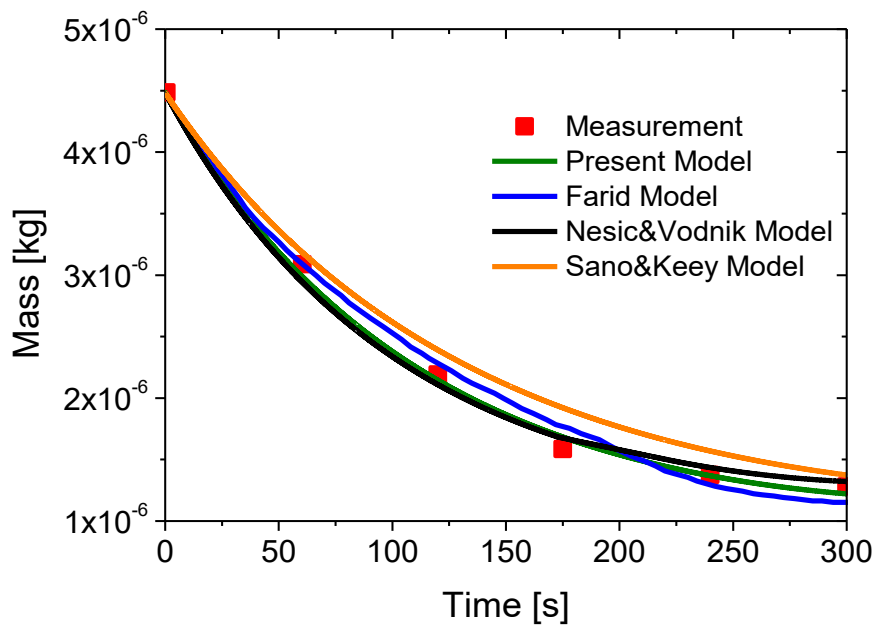


Fig 3.21: Comparison of mass as a function of time for different models (1.9 mm diameter droplet of 20 wt% (solid content) skim milk during drying with air at 343°K , $u_{\text{air}} = 1.3 \text{ m/s}$) (**case 1**).

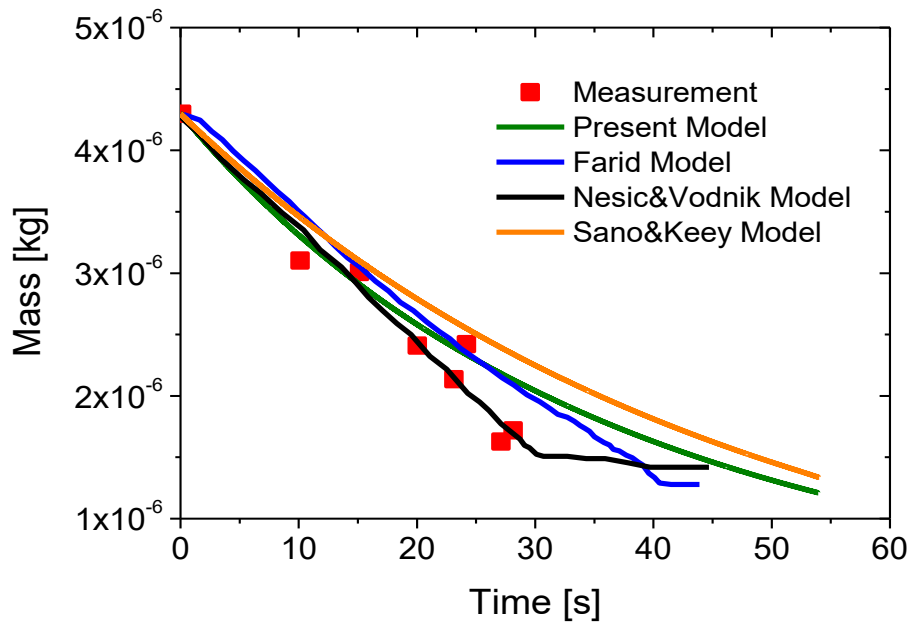


Fig. 3.22: Comparison of mass as a function of time for different models (droplet of 30 wt% (solid content) colloidal silica during drying at: $T_{\text{air}} = 451^{\circ}\text{K}$, $V_{\text{air}} = 1.40 \text{ m/s}$ and $D_d = 2.00 \text{ mm}$ (case 6).

3.5 Conclusion of the chapter

The main goal of this work was the developing of a confident CFD model for the spray drying process to describe the drying of the suspension or solution droplets under the conditions relevant for the spray dryers and furthermore, overcome some of the drawbacks recognized in the previous drying models existed in the literature. A more detailed droplet drying model which considers not only the rate of moisture loss, but also enables having a better understanding regarding the morphological evolution of the droplets throughout the drying process.

Successful applications of the developed model for the simulation of three different systems: colloidal silica, aqueous sodium sulphate and skimmed milk droplets and moreover, the comparison of the results obtained by the present model with the results provided by the literature models confirmed the ability and capability of this model for estimation of the drying behavior of different materials during the drying process both in the constant and in the falling drying rate period. As a conclusion, the study provided an efficient drying model which is able to predict successfully the drying behavior of

different single droplets and has the potential and capability in order to be applied as a sub-model for a full CFD spray dryer simulation.

4 Calculation approaches for spray dryers

4.1 Calculation approaches for the spray drying process

There are several methods which can be used for the simulation of spray dryers. Generally, Oakley (2004) classified these methods into four groups as follows:

4.1.1 Heat and Mass balances methods

This approach includes the simplest methods for description of the spray dryers behavior and uses the energy and mass balance of the incoming flows (i.e. incoming air and the atomized fluid flow) and the outgoing flows (i.e. the outgoing air flow and the powder removed from the dryer) in the drying chamber (Masters 1991, Blei 2005).

The main advantage of this approach is its ability to evaluate the thermodynamic feasibility of an operation at the earliest design stage while the low predictive power and the incapability to predict the solvent distribution between the gas and droplet phase are the main disadvantages of this approach for designing a spray drying process (Handscomb 2008).

4.1.2 Equilibrium based methods

The models which are based on the heat and mass balance can be extended by applying the information about the phase equilibrium between the gas and dispersed phase during the drying process (Blei 2005). A phase equilibrium relationship relates the particle moisture content to the humidity of surrounding gas. Supposing that the dried particles at the outlet are in equilibrium with their surroundings enables the using of sorption isotherms to estimate the moisture content of the exit particles (Handscomb 2008). The sorption isotherms are curves which graphically indicate the corresponding moisture (water) content value at a given, constant temperature for each humidity value of the surrounding gas and are determined experimentally for each product.

A rough approximation of the moisture content of exit product and the ability for investigation of ‘‘how the different operating conditions affect the moisture concentration of the exit dried particles’’ are the main advantages of the equilibrium-based models while

Oakley (2004) mentioned two drawbacks of these models which put a limitation on the applicability of this approach as:

1-the only way for determination of the sorption isotherms for each product is an experiment.

2- The dried particles at the outlet have to be in equilibrium with the exit-gas phase.

4.1.3 Rate-based models

The rate based models are applicable when the assumption of equilibrium conditions at the outlet is not correct (i.e. the dried particles at the outlet did not approach the equilibrium state with the surrounding gas). These types of models are dynamic and describe the rate at which the moisture is removed from the droplets as the droplets travel through the drying chamber. These models can also be used to determine the final particles size and moreover, to predict the particles residence time in the dryer based on the simplifying assumptions about the droplets motion within the spray drying tower. But due to not including the calculation of drying gas flow pattern as well as the injection pattern this approach is not a proper tool for a detailed design.

It seems there is no logical reason for the application of rate based models anymore because nowadays using the computational fluid dynamics (CFD) provides the more detailed and comprehensive information about the spray drying process for which the rate based models were established (Blei 2005).

4.1.4 Models based on the application of Computational Fluid Dynamics (CFD):

Since the next chapters describe extensively the application of Computational Fluid Dynamics (CFD) in the spray drying simulation, only a brief summary about the CFD models is discussed here.

Computational fluid dynamics (CFD) discusses the issue of “how the differential equations governing the transport of mass, momentum, and energy in the moving fluids can be solved by the numerical methods”. The CFD activity emerged and got superiority with the availability of the computers in the early 1960s. Today, the CFD has the extensive applications in the basic and practical research especially in the simulation of environmental and geophysical phenomena and in the designing of engineering equipment. Since the early 1970s that the commercial software packages (or computer codes) are available, the CFD has become an important component of the engineering

practice and applied research in the industrial, defense, and environmental organizations.
(Date 2005)

The general process for performing a CFD analysis can be outlined in the three steps as following:

4.1.4.1 STEP ONE: PRE-PROCESSING

It consists of following stages;

A: Formulate the Flow Problem

The first step of the analysis process is to formulate the flow problem in which some subjects such as the aim of the analysis, the best way to achieve those aims, the geometry of the problem and its dimensionality (1D, quasi-1D, 2D, axisymmetric, 3D), the operating conditions (steady or unsteady, laminar or turbulent), the number of phases and the appropriate method for modelling of each phase should be considered.

B: Model the Geometry and Flow Domain

The problem should be related to a geometrical dimension for identifying the fluid domain of interest. This generally involves the modelling of geometry (physical bounds) using a CAD software package such as ICEM CFD, Gambit, etc.

C: Establish the Boundary and Initial Conditions

After definition of the flow domain, the physical conditions governing the boundaries of flow domain should be specified. The boundary conditions are one of the most important factors which remarkably affect the final results of a CFD calculation. Besides, the proper definition of initial conditions accelerates the convergence of final flow field solution and leads obtaining the final results faster (NASA Portal 2008).

D: Generate the Grid

In a CFD calculation, the flow domain should be divided into a number of smaller, non-overlapping subdomains in order to solve the transport equations within the generated geometry domain. This leads to the generation of the grid (or mesh) of cells (elements or control volumes) overlaying the whole domain geometry. The essential fluid flows that are described in each of these cells are solved numerically so that the discrete value of the flow properties such as the velocity, temperature, pressure, and the other desired transport

parameters are calculated. This results in the CFD solution of the flow problem. The accuracy of a CFD solution is significantly affected by the numbers of cells in the mesh within the computational domain (Tu *et al.* 2012). The grid has to satisfy some quality criteria as defined by the measures of orthogonality (especially at the boundaries), the relative grid spacing (15% to 20% stretching is considered as a maximum value), the grid skewness, etc. (NASA Portal 2008).

4.1.4.2 STEP TWO: SOLVER

The numerical approaches which form the basis of the solvers accomplish the following steps:

A: Approximation of the unknown flow variables by means of the simple functions.

B: Discretization by substitution of the approximations into the governing flow equations as well as the subsequent mathematical manipulations.

C: Solution of the algebraic equations (Versteeg and Malalasekera 1995).

There are four different approaches for the numerical solution of governing equations including the finite difference, finite volume, finite element and spectral approach. The main differences between these four distinct approaches are related to the ways through which the flow variables are approximated (i.e. the discretization procedures).

4.1.4.2.1 Finite difference approach:

Finite difference methods describe the unknowns variable (ϕ) of the flow problem using the point samples at the node points of a grid of co-ordinate lines. The finite difference approximations of the derivatives of ϕ (general flow variable) in terms of the point samples of ϕ at each grid point and its immediate neighbors are often generated by the truncated Taylor series expansions. The derivatives existed in the governing equations are substituted by the finite difference approximations to obtain an algebraic equation for the values of ϕ at each grid point (Versteeg and Malalasekera 1995).

4.1.4.2.2 Finite Element approach:

Finite element methods describe the local variations of the unknown flow variables (ϕ) using the simple piecewise functions (e.g. linear or quadratic) which are valid on elements. The governing equations are precisely satisfied by the exact solution ϕ . If the piecewise approximating functions for ϕ are replaced into the equation, it does not hold exactly and a residual is defined to measure the errors. Later on, the residuals (and

therefore the errors) are minimized by multiplying them by a set of weighting functions and integrating. Finally, a set of algebraic equations for the unknown coefficients of the approximating functions are achieved (Versteeg and Malalasekera 1995).

4.1.4.2.3 Spectral approach

Truncated Fourier series or series of Chebyshev polynomials are used to generate the approximation of the unknowns in the spectral methods. Contrary to the finite difference or finite element method in which the approximations are local, in this approach the approximations are valid throughout the whole computational domain. The constraint which provides the algebraic equations for the coefficients of the Fourier or Chebyshev series is obtained by a weighted residuals concept similar to the finite element approach or by establishing the approximate function coincide with the exact solution at a number of grid points (Versteeg and Malalasekera 1995).

4.1.4.2.4 The finite volume approach:

Finite volume approach, which has been used at the present work, was originally established as a particular finite difference formulation and is the most well-established and thoroughly validated general purpose CFD technique. Hence, most of the commercial CFD software in the fluid mechanics field such as PHOENICS, FLUENT, FLOW3D and STAR-CD are developed based on this method.

The numerical algorithm in this approach contains the following steps:

- Integration of the governing equations of the fluid flow over all the (finite) control volumes of the solution domain.
- Discretization; involves the replacement of a variety of finite-difference-type approximations for the terms in the integrated equation representing the fluid flow such as the convection, diffusion and sources. This procedure transforms the integral equations into a system of algebraic equations.
- Solution of the algebraic equations by using an iterative method.

The integration of the governing equations over each finite control volume distinguishes the finite volume approach from all the other approaches. The resulting statements express the conservation of relevant properties for each finite size cell. The conservation of a general flow variable ϕ , for example a velocity component or enthalpy, within a finite

control volume can be expressed as a balance between the various processes tending to increase or decrease that variable (Versteeg and Malalasekera 1995). In other words;

$$\left(\begin{array}{c} \text{Rate of change} \\ \text{of } \phi \text{ in the} \\ \text{control volume} \\ \text{with respect to} \\ \text{time} \end{array} \right) = \left(\begin{array}{c} \text{Net rate of} \\ \text{increase of } \phi \text{ due} \\ \text{to convection} \\ \text{into the control} \\ \text{volume} \end{array} \right) +$$

$$\left(\begin{array}{c} \text{Net rate of} \\ \text{increase of } \phi \\ \text{due to diffusion} \\ \text{into the control} \\ \text{volume} \end{array} \right) + \left(\begin{array}{c} \text{Net rate of} \\ \text{creation of } \phi \\ \text{inside the} \\ \text{control volume} \end{array} \right)$$

The CFD codes comprise the discretization techniques appropriate for treatment of the main transport phenomena including the diffusion (transport due to the variations of ϕ from point to point), the convection (transport due to the fluid flow), the source terms (associated with the creation or destruction of ϕ) and the rate of change with respect to time. Furthermore, the underlying physical phenomena are non-linear and complex, and hence, an iterative solution approach is required. The most popular solution procedures are the TDMA line-by-line solver of the algebraic equations and the SIMPLE algorithm to establish correct linkage between the pressure and velocity (Versteeg and Malalasekera 1995).

4.1.4.3 STEP THREE: POST-PROCESSING

Analyzing of the simulation results will be done at this stage through the extracting and visualization of the desired properties of continuous and dispersed phase (velocity, temperature, concentration and etc.). Then the predicted results are compared with the available experimental data in order to assess the validity of modelling results.

4.2 Previous studies about CFD modelling of spray drying

Spray drying technology has many applications in the pharmaceutical, dairy and chemical industries for producing the detergents, coffee, milk powder, etc. But the complex interaction of the dispersed phase (droplets, particles) and continuous phase (drying gas) in this process caused the design of spray dryers to be difficult. Hence, due to the advantages of the CFD technique, this technique is the best option for prediction of the operation of this complicated process.

Marshall and Seltzer (1950) and Miesse et al (1957) were the first who tried to describe the spray drying process mathematically by the simple models in order to understand the mechanism of this process. Nevertheless, the main progress in this field occurred in 1970s when the principles of mass, momentum and heat balance between the continuous and dispersed phases were formulated by Parti and Palancz (1974) and when Katta and Gauvin (1975) developed an experimental-based model in which the effect of extension of spray and the non-uniformity of atomization were considered.

However, the most significant progress on the modelling of spray drying process occurred when Crowe *et al.* (1977) introduced the Particle Source in Cell (PSI-Cell) method in which the continuity and Navier-Stokes equations are solved for the continuous (gas) phase and the droplets/particles were considered as the sources of mass, momentum and energy to the gas phase. In 1980, by using the CFD and applying the PSI-cell model Crowe successfully simulated a co-current spray drying system.

Oakley *et al.* (1988) applied the CFD technique to predict the performance of a co-current spray dryer. In their work the changes of gas flow pattern in the drying tower were predicted when the angle of swirl vanes in the inlet annulus in the top of the dryer around the atomizer was altered from 25° to 30°. The comparison of the predicted results with the

experimental measurements showed that the changes of gas flow pattern were predicted well by their simulation.

Langrish and Zbicinski (1994) by applying a CFD technique simulated the behavior of dispersed phase in a drying chamber to study the wall deposition rate. They investigated that ‘‘how the change of spray cone angle and modification of the air inlet geometry influenced the wall deposition rate’’ and concluded that the turbulence enhancement and a large spray cone angle caused reduction of the wall deposition rate. The acceptable agreement between the predicted results and experimental data proved the potential capacity of their technique.

In order to investigate the sensitivity of simulation to some factors such as ‘‘the number of specified trajectories, different drift correction approaches and different particle dispersion approaches’’ Chen *et al.* (1996) accomplished several numerical predictions of the droplet phase behavior. They tried to improve the accuracy of simulations by using the experimental data which were taken from Sommerfeld’s experiments (Sommerfeld *et al.*, 1993) for defining the initial spray parameters. The droplet phase parameters were determined in the 6 distances from the atomizer and how the different approaches influenced the final predicted results were discussed in their work.

Zbicinski und Li (2006) incorporated an experimentally-determined drying kinetics in the CFD modelling of spray drying process. The drying kinetics applied in their work was developed based on the drying curves which were obtained by the experiments. The predicted results of the continuous and dispersed phase agreed well with the experimental measurements which proved that the incorporation of a realistic experimentally-determined drying model into the CFD calculations, as well as the correct definition of atomization parameters, lead to the reliable modelling of spray drying process.

However, the different kinds of droplets (i.e. different materials) show different behaviors during the drying process and hence the unique drying curve for each kind of droplet will be obtained. Therefore according to the product (material) used in the spray drying process, this curve has to be determined experimentally (for each product) to enable the developing of this kind of drying kinetics. Thus, the dependency of this approach to the experiments puts a limitation on its applicability.

Blei and Sommerfeld (2007) used the Euler-Lagrange approach to simulate a pilot plant spray dryer in which the gas phase was modeled by solving the transport equations for the mass, enthalpy and momentum combined with the k- ϵ model for the turbulence modelling while the dispersed phase calculation was performed by taking the drag, buoyancy and gravity force into account. Moreover, a drying model for the moisture evaporation, a developed collision model and an agglomeration model were also applied in their work in order to perform a 4-way coupled calculation. They concluded that for obtaining an accurate simulation of the spray drying process the consideration of collision model is necessary and without considering the collision model some characteristics of the spray drying process cannot be predicted very well.

Roustapour *et al.* (2009) used the computational fluid dynamics method for the simulation of drying of the lime juice in a drying chamber. A one-way coupling calculation was considered in this work to simulate the behavior of the continuous and discrete phase (lime juice droplets). They determined the drying kinetics of the lime juice by combination of the experimental and numerical results. In the first step, the variation of moisture content of the lime juice droplets was determined by the sampling of droplets along the length of dryer and then by using the numerical simulation the air flow pattern, the droplets distribution and their evaporation in the spray dryer were estimated. They found the significant effect of the droplets/particles size on the mean residence time so that the increase of initial droplets size resulted in the decrease of particles residence time. By estimation of the mean residence time of droplets/particles in the different heights along the drying chamber, the variation of their moisture content with time was determined according to the variation of moisture along the length of dryer (length scale) which was obtained from the experiments. It was concluded that the increase of the drying air temperature caused faster reduction of the droplets diameter and increased the rate of drying as well.

NIS Muhammad (2011) applied the computational fluid dynamics for the modelling of hydrodynamics in a co-current spray dryer to investigate the potential of different turbulence models, i.e. the Standard k- ϵ (SKE), the Realizable k- ϵ (RKE) and the

Detached Eddy Simulation (DES) for predicting the flow pattern in the spray drying process. Multiphase modelling was carried out using the discrete phase modelling to simulate the particles movement inside the drying chamber. The predicted axial velocity, temperature and humidity profile inside the drying chamber were found to be in good agreement with the experimental data for all applied turbulence models. However, the DES model provided the more accurate predictions compared to the other models tested in this work which demonstrates the great potential of this model for predicting the flow pattern in a co-current spray dryer.

A steady state, 3D, multiphase CFD modelling of a pilot-plant counter-current spray drying tower was performed by Ali *et al.* (2013) to study the drying of slurry for producing the detergent powder. They used the commercial software package 'Fluent' to solve the mass, momentum and heat transfer between the drying gas and droplets/particles and coupling of these two phases was achieved by the Eulerian-Lagrangian approach. They used the Reynolds-Stress Model (RSM) for the turbulence modelling and considered the particle-wall interaction by specifying the coefficient of restitution as a function of moisture content. They incorporated a semi-empirical drying model in the 'Fluent' using the User-Defined Functions (UDF). The obtained results showed that the particle-wall interaction is one of the main factors which leads to the significant changes in the velocity, temperature and moisture profile of the gas and droplet phase. The comparison of the predicted results with the measurements showed that the heat transfer between two phases is under-predicted and they referred this weakness to the simplifying assumptions supposed in their simulation such as the neglecting of coalescence and agglomeration and concluded that for a more reliable simulation a good estimation of the initial droplets size distribution, as well as the change of droplets/particles size due to the particle-particle interactions, should be considered.

Summarizing the literature review, although the CFD techniques provided the good insights about the spray drying process but still some issues are remained which should be solved for a more accurate simulation of this process. The future works have to focus on the developing of the reliable drying models, collision models, agglomeration models and

the agglomerate breakup models to enable the successful CFD modelling of the complex mechanisms occurred in the spray drying process.

5. Modelling Procedure

5.1 Basics of the turbulent reacting multiphase flows

The numerical approaches for solving the multi-phase flows (which the spray drying process belongs to them) can be generally categorized into three different approaches:

- The Probability Density Function (PDF) approach
- The two-fluid approach
- The Eulerian-Lagrangian approach

5.1.1 PDF approach

In this approach the dispersed phase is considered as a cloud of material elements and the equations which describe the behavior of this phase are driven using a probability function based on the mass, velocity, and temperature of dispersed phase and the species concentration, velocity and temperature of continuous phase seen by the dispersed phase.

The PDF evolution in the phase space and the unsteady evolution and convection in the physical space are described by the joint-PDF transport equation. For obtaining these equations some conditional average over the phase space, because of the phase change, heat transfer and dispersion of dispersed phase and the mass, momentum and heat transport of continuous phase seen by the dispersed phase, have to be accomplished. The Finite Volume method is used to solve the continuous phase equations along with the turbulence equations which are Reynolds time-averaged in the Eulerian coordinate while the Lagrangian approach in the phase space is used to solve the PDF model of dispersed phase (Liu *et al.* 2002, Chrigui 2005).

Throughout the PDF simulation, the droplets/particles are considered to be uniformly distributed in the physical computational domain and a random function operation for the arrangement of dispersed phase has to be accomplished, so that during all iterations the number of droplets/particles in each cell remains nearly constant. There are the random-set values of the spatial position, diameter, velocity and temperature for each droplet/particle and the continuous phase properties seen by it. The changes of these random-set values during the simulation are calculated by solving the stochastic equations in a certain time step (Simonin 1996). Furthermore, using an ensemble average of the

numbers of particles/droplets existing in each cell, the particle/droplet-averaged properties will be obtained (Chrigui 2005).

Compared to the Eulerian-Lagrangian approach that provides a little information in the low droplet/particle concentration regions, the PDF approach gives the more detailed and accurate droplets/particles statistics at all regions within the flow field.

In comparison with the Eulerian-Eulerian approach, the PDF approach is able to easily treat the droplets/particles with different initial sizes, velocities and temperatures. Moreover, this approach has the ability to provide the more accurate particle/droplet statistics when it is interested to find out more about the droplets/particles behavior in the low concentration regions.

The main disadvantage of the PDF approach is that the computation time in this approach is much more than the two other approaches. In addition, in this approach the full-droplet/particle PDF equations should be solved even in the low droplets/particles concentration regions which due to the little influence, their effect on the overall solution can be neglected and also leads to the unnecessary extra expenses and effort (Chrigui 2005).

5.1.2 Eulerian-Eulerian (two-fluid) approach

This approach which has been widely used in the multi-phase flows simulations considers both the dispersed and the gas phase as the continuous phase and the behavior of the both phases is modeled by using the Navier-Stokes equations.

When the volume fraction of the both phases is larger than 10^{-3} (i.e. dense two-phase flow) considering the dispersed phase as a continuous phase can be a relatively-realistic assumption and in such a case the application of this approach is recommended.

Some advantages of this approach can be mentioned as:

- It needs less computational costs compared to the PDF and Eulerian-Lagrangian approach.
- Even the multiple dispersed phases are treated like the continuous phase and have the similar transport equations which cause the implementation to be not very complicated.

- Considering the dispersed phase as a continuous phase causes this approach to be more time-effective and makes the parallel numerical computation possible by assigning the fluid-blocks to the CPU and not particles/droplets (Simonin 1996).

And some disadvantages of this approach are:

- In this approach the modelling of the turbulent diffusion of dispersed phase and the momentum transfer between the phases are difficult.
- It is appropriate approach only for the dense multi-phase flows, and moreover, all phases should be assumed to be incompressible.
- If there are phase transitions (e.g. evaporation) in the multiphase flows, the extra modelling effort is needed for the calculation of pressure field.
- Consideration of the particle-wall interaction, boundary conditions and fluctuations of the dispersed phase are difficult in this approach.
- In the case of poly-dispersion in the size of spray, each class of particles/droplets diameter should be treated as a separate phase which causes the high computational costs (FLUENT Manual 2001, Chrigui 2005).

5.1.3 Eulerian-Lagrangian approach

As this approach is used at the present work and in the next part is discussed in detail, only a brief explanation of this approach is presented here.

The third approach for the two-phase flows simulation is the Eulerian Lagrangian approach that considers the fluid as a continuum and the particles/droplets as the discrete entities. The solution procedure for the transport problem in the most of Eulerian-Lagrangian methods are divided into 2 distinct steps (hybrid methods).

At the first step the transport equations (i.e. The Navier-Stokes equations, enthalpy, continuity, etc.) are solved over a fixed computational grid (Eulerian framework) to model the behavior of continuous phase while at the second step the Lagrangian equations are used to describe the behavior of dispersed phase and tracking of the particles, droplets or bubbles within the flow field is carried out based on a force balance on each entity (Kohnen 1994). The source terms calculated for each variable of dispersed phase at each control volume of the flow domain are added to the transport equations of continuous

phase to establish the coupling procedure. The solution procedure is repeated between these two mentioned steps until the convergence criteria of coupling between two phases are achieved (Chrigui 2005).

In the Eulerian- Lagrangian approach the change of continuous phase volume, caused by the presence of droplets/particles, is most often overlooked. Additionally, in order to decrease the computational time a numerical parcel in this approach represents a set of real particles/droplets and not only one real particle/droplet which may result in the poor numerical predictions due to the poor statistics (Kohnen 1998). Different spatial interpolation methods such as linear, quadratic, cubic, spline, etc. are used to obtain the fluid properties on the parcel location which (these interpolation methods) can influence the numerical results provided by this approach as well.

Compared to the Eulerian- Eulerian approach, the parallel numerical computation is more difficult in this approach because the particle/droplet may move throughout all blocks of computational domain (Sommerfeld 1996, Chrigui 2005).

Nevertheless, the modelling of interaction between the continuous and dispersed phase, droplet evaporation, agglomeration, collision, wall interaction, etc. make physically more sense in the Eulerian- Lagrangian approach and this is the fundamental advantage of this approach which made it the most popular approach for the modelling of multiphase flows.

5.2 Euler-Lagrange Approach: An Extended Model for Spray Dryer Simulation

In the following chapter the Euler-Lagrange approach, as applied in the present study for the CFD calculation of a spray dryer, is discussed in more detail.

5.2.1 Fluid Phase Modelling

The well-known Reynolds-averaged Navier-Stokes equations are solved to determine the velocity field of drying gas within the spray dryer and for considering the turbulence of gas phase the standard k- ϵ model introduced by Launder and Spalding (1974) is applied in the present study.

The general transport equation used for the calculation of flow problem is represented as:

$$\frac{\partial}{\partial x}(\rho u \phi) + \frac{\partial}{\partial y}(\rho v \phi) + \frac{\partial}{\partial z}(\rho w \phi) - \frac{\partial}{\partial x} \left(\Gamma \frac{\partial \phi}{\partial x} \right) - \frac{\partial}{\partial y} \left(\Gamma \frac{\partial \phi}{\partial y} \right) - \frac{\partial}{\partial z} \left(\Gamma \frac{\partial \phi}{\partial z} \right) = S_{\phi} + S_{\phi,p} + S_{\phi,p,ev} \quad (5.1)$$

x, y and z are the coordinates of Cartesian framework, u, v, w are the three velocity components, ρ is the fluid density and ϕ represents the gas flow variable considered (see Table 5.1). S_{ϕ} , $S_{\phi,p}$ and $S_{\phi,p,ev}$ represent the source terms of gas phase, non-evaporating particles and evaporating droplets respectively and depending on the considered variable, Γ indicates the effective diffusion coefficient. The diffusion coefficients and the source terms as were used in this work can be found in Table 5.1 and Table 5.2.

How the general transport equation is derived from the Navier-Stokes equations and the rules of mass and heat conservation can be found in the standard CFD literature (Versteeg and Malalasekera 1995, Anderson 1995).

Highly inaccurate results are achieved for the gas flow patterns and droplets/particles properties if the droplets/particles source terms are not considered in the spray drying simulation (Blei and Sommerfeld 2007). Therefore, a two-way coupling procedure for considering the mass, momentum and thermal energy transfer between the continuous (gas) and dispersed phase (droplet/particle) is applied in the present study.

Table 5.2 represents the dispersed phase source terms of the general transport equation in which n_p is the number of the considered particles, $V_{i,j,k}$ is the volume of the cell, Δt the time step size, $u_{p,i}$ the particle's velocity components, $c_{p,v}$ the specific heat capacity of the particle material, h_v the specific heat of evaporation, $\dot{m}_{p,ev}$ the evaporated mass flow rate, \mathbf{g}_i the gravitation vector, $S_{p,ev}$ the volume-averaged mass transfer caused by the evaporation (Chrigui 2005), μ and μ_t are the molecular and turbulent dynamic viscosity of the fluid and $c_{\epsilon,3}^{k-\epsilon}$ is a constant value equal to 1.1 as Squires and Eaton (1992) suggested.

There is no analytical solution for the general transport equation for a real three-dimensional flow problem and hence this equation should be solved by the numerical

techniques. The numerical procedure for solving this equation is discussed in the following part.

Due to the advantages of the finite volume method in the field of fluid mechanics, this technique is applied in the present work. As described in the previous chapter, this means that the flow domain should be divided into a number of smaller subdomains (i.e. control volumes) and for each of these small control volumes the partial differential equations describing the flow behavior should be satisfied. Thereupon, the system of non-linear differential equations (governing equations) by substitution of the finite-volume-type approximations is converted into a system of algebraic equations which can be solved by the iterative methods. The more detailed description of this procedure can be found in the standard CFD literature (Fastest-3D, TU Darmstadt, Prof. Schäfer, 2004, Patankar 1980, Versteeg and Malalasekera 1995).

The system of the obtained algebraic equations is solved by a successive approach including the inner and outer solution sequences. The Inner iteration is used to the solution of the system of linear equations for each dependent variable (Azevedo 1988). The “Strongly Implicit Procedure” method developed by Stone (1968) is applied in the present work for this purpose. The more detailed explanation of this method can be found in the literature (Stone 1968).

The outer iteration is applied to the solution of the equations of mass, pressure, momentum and other desired variables, which are solved in an iterative method to fulfill the conservation laws and to meet the boundary conditions (Azevedo 1988) as well. For this purpose, an improved SIMPLE (i.e. Semi-Implicit-Method for Pressure Linked Equations) method (Patankar and Spalding 1972) developed by of Peric (1985) is applied. The more detailed description of the SIMPLE method can be found in the standard CFD literature (Patankar and Spalding 1972, Peric 1985).

Table 5.1: Diffusion terms and continuous phase source terms of the general transport equation, modified for the k - ε turbulence model.

ϕ	Γ	S_ϕ
1	0	0
u_i	$\mu + \mu_t$	$\frac{\partial}{\partial x_j} \left(\Gamma_{u_i} \frac{\partial u_j}{\partial x_i} \right) - \frac{\partial p}{\partial x_i} + \rho g_i$
$c_p T$	$\frac{\mu}{Pr} + \frac{\mu_t}{Pr_t}$	0
Y	$\frac{\mu}{Sc} + \frac{\mu_t}{Sc_t}$	0
k	$\mu + \frac{\mu_t}{\sigma_k}$	$G_k - \rho \varepsilon$
ε	$\mu + \frac{\mu_t}{\sigma_\varepsilon}$	$\frac{\varepsilon}{k} (c_1 G_k - c_2 \rho \varepsilon)$
$G_k = \mu_t \left(\frac{\partial u_i}{\partial x_j} + \frac{\partial u_j}{\partial x_i} \right) \frac{\partial u_i}{\partial x_j}$		

Table 5.2: Dispersed phase source terms of the general transport equation, modified for the k - ε turbulence model.

ϕ	$S_{\phi,p}$	$S_{\phi,p,ev}$
1	0	$-\sum_p \frac{\dot{m}_{p,ev} \cdot n_p}{V_{i,j,k}}$
u_i	$-\sum_p \frac{\dot{m}_p \cdot n_p}{V_{i,j,k}} \cdot [(u_{p,i}^{t+\Delta t} - u_{p,i}^t) - g_i \cdot \Delta t]$	$\sum_p \frac{\dot{m}_{p,ev} \cdot n_p}{V_{i,j,k}} u_{p,i}$
$c_p T$	$-\sum_p \frac{\dot{m}_p \cdot n_p}{V_{i,j,k}} \cdot c_p \cdot (T_p^{t+\Delta t} - T_p^t)$	$\sum_p \frac{\dot{m}_{p,ev} \cdot n_p}{V_{i,j,k}} \cdot (c_{p,v} \cdot T_p - h_v)$
Y	0	$\sum_p \frac{\dot{m}_{p,ev} \cdot n_p}{V_{i,j,k}}$
k	$\overline{u_i S_{u_i,p}} - \bar{u}_i \cdot \overline{S_{u_i,p}}$	$\overline{u_i S_{u_i,ev}} - \bar{u}_i \cdot \overline{S_{u_i,ev}}$ $+ \frac{1}{2} (\bar{u}_i \bar{u}_i \overline{S_{p,ev}} - \overline{u_i u_i S_{p,ev}})$
ε	$c_{\varepsilon,3}^{k-\varepsilon} \cdot \frac{\varepsilon}{k} \cdot S_{k,p}$	$c_{\varepsilon,3}^{k-\varepsilon} \cdot \frac{\varepsilon}{k} \cdot \overline{S_{k,p,ev}}$

Table 5.3: The constant values and variables given in Table 5.1 and Table 5.2

$\mu_t = c_\mu \rho \cdot \frac{k^2}{\varepsilon}$	$c_\mu = 0.09$	$c_1 = 1.44$	$c_2 = 1.92$	$\sigma_k = 1.0$	$\sigma_\varepsilon = 1.3$
--	----------------	--------------	--------------	------------------	----------------------------

The information about the fluctuation values of the transport variables are lost due to the time-averaging of the system of differential equations, therefore the turbulence models should be applied to balance this loss of information (Blei and Sommerfeld 2007). For this purpose, the standard k- ε turbulence model of Launder and Spalding (1974) is applied in the present work. The complete description of this well-known turbulence model can be found in the standard literature regarding the turbulent flows (McComb 1990, Pope 2000) and thus just a brief discussion about this turbulence model is presented here:

It is a two-equation model consists of the transport of turbulent kinetic energy k and the rate of turbulent dissipation ε . The turbulent kinetic energy is described as:

$$k = \frac{1}{2} \cdot \overline{u'_i u'_i} \quad (5.2)$$

and signifies half of the sum of the Reynolds stress tensor.

The rate of dissipation ε defines the dissipation of turbulent energy by the molecular viscosity. It is a function of the fluctuation velocities u' as:

$$\varepsilon = \frac{\mu}{\rho} \cdot \overline{\frac{\partial u'_i}{\partial x_j} \frac{\partial u'_i}{\partial x_j}} \quad (5.3)$$

Prandtl's eddy-viscosity theory (1945), which relates the turbulent stresses of flow to the deformation velocities, introduced the concepts of eddy-viscosity μ_t and eddy-diffusivity λ_t which both are the characteristics of the flow structure and are not the fluid properties (Blei 2005). These two concepts are defined mathematically as:

$$\mu_t = \rho \cdot c_\mu \cdot \frac{k^2}{\varepsilon} \quad (5.4)$$

$$\lambda_t = \rho \cdot c_p \cdot l_m \cdot l_t \cdot \left| \frac{\partial u}{\partial y} \right| \quad (5.5)$$

l_m and l_t represent the hydrodynamic and thermal mixing length respectively. By the turbulent Prandtl number these parameters are related to each other as:

$$\text{Pr}_t = \frac{\mu_t \cdot c_p}{\lambda_t} = \frac{l_m}{l_t} \quad (5.6)$$

The turbulent Prandtl number values are generally specified experimentally (Eckert and Drake 1987) and as the empirical constants are involved in the transport equations. The transport equations of k and ε can also be found in Table 5.1 and Table 5.2.

5.2.2 Dispersed Phase Modelling

When the particles/droplets are dispersed in a fluid phase, some forces act on the particles/droplets and lead to the particles/droplets motion and their acceleration or deceleration. The forces which act on the particles/droplets can be categorized into two main groups including the fluid dynamic and external-field forces. The fluid-dynamic forces consist of the drag-, Magnus-, Basset-, Saffman-, added mass- and pressure force and the field forces are the magnetic, gravity and electrostatic forces.

Due to this fact that all forces \vec{F}_p can be considered as independent, using the superposition principle to compute the overall force \vec{F}_p acting on a particle/droplet yields the Newton's law of motion as (Blei 2005):

$$m_p \cdot \frac{d\vec{u}_i}{dt} = \vec{F}_p = \sum \vec{F}_i \quad (5.7)$$

Description of the forces acting on a particle/droplet and related resistance coefficients can be found in works of Crowe *et al.* (1998), Sommerfeld (2002) and Sommerfeld *et al.* (2008). As a brief review:

5.2.2.1 Drag Force

The drag force, established due to the presence of fluid flow field around the particle, can be divided into two terms. The first term comes from the shape of particle while the second term describes the friction which the particle experiences. It is estimated that the shape drag contributes around 1/3 to the overall drag force within the Stokes-flow regime. The particle Reynolds number is usually a criterion for describing the different regimes of drag force (Blei 2005).

A laminar flow is observed around a spherical particle when the particle Reynolds number is less than 0.5. In such cases, by integrating the pressure field and shear stress across the particle surface the corresponding drag force can be calculated as:

$$F_{\text{stokes}} = 3 \cdot \pi \cdot \mu_f \cdot d_p \cdot \overline{u_{rel}} \quad (5.8)$$

There is no analytic solution for the higher Reynolds numbers, therefore the interpolation functions of the drag force versus the Reynolds number are derived using the experimental data (Blei 2005). Different approximation functions for this force are proposed and can be found in the literature (Schmidt and Mueller 1997). In these

approaches the drag coefficient c_d according to the experimental data is introduced and the drag force is defined as:

$$\overrightarrow{F}_{\text{Drag}} = \frac{3}{4} \cdot m_p \cdot \frac{\rho_f}{\rho_p \cdot d_p} \cdot c_d \cdot (\overrightarrow{u}_f - \overrightarrow{u}_p) \cdot |\overrightarrow{u}_f - \overrightarrow{u}_p| \quad (5.9)$$

A relationship for the drag coefficient which is commonly used for the spherical particles is that of Schiller and Naumann (1933) as:

$$c_d = \frac{24}{\text{Re}_p} \cdot (1 + 0.15\text{Re}_p^{.687}) \quad \text{For } \text{Re}_p < 800 \quad (5.10)$$

Compared to the experimental data, the deviation of this relationship is less than 6%. In the severely turbulent regimes (above the Reynolds number of 800) the role of friction can be neglected for the drag force. In such cases, c_d is usually considered to be a constant value equal to 0.445 in agreement with the experimental data (Blei and Sommerfeld 2007).

5.2.2.2 Virtual Mass Force

If a particle is accelerated through a fluid, there is a corresponding acceleration of the surrounding fluid as well. ‘The virtual mass effect’ relates the force required to overcome the inertia of surrounding fluid (Crowe *et al.* 1998). This force is described by Crowe *et al.* (1998) as:

$$\overrightarrow{F}_{\text{vm}} = m_p \cdot c_{\text{vm}} \cdot \frac{\rho_f}{\rho_p} \cdot \left(\frac{D\overrightarrow{u}_f}{Dt} - \frac{d\overrightarrow{u}_p}{dt} \right) \quad (5.11)$$

In order to extend the validity of this relationship to the higher Reynolds numbers the coefficient c_{vm} was introduced. A constant value of 0.5 has been suggested by Magnaudet (1997) for this coefficient (Blei 2005).

5.2.2.3 Basset Force

The Basset term accounts for the viscous effects and addresses the temporal delay in the boundary layer development as the relative velocity changes with time (i.e. accelerations or decelerations of the particle and flow). When the density ratio $\frac{\rho_f}{\rho_p}$ is very small, this force can be considered insignificant and therefore can be neglected. In fact, this force

contains an integral term along the entire particle trajectory which makes the consideration of this force very time-consuming in the numerical simulation.

5.2.2.4 Forces caused by pressure gradients in the fluid

Pressure gradients of the fluid field can generate the additional forces acting on the particle. Supposing that the shear across the surface of particle is constant, the force can be expressed as (Crowe *et al.* 1998):

$$\vec{F}_p = m_p \cdot \frac{\rho_f}{\rho_p} \cdot \frac{d\vec{u}_f}{dt} - m_p \cdot \frac{\rho_f}{\rho_p} \cdot \vec{g} \quad (5.12)$$

The first term of this equation is usually named the pressure force and the second term is named the Archimedes buoyancy force.

5.2.2.5 Magnus Force

If a particle rotates, the pressure differences observed on the surface of particle can generate the additional forces. The following equation suggested by Sommerfeld (2002) can be used to calculate the Magnus force:

$$\vec{F}_M = \frac{\pi}{8} \cdot d_p^2 \cdot \rho_p \cdot c_M \cdot \frac{|\vec{u}_{rel}|}{|\vec{\Omega}_{rel}|} \cdot (\vec{u}_{rel} \times \vec{\Omega}_{rel}) \quad (5.13)$$

Where \vec{u}_{rel} represents the relative velocity vector between the particle and fluid, $\vec{\Omega}_{rel}$ the vector of the relative angular velocity and c_M the associated resistance coefficient (Blei 2005).

5.2.2.6 Saffman Lift Force

The non-uniform pressure distribution across the particle surface within a shear flow generates the saffman (shear) force which acts in a direction perpendicular to the flow gradient (Blei 2005). Mei (1992) proposed the following equation to express this force:

$$\vec{F}_s = 1.615 \cdot d_p^2 \cdot \sqrt{\rho_f \cdot \mu_f} \cdot c_s \cdot \frac{[\vec{u}_{rel} \times \vec{\omega}_f]}{\sqrt{|\vec{\omega}_f|}} \quad (5.14)$$

Where $\vec{\omega}_f$ is the rotational velocity of the fluid and c_s represents the resistance coefficient for the higher Reynolds number values proposed by Mei (1992).

5.2.2.7 Gravitational Force

This force is generated by the gravitational acceleration (g) and can be described as:

$$\vec{F}_g = m_p \cdot \vec{g} \quad (5.15)$$

The importance of the aforementioned forces is dependent on the simulation condition and regarding the simulation condition some of them lose their importance and therefore can be neglected. At the present work which consists of the droplets in the size range of microns moving in a drying chamber, the drag force (having the highest importance), the gravitational force as well as the buoyancy force are taken into account.

5.3 Particle Tracking

Using the Newton's law of motion the change of the particle/droplet location and the change of the particle/droplet velocity can be described as:

$$\frac{dx_{p,i}}{dt} = u_{p,i} \quad (5.16)$$

$$m_p \frac{du_{p,i}}{dt} = \frac{3}{4} m_p \frac{\rho_f}{\rho_p d_p} c_d (u_i - u_{p,i}) |\vec{u} - \vec{u}_p| + m_p g_i \left(1 - \frac{\rho_f}{\rho_p}\right) \quad (5.17a)$$

Furthermore, based on the drying stage that the droplet belongs to it (see chapter 3), the change of droplet temperature is calculated using:

$$\frac{\partial T}{\partial t} = \frac{\alpha}{r^2} \left[\frac{\partial}{\partial r} \left(r^2 \frac{\partial T}{\partial r} \right) \right] \quad (5.17b)$$

$$\text{or} \quad 2\pi R \text{Nu} \lambda_{\text{air}} (T_\infty - T_s) = m C_v \frac{dT}{dt} + L \frac{dm}{dt} \quad (5.17c)$$

$$\text{or} \quad \frac{dT}{dt} = \frac{r}{R_v} \frac{dR_v}{dt} \frac{\partial T}{\partial r} + \frac{\alpha}{r^2} \left[\frac{\partial}{\partial r} \left(r^2 \frac{\partial T}{\partial r} \right) \right] \quad (5.17d)$$

and the change of droplet radius is calculated using:

$$\frac{dR}{dt} = - \frac{1}{\rho_d 4 \pi R^2} \frac{dm}{dt} \quad (5.17e)$$

In the present study the drag, gravity and buoyancy are considered as the forces acting on the particles. The standard correlation for a sphere introduced by Schiller and Naumann (1993) is used to calculate the drag coefficient c_d as:

$$c_d = \frac{24}{\text{Re}_p} (1 + .15 \text{Re}_p^{.687}) \quad \text{Re}_p < 800 \quad (5.18)$$

$$c_d = .44 \quad \text{Re}_p \geq 800 \quad (5.19)$$

Calculation of the particle/droplet trajectory requires the instantaneous fluid velocity to be determined throughout the particle trajectory (Blei 2005). The Reynolds averaging of the

fluid turbulence provides the transport equations for the mean variables and hence the detailed information about the instantaneous fluid properties is missing. In order to reconstruct the instantaneous fluid velocity seen by the particles/droplets in addition to mean part (which are attained from the continuous phase computation and interpolated at particle/droplet location), the fluctuating components should be modeled using the turbulent dispersion models (Lain 2010).

5.4 Dispersion modelling

The dispersion describes the influence of the fluid (continuous phase) turbulence on the particles/droplets distribution. The interaction of particles with the turbulent eddies causes the preferential concentration effects which may change severely the mass flow distribution of the dispersed phase. Subsequently, these effects can enhance the inhomogeneity of the species (e.g. vapor concentration) (Chrighui 2005). In order to consider this phenomenon, a stochastic Lagrangian process can be used to produce the instantaneous fluid velocity based on the computed fluid turbulent variables. For this purpose, the so-called standard dispersion model introduced by Sommerfeld et al (1993) is applied in the frame of this study to taking this phenomenon into account.

In this approach the fluctuating fluid velocity seen by the particle/droplet is consist of a random contribution of the local fluid fluctuation velocity and a term that stands for the correlation of the fluid fluctuation at the current particle/droplet location with that of the particle/droplet location one time step earlier (Blei 2005). This can be described by the following equation as:

$$u_{i,n+1}^f = R_{p,u_i}(\Delta t, \Delta r) \cdot u_{i,n}^f + \sigma_{u_i}^f \cdot \xi_i \cdot \sqrt{1 - R_{p,u_i}^2(\Delta t, \Delta r)} \quad (5.20)$$

Where, ξ_i represents a vector of three independent Gaussian random numbers with a mean value of zero and a standard deviation of one. Using these values, the local fluid rms values σ_{u_i} and the correlation term $R_{p,u_i}(\Delta t, \Delta r)$, the random contributions for the three velocity directions ($i=1, 2, 3$) are composed. Furthermore, the correlation term includes an Eulerian and Lagrangian part as:

$$R_{p,u_i}(\Delta t, \Delta r) = R_{E,ij}(\Delta r) \times R_L(\Delta t) \quad (5.21)$$

In this approach, the Lagrangian term is described by means of the Lagrangian time scale T_L and the current time step of tracking procedure:

$$R_L(\Delta t) = \exp\left(-\frac{\Delta t}{T_L}\right) \quad (5.22a) \quad T_L = \frac{2}{3} C_T \cdot \frac{k}{\varepsilon} \quad (5.22b)$$

According to the research by Sommerfeld (1996) C_T is set to 0.24 (Stübing 2014).

The Eulerian part of the correlation term can be determined by applying the longitudinal and transversal correlation functions $f(\Delta r)$ and $g(\Delta r)$ (Karmann and Horwarth 1938) as:

$$R_{E,ij}(\Delta r) = \{f(\Delta r) - g(\Delta r)\} \cdot \frac{\Delta r_i \Delta r_j}{\Delta r^2} + g(\Delta r) \cdot \delta_{ij} \quad (5.23)$$

Where:

$$f(\Delta r) = \exp\left(-\frac{\Delta r}{L_{E,i}}\right) \quad (5.24)$$

$$g(\Delta r) = \left(1 - \frac{\Delta r}{2L_{E,i}}\right) \exp\left(-\frac{\Delta r}{L_{E,i}}\right) \quad (5.25)$$

The integral length scales $L_{E,i}$ are expressed as (Sommerfeld 2001):

$$L_{E,x} = 3 \cdot T_L \cdot \sqrt{\frac{2}{3}k} \quad (5.26a) \quad \text{and} \quad L_{E,y} = L_{E,z} = 0.5L_{E,x} \quad (5.26b)$$

Here, $L_{E,x}$ represents the length scale in the flow direction while the other two are the lateral components (Blei 2005).

5.5 Turbulence modulation modelling

The presence of dispersed phase may influence the turbulence of continuous phase especially in the dense multi-phase flows in which the particle/droplet concentration is high. The particles/droplets dispersed in a fluid phase can lead to the distortion of streamlines so that the velocity gradients are modified due to the shear forces existed between the different phases. In the opposite way, the wakes generated behind the particles/droplets yield a damping effect of the drag force on the dispersed phase. This phenomenon, called turbulence modulation, is very complicated and is not completely understood up to now (Chrigui 2005).

The effect of dispersed phase on the fluid motion can be considered as an additional force exerted on the gas (continuous) phase if the density of dispersed phase is much larger than that of the gas phase. The momentum transfer from the dispersed phase to the continuous

phase can be taken into account by adding the reaction force against the surface force acting on the particle/droplet to the Navier-Stokes equation (Eq. (5.1)). This approach is called source terms approach or particle-source-in-cell (PSI-Cell) model introduced by Crowe *et al.* (1977). Crowe proposed many models for the modelling of turbulence modulation in the multi-phase flows. In his last model (Crowe 2000) based on the energy balance and experimental observations the correlations describing the source terms for the $k - \varepsilon$ turbulence model in the framework of Eulerian-Eulerian approach was proposed (Chrigui 2005). Later on, this correlation has been transformed to the Eulerian-Lagrangian notation by Lain *et al.* (2000). The detail of this model which is used in the present work can be found in the work of Lain *et al.* (2000).

5.6 Two-way Coupling Procedure

Considering the effect of dispersed phase on the continuous phase requires a consecutive solution of the Eulerian and Lagrangian part. When a converged solution of the single phase flow (i.e. the gas phase without consideration of the droplet phase) is achieved, the particle/droplet tracking is carried out and subsequently the drying model described in chapter 3 is applied to consider the exchange of heat and mass between the continuous (gas) and dispersed (droplet) phase and then the dispersed (droplet) phase properties and the source terms are sampled for every control volume. After that, again the calculation of continuous phase is accomplished by taking the dispersed (droplet) phase source terms into account (Blei 2005, Chrigui 2005). Using the following equation an under-relaxation procedure is applied to improve the numerical stability and prevent the divergence problem:

$$S_{\phi,p}^{\text{new}} = (1 - \gamma) S_{\phi,p}^{\text{old}} + \gamma S_{\phi,p}^{\text{samp}} \quad (5.27)$$

Where $S_{\phi,p}^{\text{new}}$ represents the source terms used to calculate the new flow field, $S_{\phi,p}^{\text{old}}$ the source terms used in the previous Eulerian calculation, and $S_{\phi,p}^{\text{samp}}$ the new source terms sampled in the Lagrangian calculation and γ indicates the under-relaxation factor which varies between zero and one (Kohnen *et al.* 1994, Sommerfeld *et al.* 2008).

When the calculation of continuous (gas) phase by consideration of the source terms is reached to the certain degree of convergence, again the calculation of dispersed phase and the computation of the new source terms are performed. Thereafter, by using the new sampled source terms the continuous phase is again solved and this algorithm continues

repeatedly until the convergence of the Eulerian-Lagrangian coupling procedure is obtained (Blei 2005, Chrighui 2005). The convergence of the Eulerian-Lagrangian system is achieved based on the evolution of a certain reference value (Kohnen *et al.* 1994), for instance the evolution of fluid velocity at a monitoring location (Blei 2005). Figure 5.1 displays the diagram of numerical computing procedure for a 2-way coupled Euler-Lagrange computation as performed in the present study. The experience attained through this study indicated that by applying the under-relaxation factor of 0.2 and the total Eulerian- Lagrangian coupling number of 30 a stable numerical computation and a converged Eulerian-Lagrangian coupling procedure can be achieved.

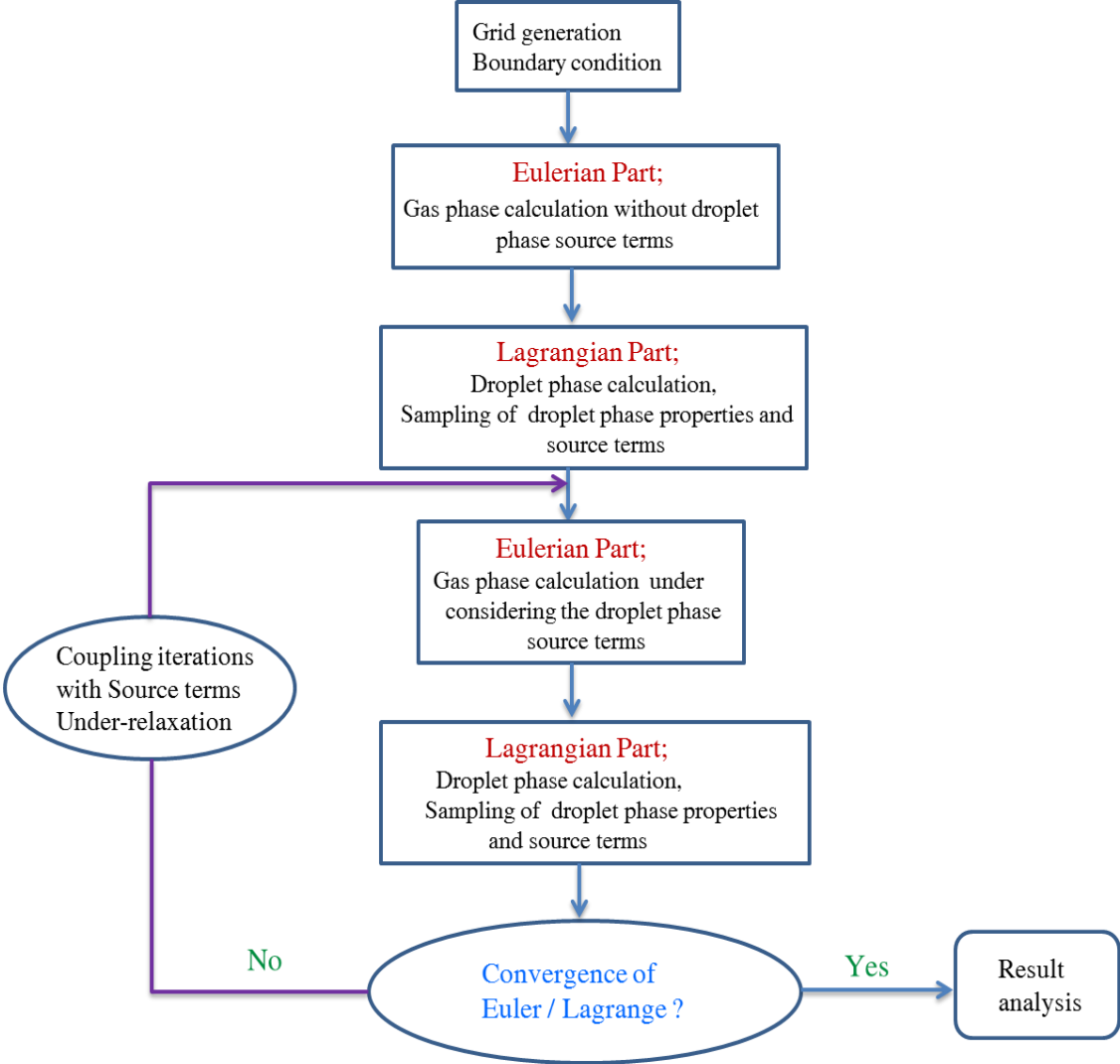


Figure 5.1: Diagram of the numerical computing procedure for a 2-way coupled Euler-Lagrange computation.

5.7 Numerical methodology

The governing equations of the multiphase flows are mainly the ordinary and partial differential equations which cannot be solved by the analytical methods. The development and application of the discretization methods for the systems of ordinary and partial differential equations and transformation of these equations into a system of algebraic equations and solving this system by the computers codes are the only way to make practical applications for these theoretical equations and obtain the usable results.

The following section consists of the explanations about the numerical methods which are used for the gas and dispersed phase and describes the statistical method which is used for the properties sampling as well.

5.7.1 Numerical method for gas phase

Generally, a numerical solution method comprises a mathematical model (governing equations), a discretization method and finite approximation, a numerical grid, a coordinate and basis vector system as well as a solution method (Ferziger and Peric 1999). In this study for the purpose of numerical solution of the governing equations of gas phase, the CFD package of FASTEST-3D (Flow Analysis Solving Transport Equations Simulating Turbulence 3 Dimensional) which was developed initially by INVENT Computing GmbH (Erlangen, Germany) has been used. The features of the numerical solution method as applied in this study are based on the characteristics of FASTEST-3D including:

- Using the Finite volume approach for discretization of the governing equations
- Cartesian coordinate and basis vector system
- Boundary-fitted non-orthogonal block-structured grid with matching interfaces and collocated variable arrangement
- Implicit and semi-implicit temporal and first and second order spatial discretization schemes
- Strongly implicit procedure for the iterative solution of the linearized equation system
- Full geometrical multigrid solver for the convergence acceleration
- Parallelization based on the domain decomposition in space (Chrigui 2005)

In the following part, some features of the numerical solution will be explained.

5.7.2 Features of numerical solution

In the present study, the finite volume method is applied to describe the behavior of continuous (gas) phase and the basis of this method is resolving of the governing equations of continuous (gas) phase in the integral form.

The storage of the flow information of each control volume divides the discretization problem into two different arrangements including collocated grid and staggered grid. The collocated grid is applied in the present work at which the pressure and velocity variables share the same grid and therefore all variables will be stored on the same grid point (i.e. the same control volume is used for all variables) (Ferziger and Peric 1999, Harlow and Welch 1965).

In the frame of the present work, the value of ϕ is approximated using three basic discretization schemes including the Central Differencing Scheme (CDS), Upwind Differencing Scheme (UDS), and Flux Blending scheme (Chrigui 2005).

Contrary to the compressible flows in which the pressure is obtained by the equation of state, in an incompressible flow (the case considered in this study) one does not have any direct equation for the pressure calculation and therefore the continuity equation should be used as an indirect equation for the pressure calculation. This method is called SIMPLE (Semi Implicit Method for Pressure Linked Equation) and is used in the present work.

In the steady calculations, a steady state solution of the governing equation system is required. In such cases either the unsteady terms in the governing equations can be neglected or it is possible to march in time without any requirement to the full satisfaction of equations at each time step.

The iterations, leading to march in time or during the steady calculation, in which the coefficient matrices and source vectors are updated can be named outer iterations to distinguish them from the inner iterations implemented on the system of linear equations for each dependent variable with fixed coefficients (in the SIP solver) (Chrigui 2005).

The change in the variables after each outer iteration can be important especially at the beginning of calculation in which they can lead to the instability. Hence, the under-relaxation of variables is used to reduce this effect as:

$$\phi^n = \alpha_\phi \phi^n + (1 - \alpha_\phi) \phi^{n-1} \quad (5.28)$$

Here ϕ^n and ϕ^{n-1} represent the values of the variable ϕ after n-th and (n - 1)st outer iteration and α_ϕ is the under-relaxation factor which satisfy $0 < \alpha_\phi \leq 1$. The detailed description of this idea (using the under-relaxation) can be found in the Patankar (1980).

5.7.3 Numerical method for dispersed phase

The equation (5.17) is an ordinary differential equation and hence one can solve it using the classical numerical methods. One of these classical numerical methods is the Euler forward integration method (used for the dispersed phase in this study) which is a simple approach for the implementation and has the acceptable accuracy as well. Using this method:

$$x_{p,i}^{n+1} = x_{p,i}^n + \Delta t u_{p,i}^n \quad (5.29)$$

$$u_{p,i}^{n+1} = u_{p,i}^n + \frac{\Delta t}{m_p} \sum \vec{F}_1 \quad (5.30)$$

Here $x_{p,i}$ and $u_{p,i}$ represent the parcel location and the velocity component respectively.

From one given time point (t^n) finding the next point at the next time step (t^{n+1}) along the same streamline is possible and thus the tracking of the whole line can be done (Chrigui 2005).

The Euler forward integration method is strongly dependent on the quality of initial velocity field and in some situations can lead to the spirals. Hence, it requires some additional stopping conditions to prevent such situations.

Although the Euler method is fast and simple for the implementation but it is a first order method and therefore does not have high accuracy. Hence in order to have a very high accurate solution, it needs a large number of small time steps which leads to the impractically long simulation time (Chrigui 2005).

As mentioned above, in the Euler forward method the time steps are limited with regard to the condition of physical processes and numerical stability based on the following equation:

$$\Delta t = 0.1 \min(\tau_p, t_E, t_W, t_{CV}) \quad (5.31)$$

Here t_E is the turbulent integral time scale defined by the following equation in which C_T is a constant value equal to 0.24;

$$t_E = C_T \frac{\varepsilon}{k} \quad (5.32)$$

t_W is the time which is required a parcel traverse a turbulent eddy:

$$t_W = \frac{L_E}{|\bar{u} - \bar{u}_p|} \quad (5.33)$$

$$L_E = t_E \sqrt{\frac{2}{3} k} \quad (5.34)$$

t_{CV} is the time which is required a parcel cross the control volume:

$$t_{CV} = \frac{\Delta x_i}{|u_{p,i}|} \quad (5.35)$$

Where τ_p is the particle relaxation time which describes the ability of a particle to react to the carrier fluid. This parameter represents the time which takes a particle respond to the carrier fluid velocity modification (Crowe *et al.* 1998) and is defined as:

$$\tau_p = \frac{\rho_p d_p}{18 \mu_f} \quad (5.36)$$

Here ρ_p and d_p are the particle density and diameter and μ_f is the fluid dynamic viscosity.

5.7.4 Averaging technique

Considering of all small scale fluctuations occurred in the flow field is not feasible and necessary especially in the case of high turbulent flows. Hence the averaging or smoothing operators are introduced to describe only the averaged values which are sufficient for the engineering purposes.

As it was mentioned in this chapter, the Reynolds-averaged equations have been used to describe the continuous phase characteristics in the present study. The Reynolds averaging refers to the averaging process of a variable or an equation in time. The detail of Reynolds averaging process for the transport equations (mass, momentum and enthalpy) of

continuous phase can be found in the standard CFD literature (Versteeg and Malalasekera 1995, Cebeci et al 2005).

Similar to the Eulerian part in which the equations averaged for the flow quantities (mass, velocity, temperature, etc.) have been solved, in the Lagrangian part the momentaneous quantities have to be sampled and averaged as well.

The mean values and variances of the droplet characteristic variables (such as the velocity components, temperature, diameter, etc.) in each cell are calculated based on (Sommerfeld 1996, Decker 2005):

$$\overline{\phi_p} = \frac{\sum_{k=1}^{k_p} \left(\sum_{n=1}^{N_{CV}} \phi_{p,i,j,k} N_{p,k} \right)}{\sum_{k=1}^{k_p} N_{CV}} \quad (5.37)$$

$$\overline{(\phi_p)'^2} = \frac{\sum_{k=1}^{k_p} \left(\sum_{n=1}^{N_{CV}} \phi_{p,i,j,k}^2 N_{p,k} \right)}{\sum_{k=1}^{k_p} N_{CV}} - \left(\overline{\phi_p} \right)^2 \quad (5.38)$$

Here k_p represents the total number of numerical droplets in a considered cell, N_{CV} the number of time steps which a droplet needs to cross the cell and $N_{p,k}$ the number of real particles represented by a numerical one (Chrigui 2005).

The regions where the particles/droplets are not able to reach them because of the high shear flow or total evaporation, have been characterized by the non-uniform properties profiles. The interested readers are referred to the works of Sommerfeld (1996) and Decker (2005) to find more information about these issues.

6 CFD Modelling of spray drying process

6.1 Measuring procedure

Developing a reliable drying kinetics for the successful simulation of spray drying process was the main aim of the present work. After successful applications of the developed drying kinetics for prediction of the behavior of different single droplets during the drying process, here this model is applied for the modelling of a pilot-scale dryer to evaluate the potential and capability of this drying model in the large scale.

The experimental data required to determine the initial and boundary conditions and to validate the numerical predictions are provided by Professor Ireneusz Zbiciński at Technical university of Lodz in Poland (Li and Zbiciński (2005), Li X. (2004)). The experiment was performed in a long co-current spray-drying tower in which the pneumatic spray nozzle was used to spray the suspension of baker's yeast with 90% initial moisture (water) content. The drying tower was equipped with a 60 kW heating, waste air cooling, dedusting and atomization system which enabled to carry out extensive trials of the co-current spray drying process.

The 50 optical glass windows at the tower walls allowed the performing of the PDA/LDA analysis (Particle Dynamic Analysis/ Laser Doppler Anemometry) as well as the micro-separator measurements to determine the characteristics of the droplet phase.

To determine the structure of spray in the different cross-sectional areas and along the length of drying tower, the PDA technique was applied through which the initial atomization parameters, distributions of droplets size and velocity of droplet phase in the different cross sections of drying chamber were measured (Li X. 2004).

The drying chamber walls consist of the several portholes which enabled the laser measurements in the selected points in each cross section at the different vertical positions. A transport system of the laser device was designed which allowed the movement of laser unit between the arbitrary height of the column.

The construction of the dryer also enabled to take the samples of material from the different heights of drying chamber for the laboratory analysis of the droplets moisture content.

A sampler was a rectangular plate (6.5 cm wide and 25 cm long equal to the radius of column) and such structure of this device allowed the measurement of the average moisture content of material at the different distances from the atomizer.

The micro-separator was used to measure the temperature distribution of the liquid phase in the different cross sections of drying chamber at the different vertical locations.

The temperature measurements of the liquid phase were carried out in the 4 points along the radius of chamber (at 0, 0.06, 0.12 and 0.18 m from the axis) in the different positions along the length of chamber (Li X. 2004).

6.2 Geometry and numerical procedure

The same geometry as the experimental test case is generated to enable the employing of the provided experimental measurements for definition of the initial and boundary conditions and to validate the modelling results (see Fig. 6.1) as well. The data collected at the first experimental measuring section located at 25 mm from the spray nozzle exit (in which the laser system was able to collect the data) was used to specify the initial atomization parameters. Hence, the simulated part of the spray dryer begins from the first measuring section (shown in Figure 6.2) and finishes at the outlet of dryer.

The simulation of the continuous phase was carried out at the Eulerian reference system at 175°C inlet drying air temperature, 1.5 m/s inlet drying air velocity, air mass flow rate of 39 kg/h while the spray rate of 10 kg/h, the initial temperature of spray was 293 K and the solvent vapor mass concentration (X) is defined as 0.01 (kg water vapor /kg dry gas) at the inlet as well.

Table 6.1 shows the full set of boundary conditions for both the continuous and the dispersed phase as applied in the present simulation.

Table 6.1: Boundary conditions used for simulation of spray dryer

Drying air inlet temperature	448 K
Air mass flow rate	39 kg/h
Inlet drying air velocity	1.5 m/s
water vapor mass concentration at inlet	0.01 kg/kg (dry gas)
The initial temperature of spray	293 K
Spray rate	10 kg/h
Atomizing air velocity	30 m/s
Initial Droplets Size distribution	Figure 6.3
Initial Droplets velocity distribution	Figure 6.4
Initial Droplets rms velocity	Less than $\pm 5\%$ initial velocity
Interaction between wall and droplet	Reflection
Dryer wall boundary condition for velocity	No-slip
Dryer wall boundary condition for temperature:	Insulated (adiabatic)
Number of parcels	around 500000
spray nozzle type	Pneumatic
droplets liquid	Baker's yeast
Initial moisture content	90% (kg water/kg total)
Inlet radius of spray	0.02m
Critical moisture content value	5.62 kg water/kg solid

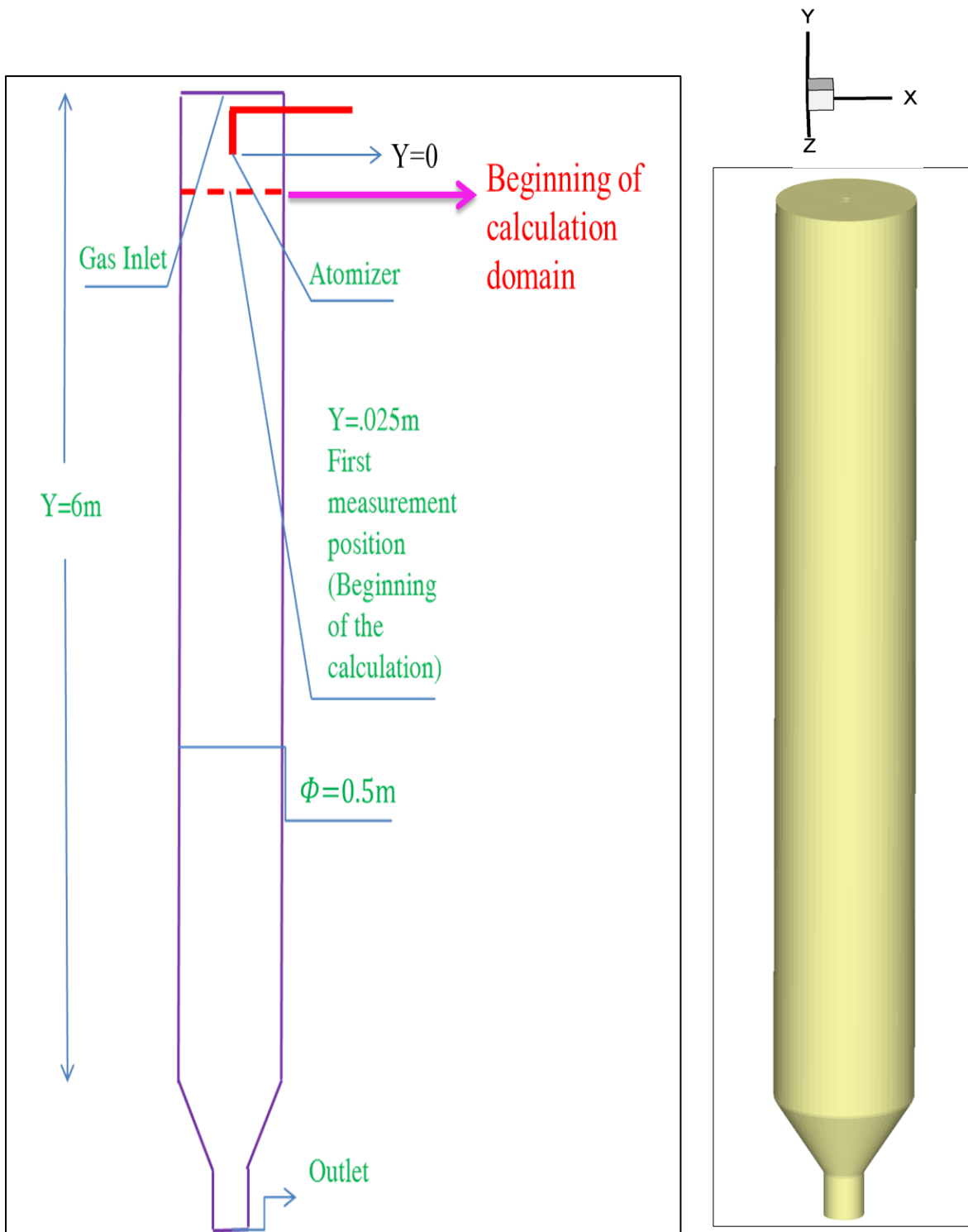


Figure 6.1: Geometry of the modeled spray drying tower.

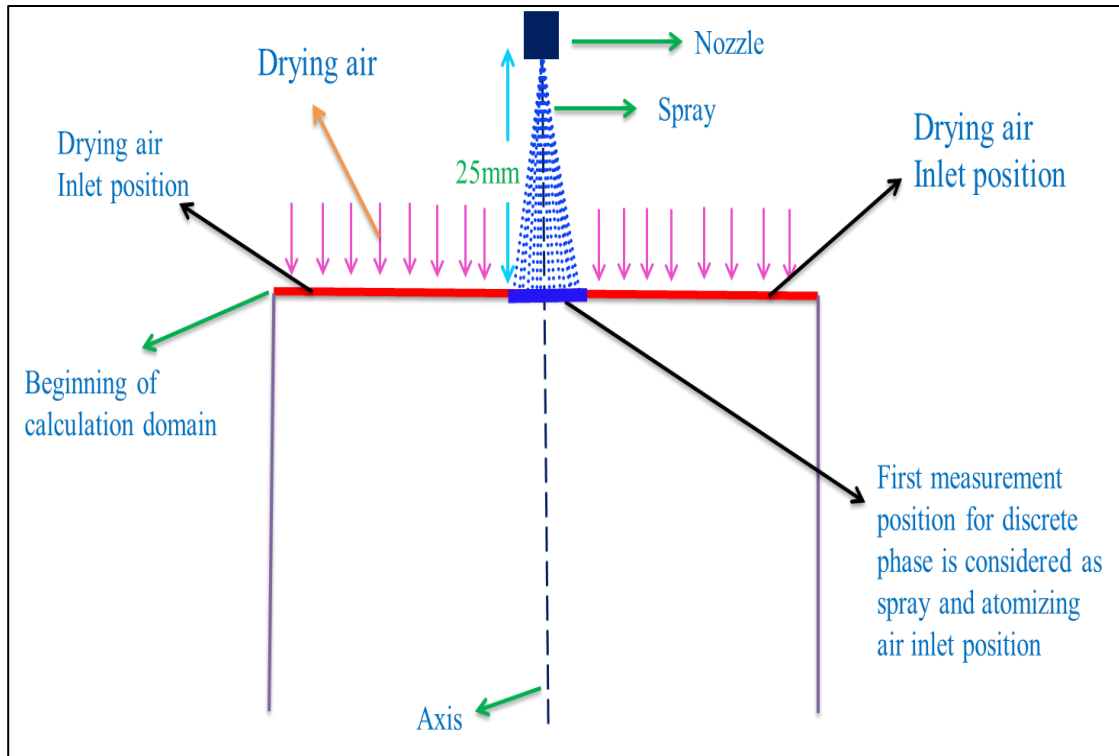


Figure 6.2: Schematic of the construction of inlet region for the continuous and dispersed phase.

The Lagrange reference system is applied to model the dispersed phase at which the droplet phase is represented by using 100 classes of size fractions each consist of 555 numbers of parcel with the identical properties. The streams of droplets are introduced in the 9 different radial positions and the parameters of each stream such as the initial diameter distributions and velocities are sampled from the experimental measurements as follows:

Figure 6.3 (a) shows the initial droplets size distributions measured at 25 mm downstream the spray nozzle exit. As it can be seen, this figure indicates that at each radial position almost an identical droplets size distribution exists. Therefore for simplicity, in the numerical simulation the averaged profile is taken to be used for all injection positions (see Fig. 6.3(b)).

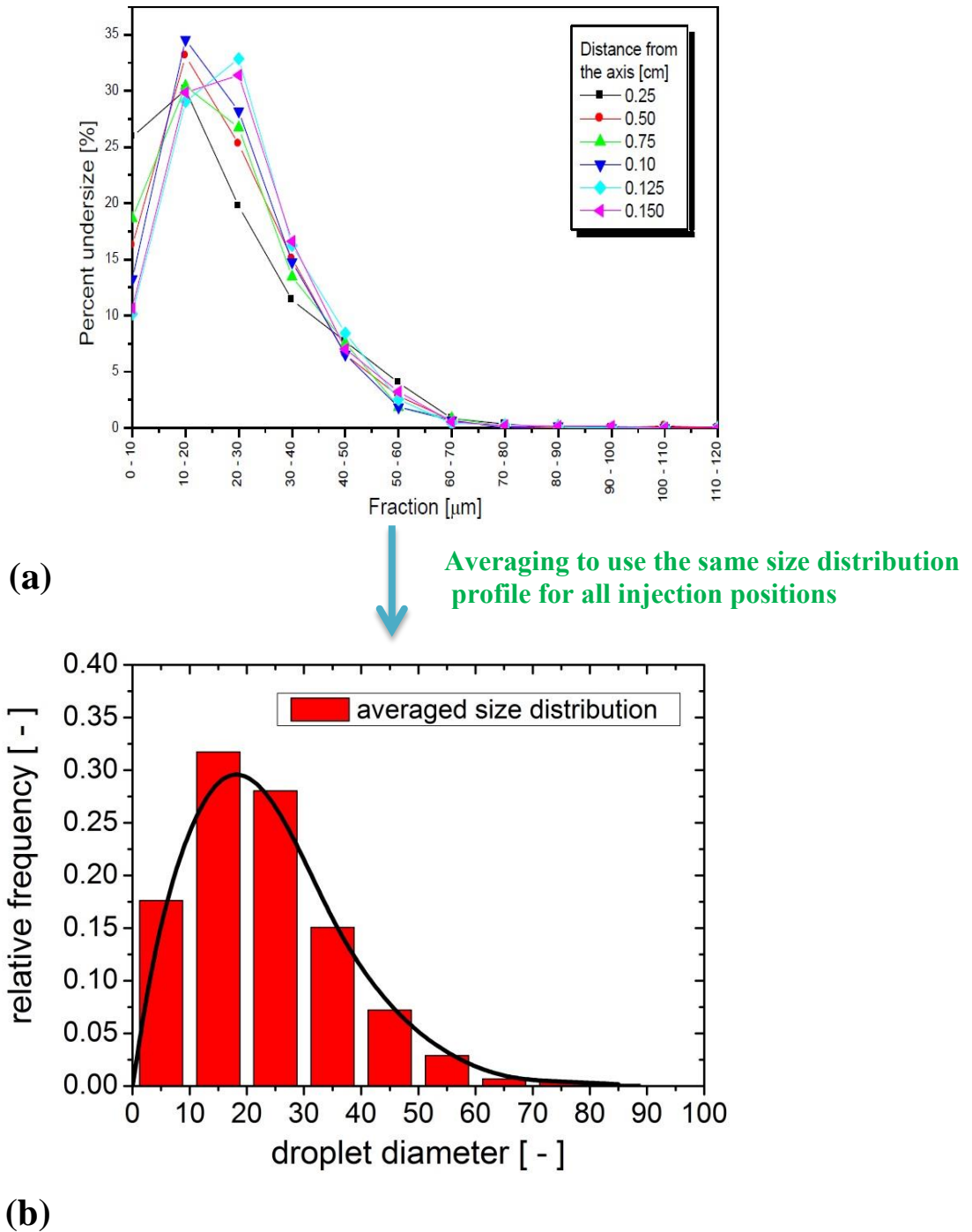
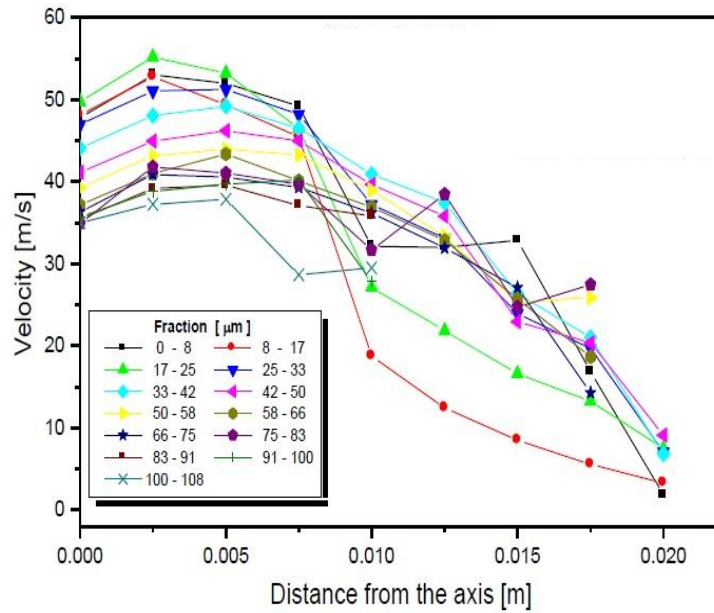


Fig. 6.3: Initial droplets size distribution (a) measured profiles (b) averaged profile

Figure 6.4(a) displays the initial axial droplets velocity profiles measured at 25 mm downstream the spray nozzle exit for several radial positions. As it can be observed, this figure indicates that the initial axial droplets velocity is a function of both the droplet diameter and the distance from the center line. The velocity of each droplet fraction is not constant at the beginning and varies according to the distance from the center line (i.e. in

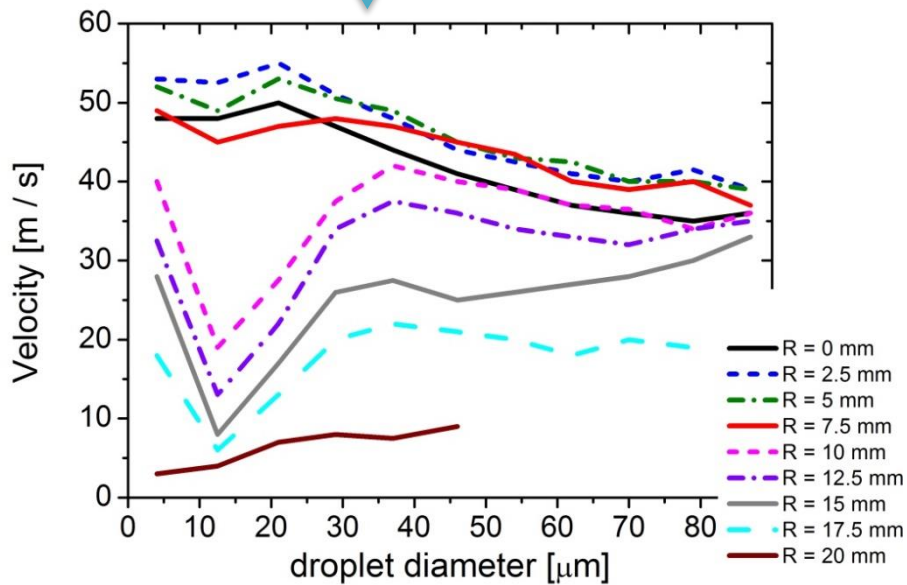
the radial position), for example from around 40 m/s at the axis to around 10 m/s at the edge of spray envelope for the size fraction of 40-50 μm .

Using Figure 6.4(a) and extracting the axial velocity of each droplets fraction for each injection position Figure 6.4(b) is obtained to be used in the numerical simulation.



(a)

Determination of axial velocity for each Position of injection for different Classes of droplets



(b)

Fig. 6.4: Initial axial droplets velocity distribution (a) measured profiles (b) extracted profiles.

Fig. 6.5 displays the initial mass flow rate distributions obtained by measurements. Like initial axial droplet velocity distributions, each droplet fraction has mass flow rate distribution that is a function of the distance from the center line (axis).

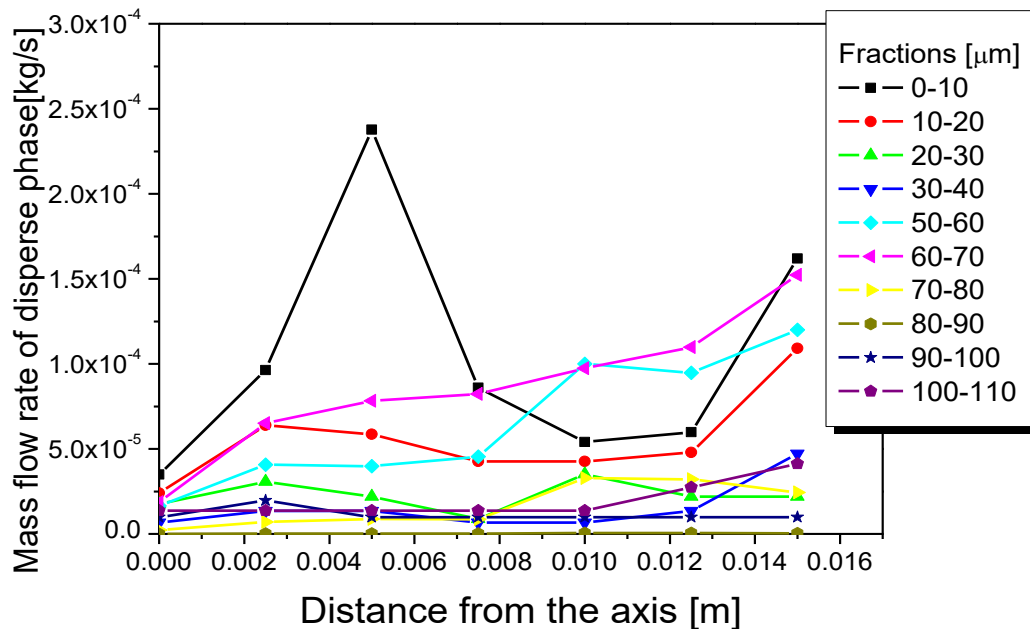


Fig. 6.5: Initial mass flow rate distribution.

6.2.1 Injection procedure

The droplet velocity-size correlation was extracted from the measurements (Fig. 6.4(a)) and is shown in Figure 6.4(b). Radial and tangential mean velocities were unfortunately not available from the measurements. Therefore, the droplet injection procedure at the inlet plane is as follows, respecting the size distribution (Fig. 6.3(b)) and the velocity-size correlation (Fig. 6.4b); for each droplet parcel:

- Random determination of a droplet size from Fig. 6.3(b) by using the cumulative distribution and equal distributed random number between [0;1].
- Based on the droplet mass flow rate in each injection control volume (Fig. 6.5), the droplet mass and the number of parcels injected in each location the real number of droplets in a parcel is determined.
- According to the considered radial position the axial droplet mean velocity is selected from the velocity-size correlation (Fig. 6.4(b)).

- Since the standard deviation of the axial velocity was not provided it was assumed to be 5% of the mean droplet velocity.
- The parcel axial velocity is then drawn from a normal distribution with the obtained mean velocity and a standard deviation of 0.05 times the mean velocity using a Gaussian random process.
- Unfortunately no measurements were available for the radial and tangential droplet velocity so that they were assumed to be zero. This may of course introduce larger errors with respect to the radial droplet velocity which is for spray modelling essential.
- Now the droplet parcel radial and tangential velocities were drawn randomly from normal distribution with zero mean and a standard deviation of 0.05 of the local droplet size dependent axial mean velocity.

6.2.2 Characteristics of the dispersed phase

The convergence of the Eulerian-Lagrangian coupling procedure depends sensitively on the total numbers of numerical droplets. Calculations using high numbers of droplets will provide reliable statistical source terms, which in turn enable to have overall fast convergence. Furthermore, obtaining the statistical mean values of the dispersed (droplet) phase properties needs the high numbers of droplets as well. Hence, in order to achieve the statistically reliable dispersed (droplet) phase properties and source terms, the droplet phase is calculated by tracking around 500,000 parcels through the gas field in every coupling iteration and increasing the numbers of parcels resulted in no influences on the statistical droplets properties.

Besides, at the dryer wall the no-slip condition is applied as a boundary condition for the gas phase velocities and the dryer is considered to be perfectly insulated (i.e. the amount of heat transfer through the dryer wall is not considered) as well.

Moreover, the primary simulations and experimental observations revealed that only a few droplets with high moisture content hit the dryer wall (Li 2004). Thus, in the simulation if the droplets tracked in the flow field hit the dryer wall the 'reflection' type condition is applied in which the bounce of particles is supposed (i.e. no momentum loss). The full set of boundary conditions is shown in Table 6.1

The properties of baker's yeast can be found in Table 6.2 and the internal diffusion coefficient of baker's yeast was calculated based on the following equation (Yüzgeç 2008):

$$D_{AB} = D_{Ref} \exp\left(\frac{E_a}{R} \left(\frac{1}{T_{Ref}} - \frac{1}{T}\right)\right) \left[\frac{\omega_A - \omega_e}{\omega_0 - \omega_e}\right]^z \quad (6.1)$$

Here ω_0 , ω_A and ω_e are the initial, current and equilibrium dry based moisture content $\left[\frac{\text{kg Water}}{\text{kg dry solid}}\right]$ respectively and E_a represents the activation energy for the diffusion calculated as:

$$E_a = 80000 \left(\frac{1}{1+10\omega_A} + 0.147\right) \quad (6.2)$$

z is the power in concentration dependence of diffusion coefficient, R the gas constant and T_{Ref} reference temperature equal to 323 K. The values of z and D_{Ref} are determined based on the experimental data as $z = .0154$ and $D_{Ref} = 7.89 \times 10^{-10} \text{ m}^2/\text{s}$.

In order to solve the transport equations for calculation of the air flow, species and temperature field, the discretization of geometry in a grid structure is required. Therefore a non-orthogonal, block-structured hexahedral grid type consists of 27 blocks with 573,104 computational volumes is applied as the final grid as shown in the Figure 6.6. Figure 6.7 displays the view of mesh at drying air and injection position

Table 6.2: *Physical properties of baker's yeast*

Test case	D_{cru} [m ² /s]	k_{core} [W/(m·K)]	k_{crust} [W/(m·K)]	ρ [kg/m ³]	C_{sat} Kg solid/kg solution
baker's yeast	1.0×10^{-6}	0.4	0.2	1050	0.15

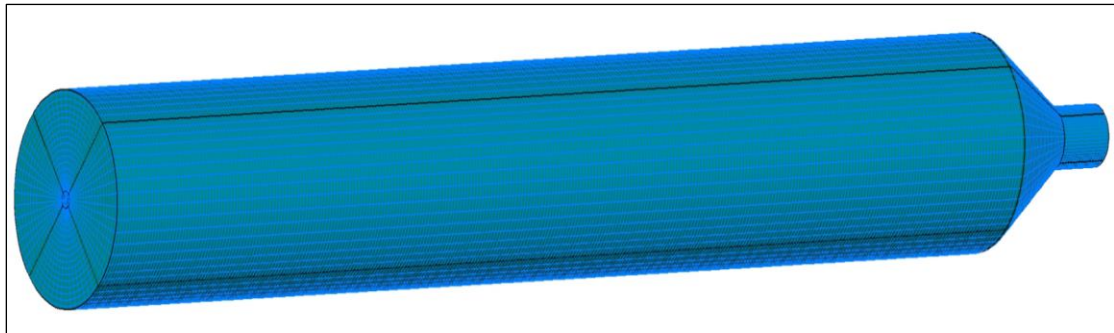


Fig. 6.6: View of mesh at geometry surface

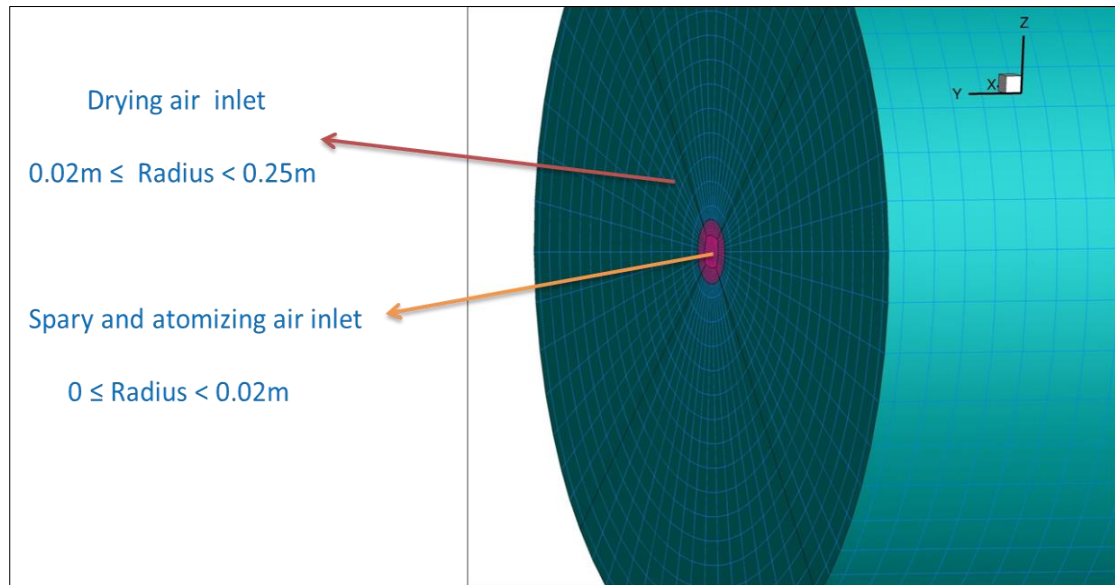
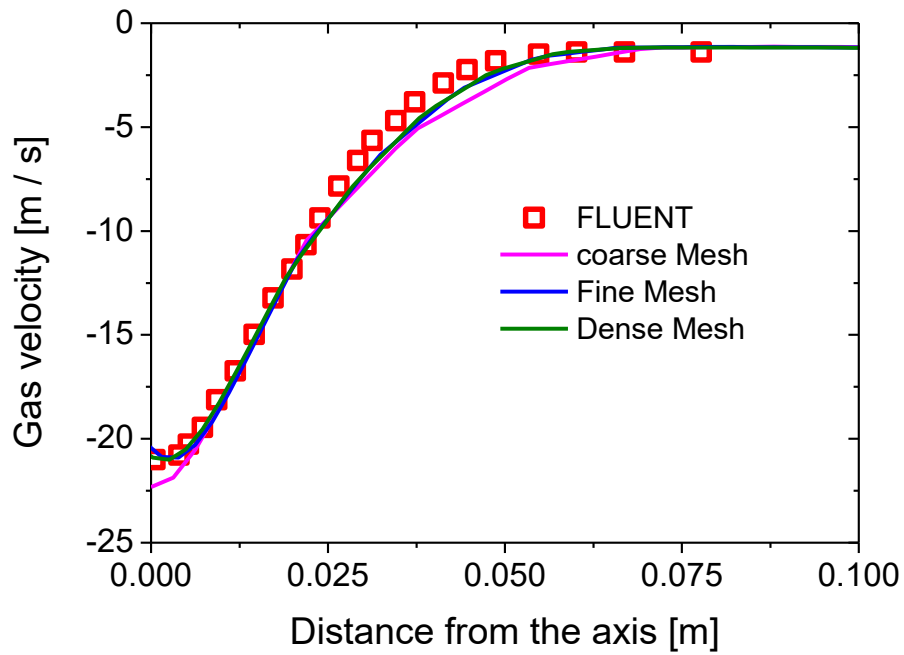


Fig. 6.7: View of mesh at drying air and injection position.

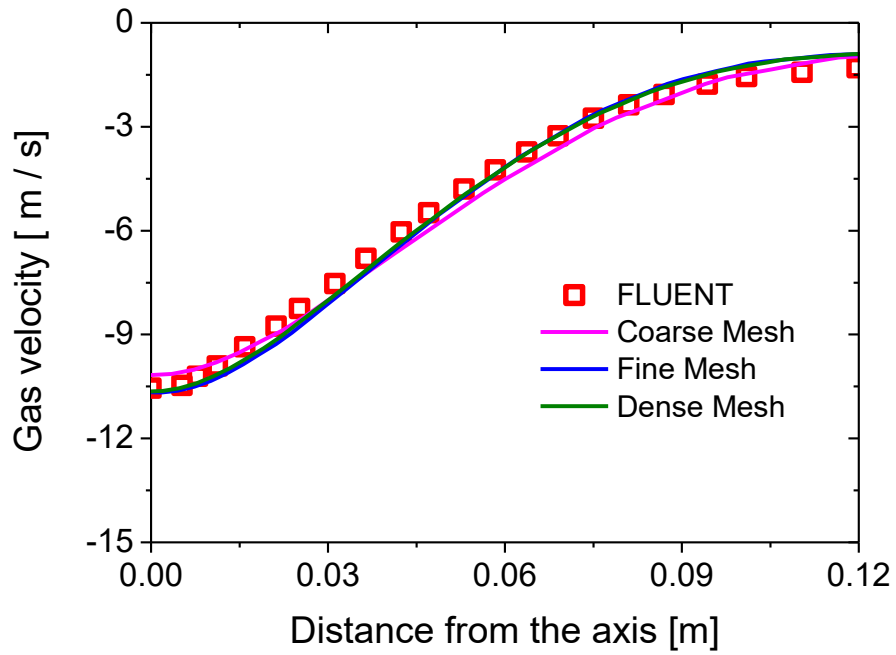
6.3 Grid independence study

Figure 6.8 displays the grid study for the drying gas (air) velocity profiles in the different cross-sections at 0.2 and 0.5m downstream from the beginning of calculation domain. Due to the lack of experimental data, the predicted results are compared with the results provided by the commercial software FLUENT (Li and Zbicinski 2005).

Grid resolution study is performed using 3 different grids including the coarse, fine and dense grid consisting of 174,220, 354,861 and 573,104 numbers of nodes respectively. The results provided by the simulations with the fine and dense grid have better agreement with the results provided by FLUENT (Li and Zbicinski 2005), and furthermore, the difference between the results for these two grids (fine and dense) are not considerable therefore the dense grid has been selected for the final simulation.



(a)



(b)

Fig. 6.8: Grid study of gas velocity distributions at (a) 0.2 and (b) 0.5 m from the beginning of calculation domain.

6.4 Simulation results and discussion

In the following sub-sections, the results obtained from the CFD simulation are presented in terms of the gas (air) velocity, temperature, vapor concentration profiles as well as the droplet phase characteristics such as the droplets velocity, temperature, size distributions, and moisture content. Furthermore, the CFD results are compared with the experimental data to evaluate the accuracy of the developed drying model in the large scale.

6.4.1 Results for the Fluid Phase

Figure 6.9 displays the predicted air velocity contour. As shown in this Figure, the air flow pattern looks to be almost axisymmetric throughout the drying chamber and the influence of jet produced by the pneumatic atomizer on the hydrodynamics of gas phase is obvious, predominantly in the vicinity of nozzle. Here the gas velocity significantly increased because the drying gas is carried away by the injected droplets, thus it is speeding up. This is the result of the large momentum exerted on the gas phase by the droplets in this region (vicinity of the nozzle). Moreover, the velocity distribution flattened as the flow proceeds downstream.

The figures 6.10 and 6.11 show the contours of the predicted water vapor concentration and gas temperature respectively. As shown, the influence of injected droplets is also noticeable in the gas temperature and species concentration contours. The concentration of water vapor in the drying gas increased in the areas of droplets evaporation especially in the upper part of drying chamber along the column because the most of heat and mass transfer (i.e. drying process) occur in this part of drying chamber. The droplets initially have the free moisture (water) at the surface and their velocity is maximum in this part of drying chamber (i.e. the upper part) which coupled with the large temperature driving force existed in this region resulted in the high drying rate and thus the increase of the water vapor concentration in this area.

The vapor concentration distribution flattened further down the chamber so that the drying air leaving the drying chamber has almost a uniform moisture distribution.

In Figure 6.11 the decrease of the drying air temperature in the area of droplets injection can be obviously observed. The injected droplets absorbed the heat from their environment; warmed up and finally their moisture (water) evaporated until the dry

particles are achieved. The absorption of heat from the surrounding hot air by the droplets resulted in the reduction of drying gas temperature especially near the atomization zone, and further down along the column the cooled air is mixed with the hotter air from the outer injection layers which caused the increase of the gas temperature again, so that the drying air flowing towards the dryer outlet has a quite uniform temperature. The minimum temperature in the dryer chamber is observed near the atomization zone due to the high mass and heat transfer rate during the initial contact between the drying gas and spray in this zone which are the results of the high relative velocities between the drying air and droplets combined with the large temperature driving force existed in this region (atomization zone).

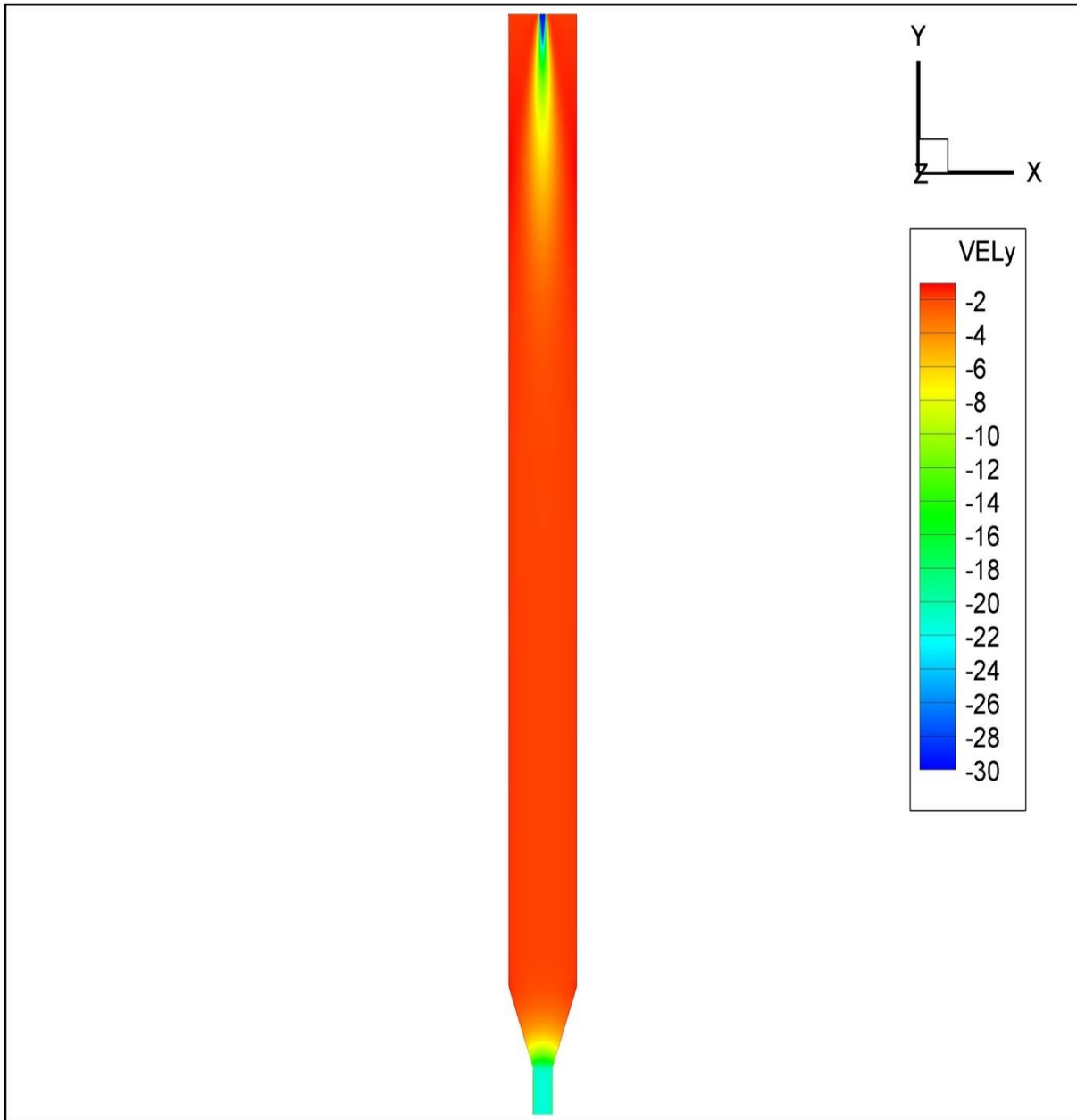


Fig. 6.9: Gas (air) velocity contour [m / s] in 2-way coupled calculation.

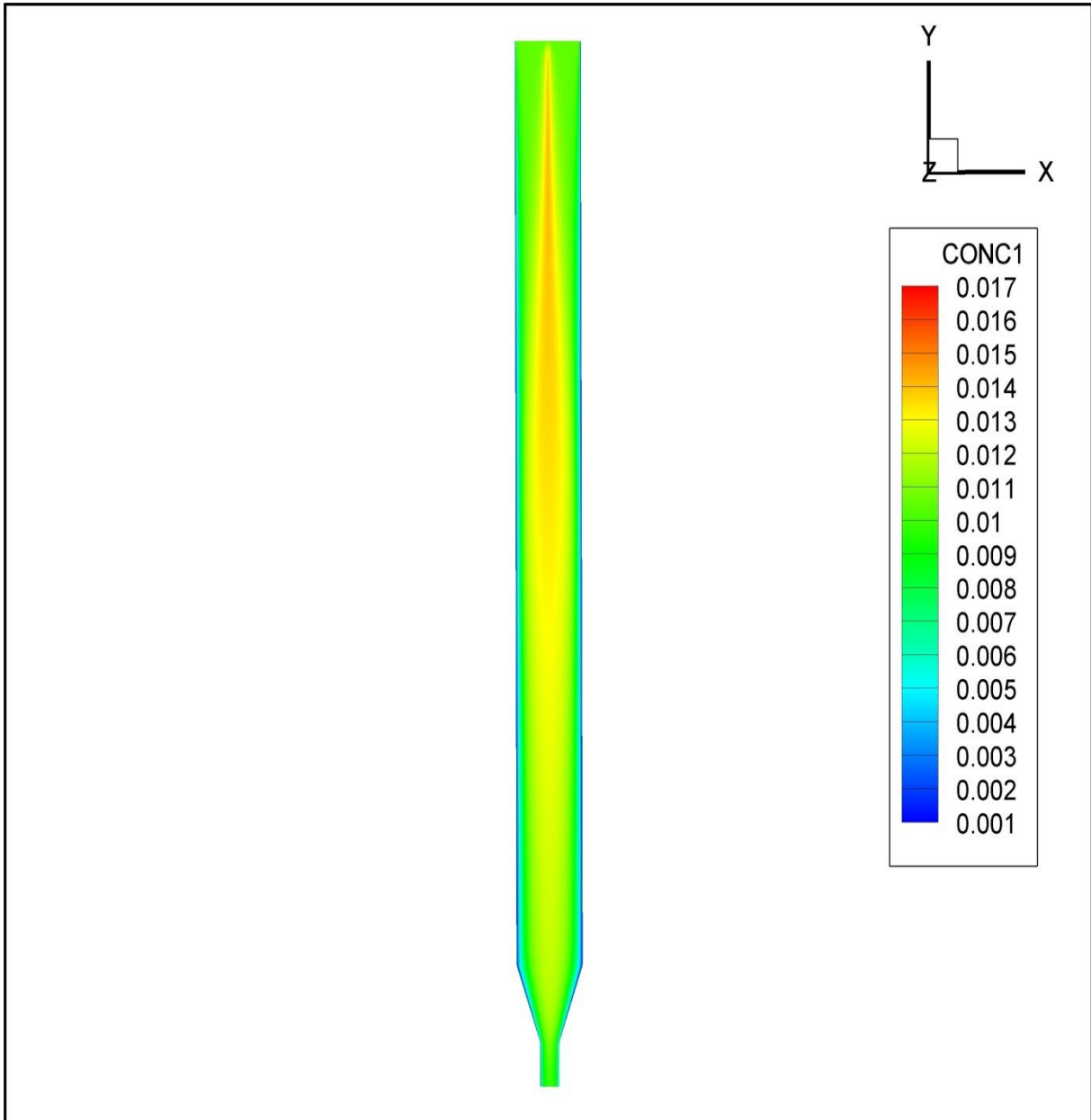


Fig. 6.10: Water vapor concentration contour [kg_{vapor}/kg_{dry Air}] in the spray dryer in 2-way coupled calculation.

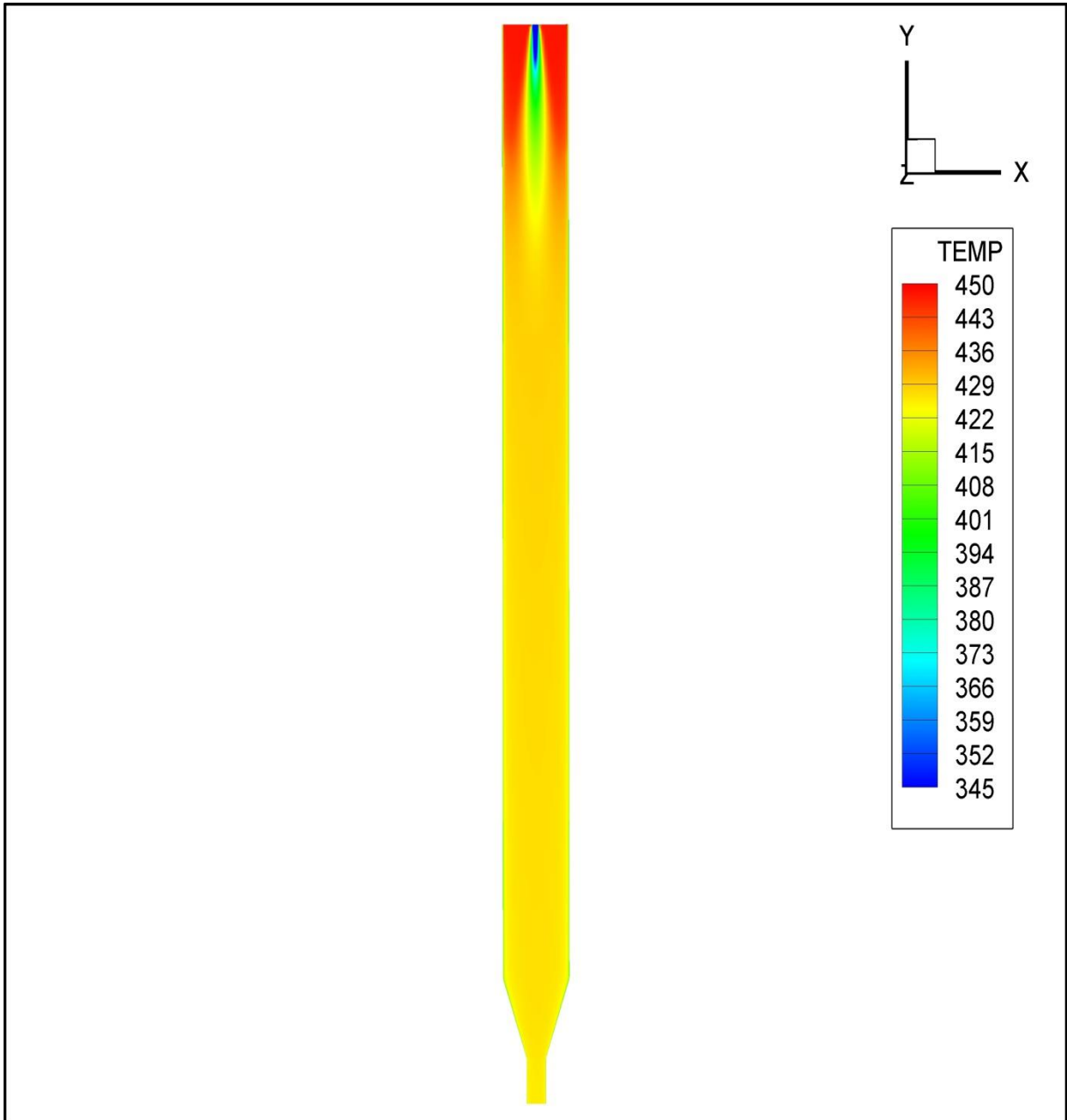


Fig. 6.11: Gas temperature contour [K] in 2-way coupled calculation.

6.4.2 Results for the Dispersed Phase

In the following sections, the results obtained from the CFD simulation are presented for the dispersed phase based on 2-way coupled calculation procedure.

The figures 6.12 and 6.13 display the predicted contours for the droplets temperature and solid content respectively. As shown in these figures, the continuous increase of the droplets temperature (Fig. 6.12) and solid content (Fig. 6.13) can be clearly observed. Right after the atomization the droplets contacted the hot inlet air and their temperature increased (initial warm-up period) and subsequently the moisture (water) evaporation occurred rapidly from the surface of droplets in the ‘quasi-equilibrium evaporation’ period in which the most of the heat transferred from the hot air to the droplets are employed for the evaporation. During these periods which form the constant drying rate period the droplets temperature gradually increased from initially 293K to about 320 K due to the initial contact of droplets with the hot drying air and growing concentration of solid matter (i.e. solid content) at the droplet surface (from initially 0.1 to about 0.15 ($\text{kg}_{\text{solid}} / \text{kg}_{\text{total}}$)). Further down the chamber, the droplets were in the falling drying rate period in which the droplets temperature increased consistently with distance down the column and finally reached almost to the drying air temperature. The solid content of droplets also increased constantly until the complete drying of particles is achieved at the solid content of about 95% at the upper half of drying chamber which proves the size of this drying chamber is big enough to provide a complete drying process.

Figure 6.14 displays the dry basis moisture content of droplets, which contrary to the solid content, decreased continuously due to the evaporation of water from the droplets and reached to 0.1 ($\text{kg}_{\text{water}} / \text{kg}_{\text{solid}}$) at the upper half of drying chamber.

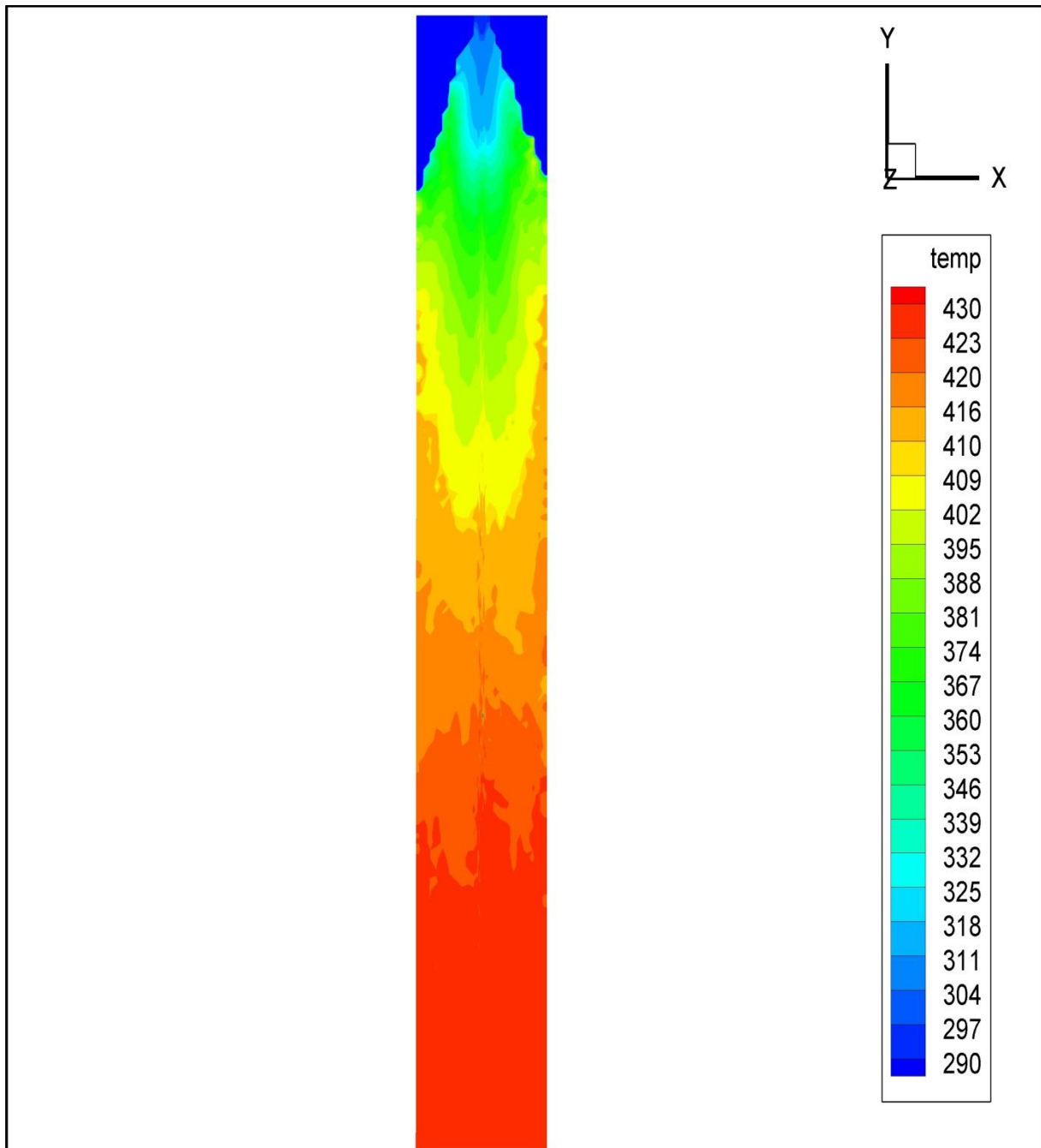


Fig. 6.12: Droplets temperature contour [K] at upper half of tower in 2-way coupled calculation.

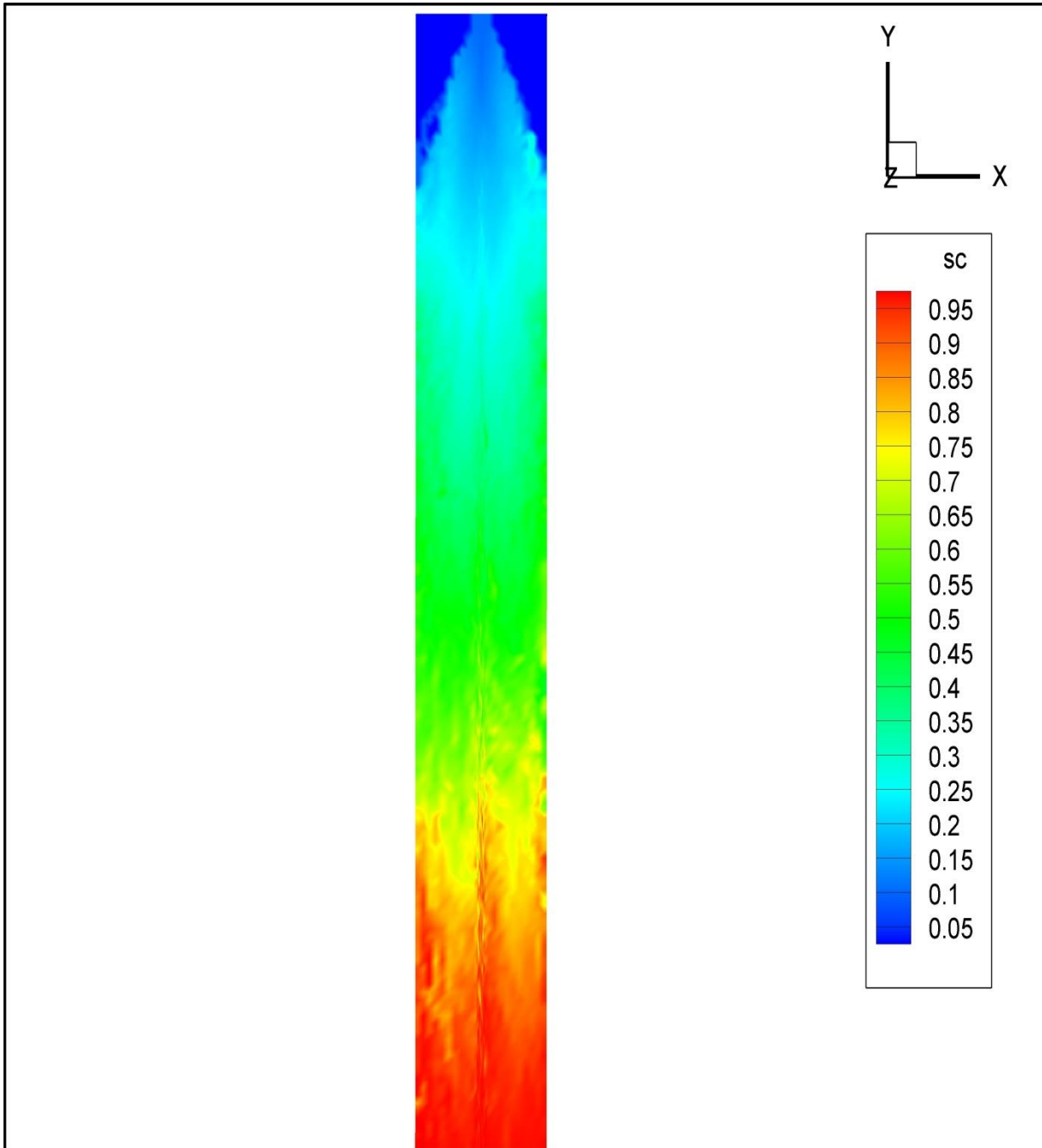


Fig. 6.13: Droplets solid content contour [$\text{Kg}_{\text{Solid}} / \text{Kg}_{\text{Solution}}$] at upper half of tower in 2-way coupled calculation.

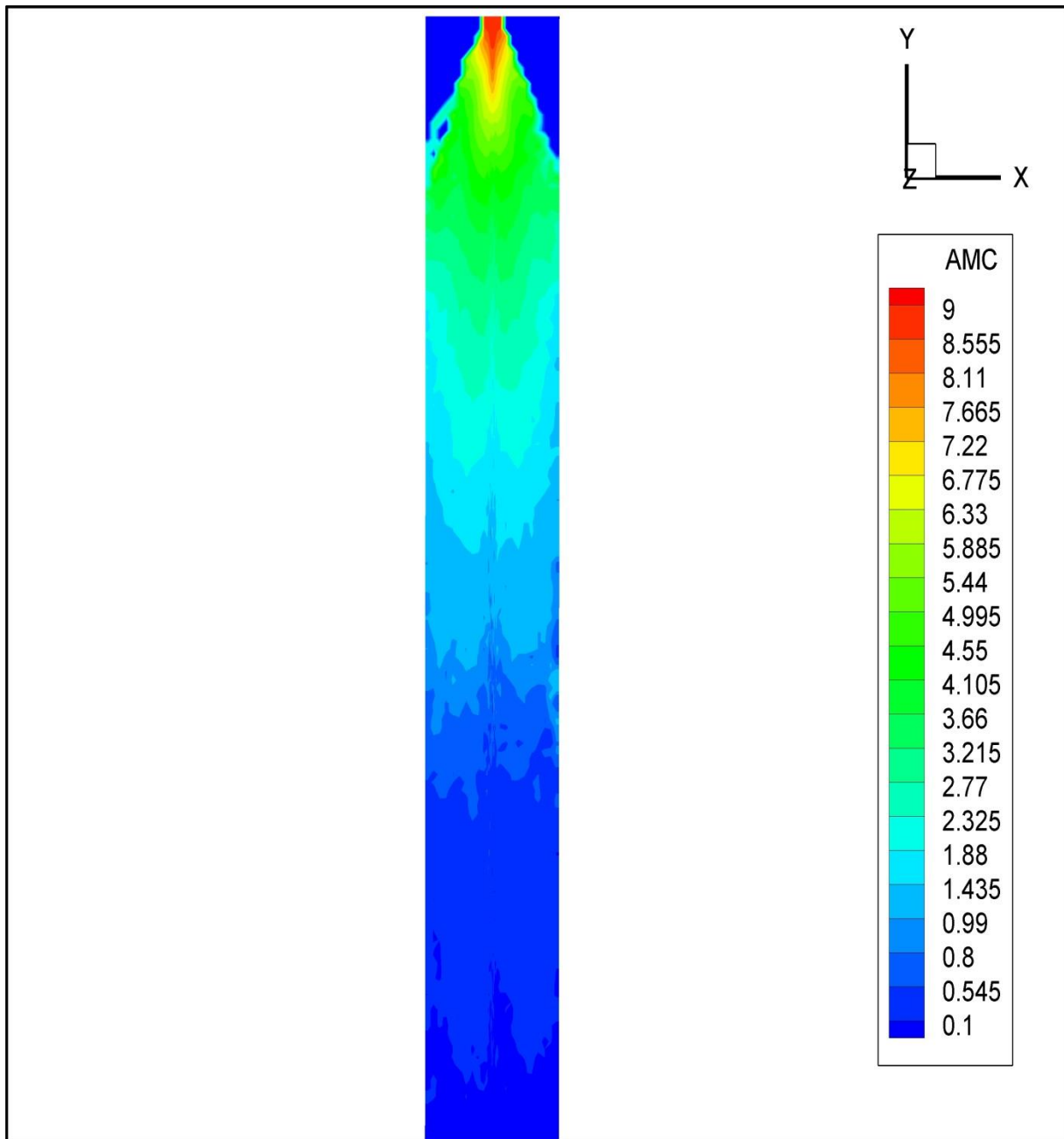
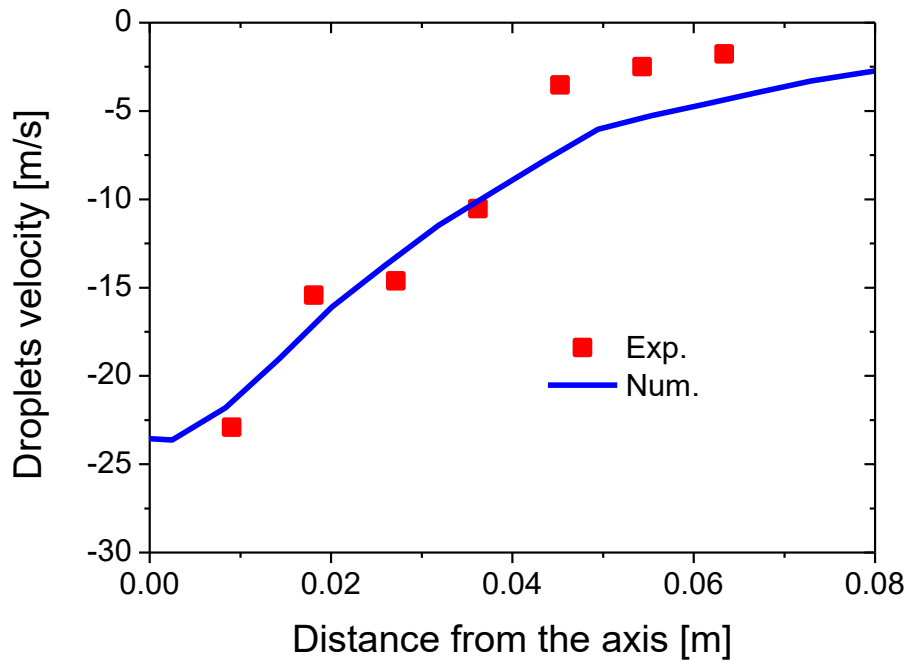


Fig. 6.14: Droplets dry basis moisture content contour [$\text{Kg}_{\text{water}} / \text{Kg}_{\text{solid}}$] at upper half of tower in 2-way coupled calculation.

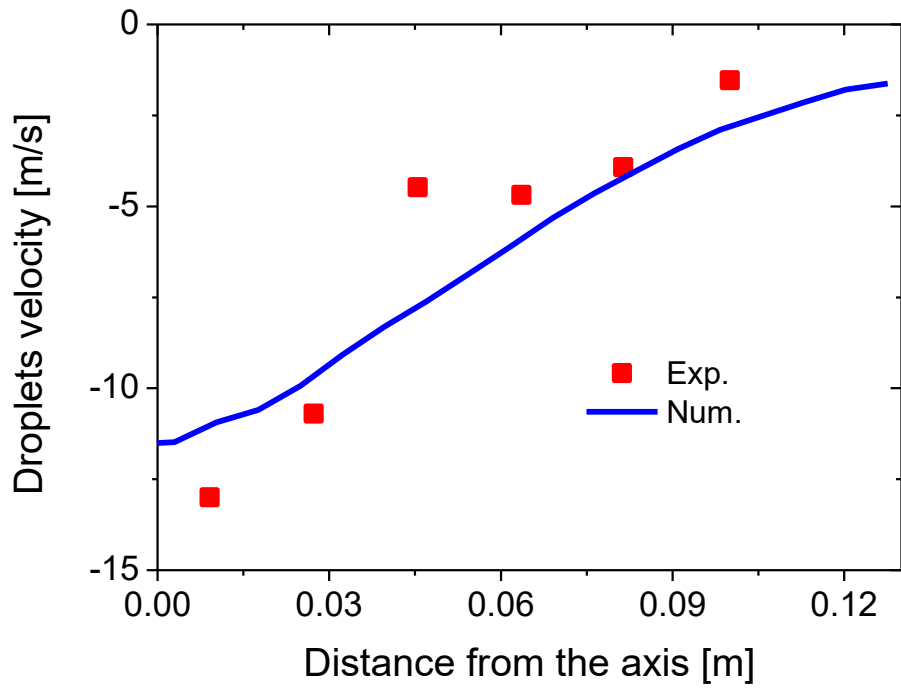
6.4.2.1 Droplets velocity

Droplets velocity distributions in the different cross-sections are plotted in Figure 6.15. As shown in this Figure, the comparison of the predicted results with the experimental measurements indicates that the predictions of current simulation are in good agreement with the experimental results.

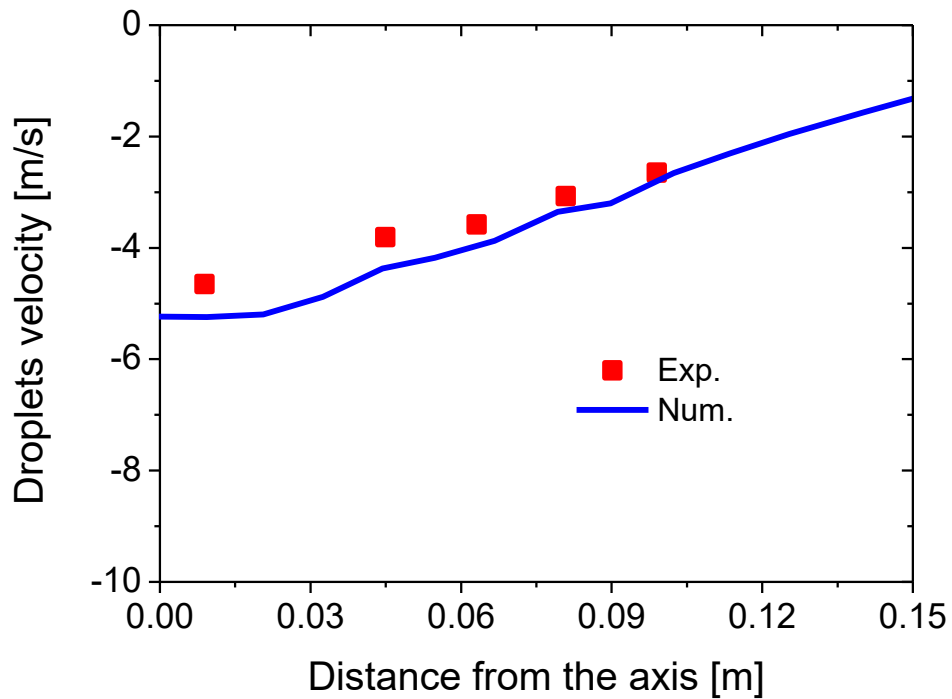
In the cross sections near to the atomizer (0.2 m and 0.5 m from the beginning of calculation domain) droplets velocity is higher on the axis, especially in the vicinity of nozzle due to the jet generated by the pneumatic nozzle, while the velocity profile flattened further down the chamber at 0.8 m from the beginning of calculation domain.



(a)



(b)



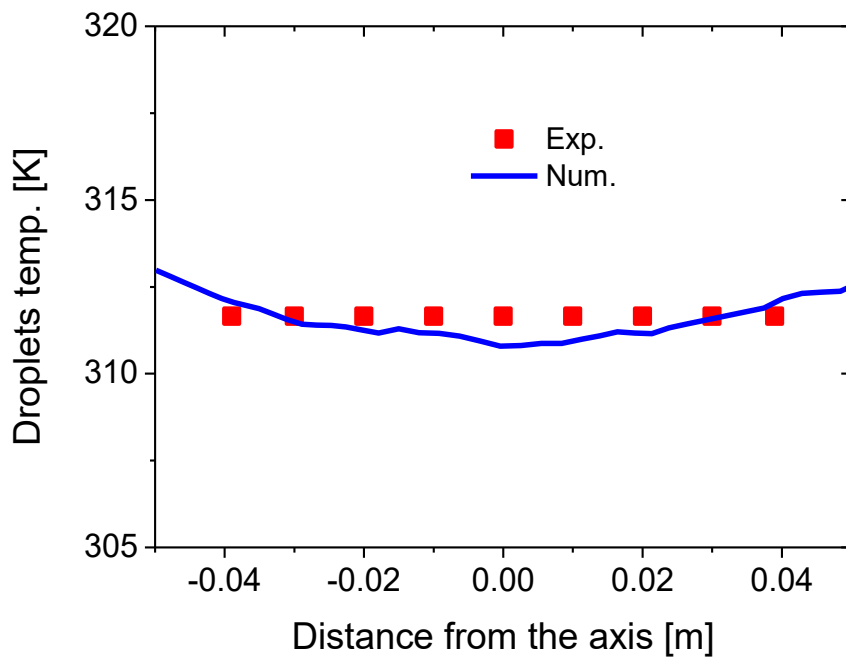
(c)

Fig. 6.15: Droplets mean velocity distributions at (a) 0.2 m, (b) 0.5 m and (c) 0.8 m from the beginning of calculation domain compared with experimental measurement.

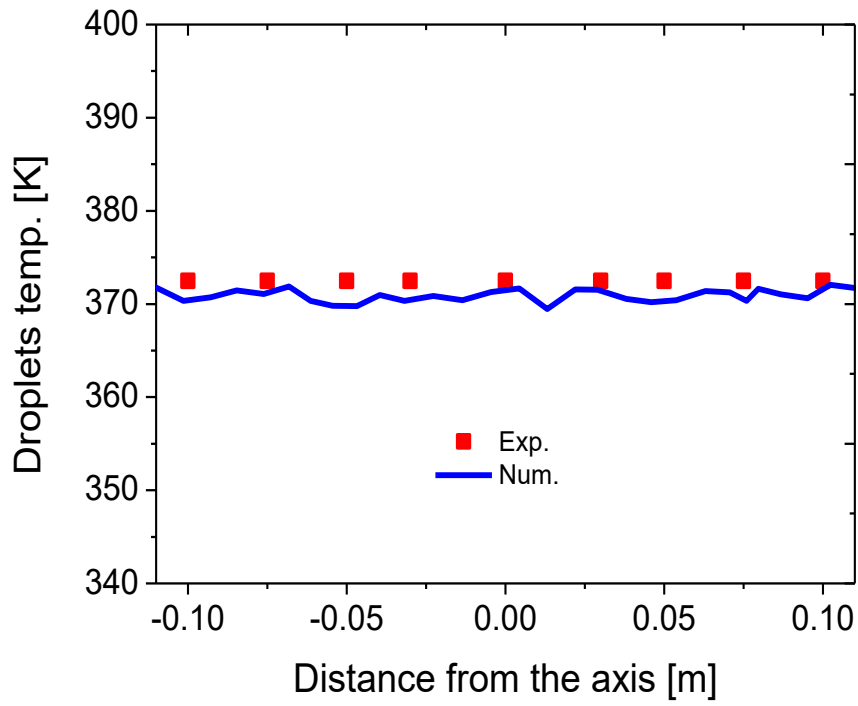
6.4.2.2 Droplets temperature

Figure 6.16 compares the results obtained by the numerical simulation with the experimental data for the droplets temperature in the different cross-sections at 0.2, 0.5, 0.8 and 1.25m downstream from the beginning of calculation domain. The experimental results show the averaged value of temperature in each cross-section measured through the experiment and hence show a constant value at each cross-section.

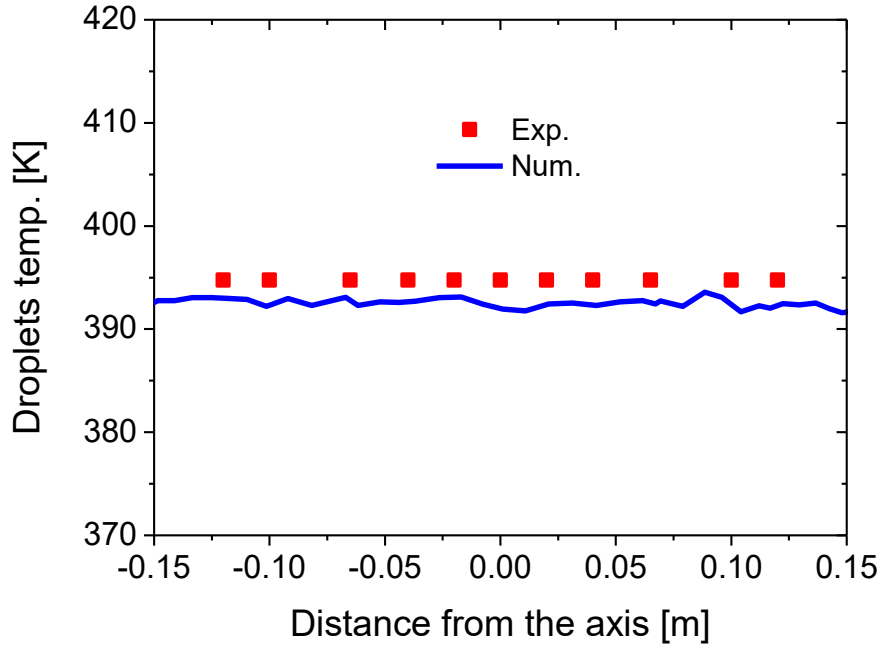
As previously mentioned; the injected droplets absorbed the heat from the surrounding environment and their temperature increased consistently with distance down the column and finally reached nearly to the drying air temperature. By considering the complexity existed in the drying process as well as the uncertainty in the measurement results, it can be said that the good agreements between the numerical and experimental results are obtained.



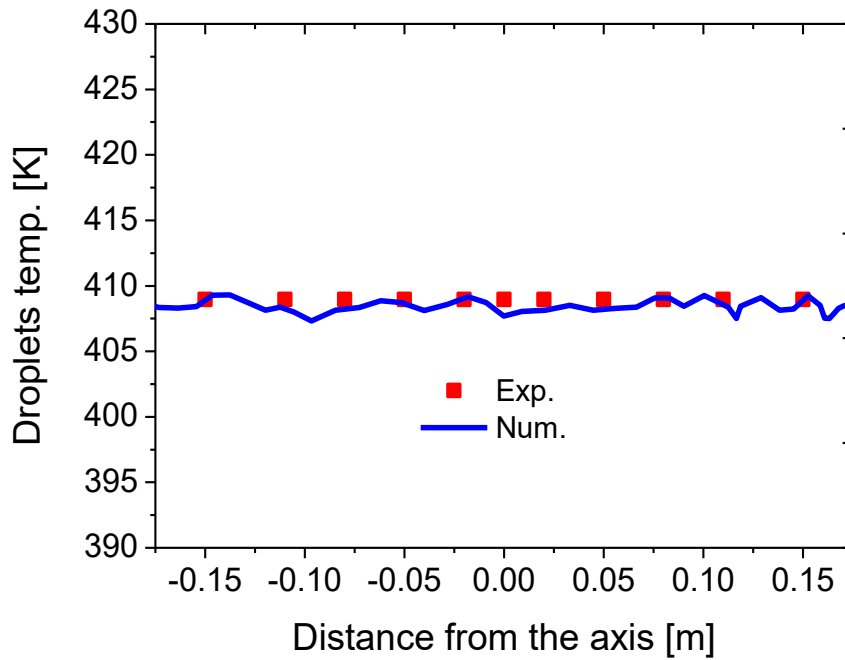
(a)



(b)



(c)



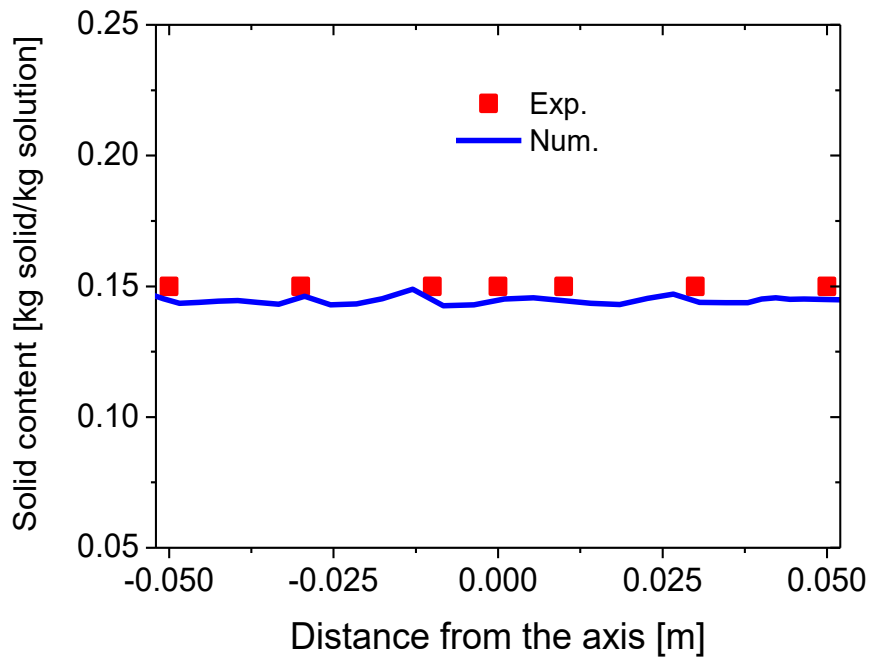
(d)

Fig. 6.16: Droplets temperature distributions at (a) 0.2 m, (b) 0.5 m, (c) 0.8 m and (d) 1.25 m from the beginning of calculation domain compared with experimental measurement.

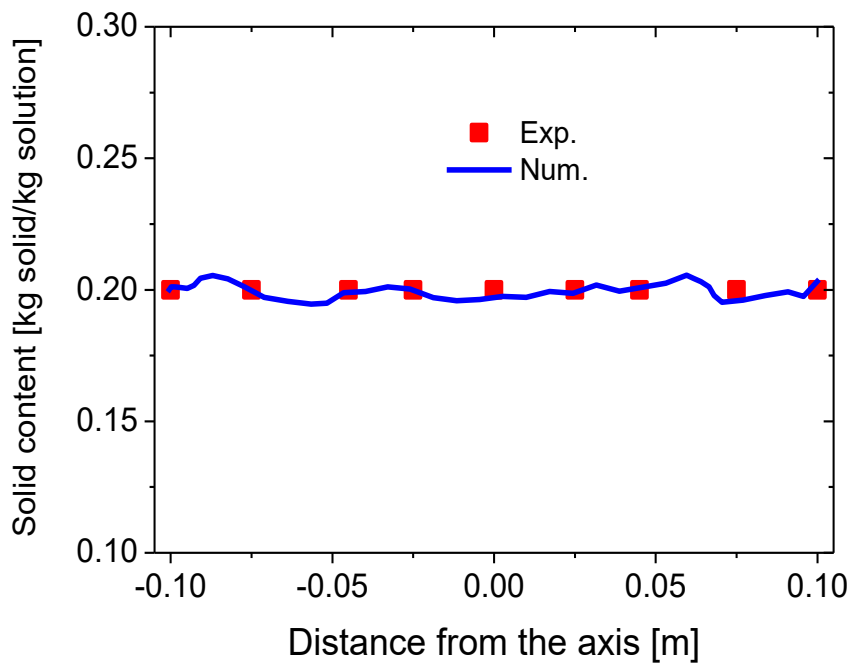
6.4.2.3 Material solid content

Figure 6.17 presents the predicted and measured results for the material solid content in the different cross-sections. The experimental results show the averaged value of solid content in each cross-section measured through the experiment and hence show a constant value at each cross-section.

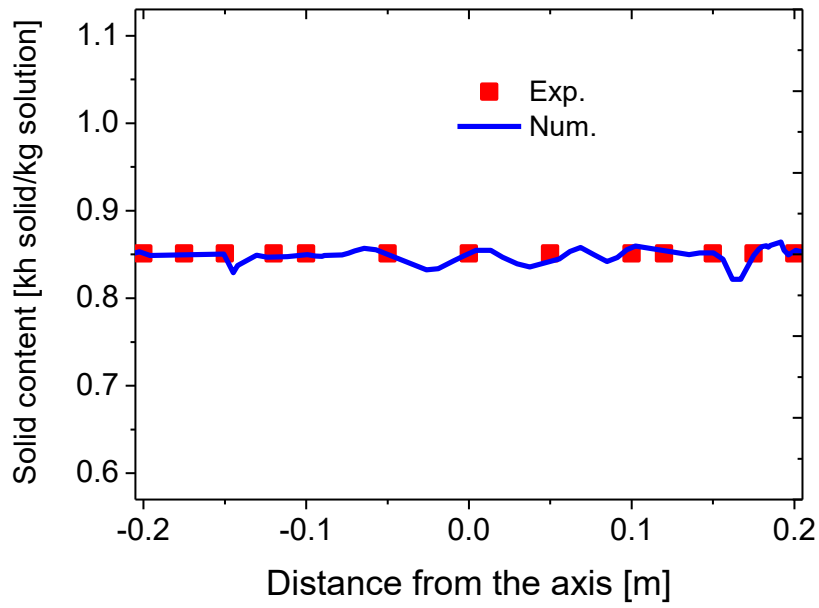
During the drying, the solid content of droplets grew gradually until the complete dried particles are achieved at the solid content of about 95% at 3.5 m downstream from the beginning of calculation domain which means the height of the present drying tower (about 6 m) is quite enough to produce a completely dried product. As shown, the model predictions are in good agreement with the experimentally measured values for this characteristic of dispersed phase as well.



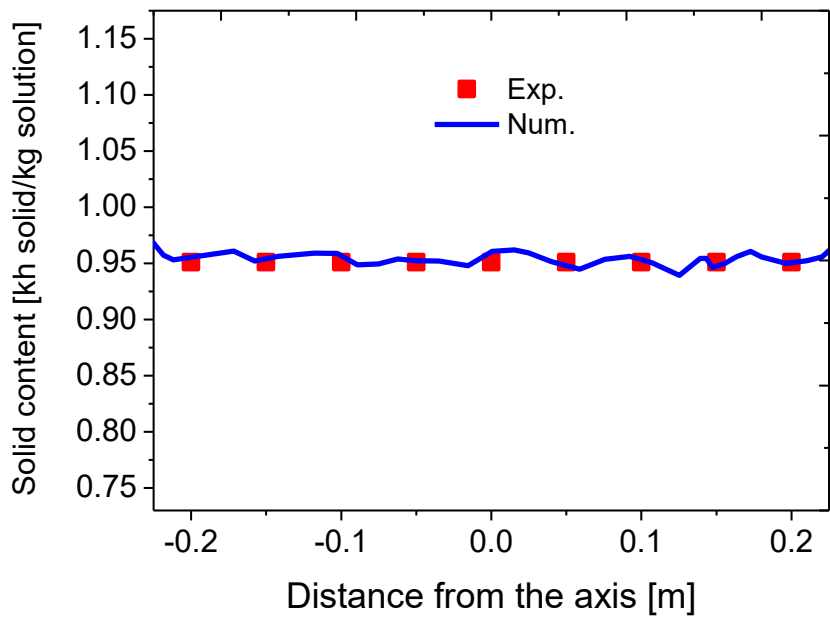
(a)



(b)



(c)



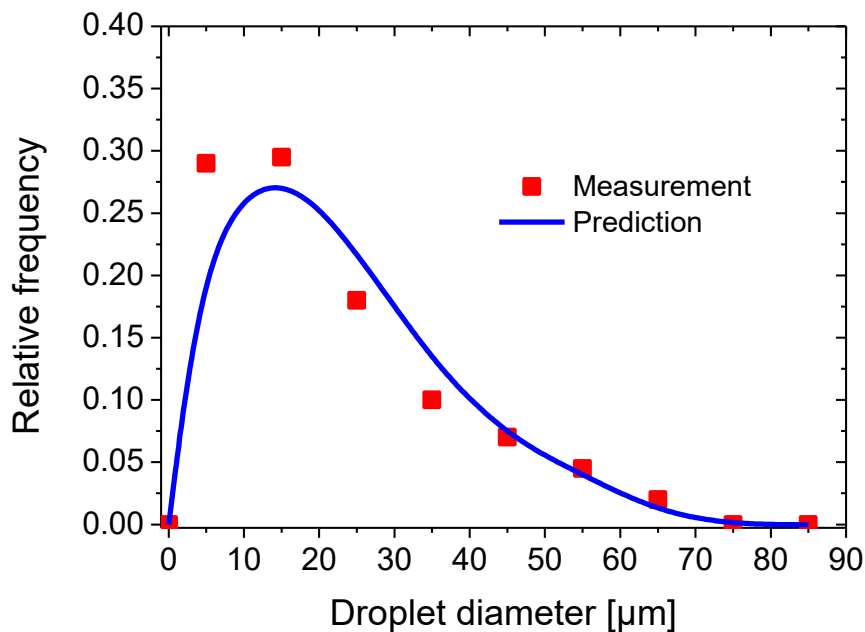
(d)

Fig. 6.17: Droplets solid content distributions at (a) 0.2m, (b) 0.5 m, (c) 2.25 m and (d) 3.5 m from the beginning of calculation domain compared with the experimental measurement.

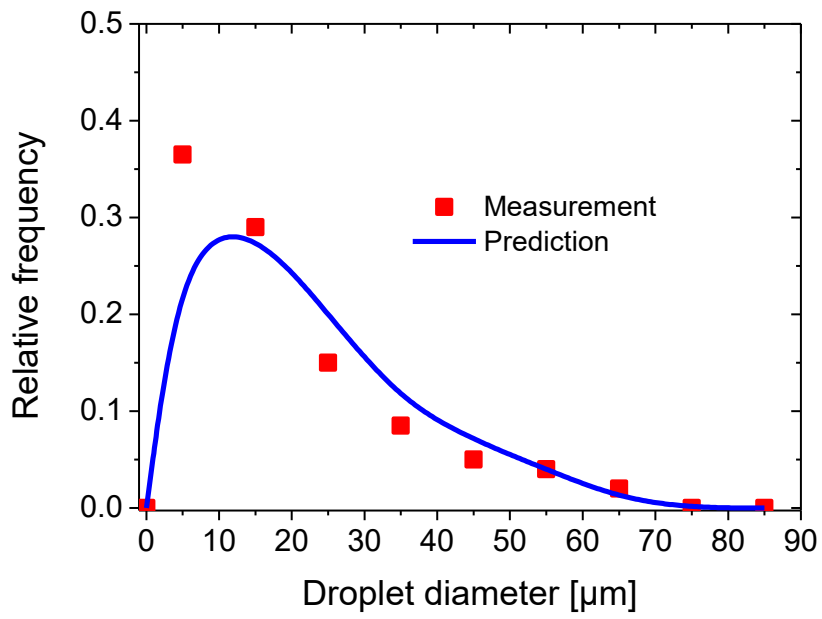
6.4.2.4 Particle size distribution

Figure 6.18 displays the predicted particles size distributions in the cross-sections at 0.2m, 0.8m and 3.5m from the beginning of calculation domain compared with the experimental results.

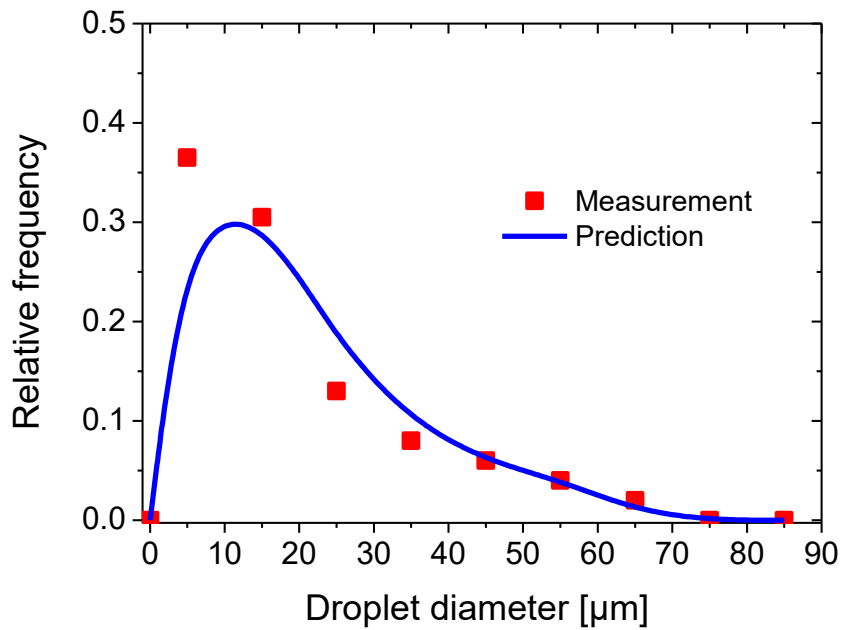
The measurement (Li 2004) showed that the shrinkage of droplets (i.e. reduction of droplets diameter) occurs before the distance of 0.4 m from the beginning of calculation domain (in the constant drying rate period) and in the downstream where the solid concentration of droplets reaches the saturation concentration formation of the solid crust on the droplets surface starts and the shrinkage of droplets stops, hence the droplets size in the dryer remains unchanged in this region (i.e. in the downstream after 0.4 m from the beginning of calculation domain (in the falling drying rate period)). That is why, as seen in this Figure in the downstream (at 0.8m and 3.5m from the beginning of calculation domain) there are almost the identical droplets size distributions. Appropriate drying model and correct specification of the critical moisture content value determined based on the experiment (5.62 kg water/kg solid for this case) resulted in the reasonable agreement between the numerical predictions and experimental data at any distance from the atomizer.



(a)



(b)



(c)

Fig. 6.18: Average particle size distribution at (a) 0.2 m (b) 0.8 m and (c) 3.5 m from the beginning of calculation domain compared with experimental measurement.

6.5 Comparison with other models

The predicted results provided by the present model are compared with the results obtained by the other drying models such as the Nesic & Vodnic (1991) and Abramzon & Sirignano (1989) model. Figure 6.19 depicts the droplets temperature profiles in the different distances from the atomizer calculated by the different models.

As it can be seen, the results achieved by the new model fit better with the experimental data compared to the other models. Besides, the Nesic & Vodnic (1991) drying model also predicted the droplets temperature profiles very good but still not as good as the developed model.

The reason of good predictions of the droplet phase temperature by the Nesic & Vodnic model might be due to the consideration of the role of solid crust formation in the temperature equation since in their model both the resistance for heat transfer in boundary layer and the resistance for heat transfer in the solid crust region are taken into account.

As it was expected, the Abramzon & Sirignano (1989) model, which is in principle a model for simulation of the evaporation of pure droplets (e.g. fuel droplets), was not able to predict the temperature profiles correctly especially in the cross-section of 1.25m from the beginning of calculation domain where the droplets are in the falling drying rate period.

This weakness of the Abramzon & Sirignano model is mainly due to the lack of consideration of crust formation and its role in the heat and mass transfer which caused the over-prediction of temperature calculations.

Since the crust formation and its growth create the new resistance for the heat and especially mass transfer in the drying process and affect the drying kinetics consequently, therefore for the correct prediction of this process must be considered.

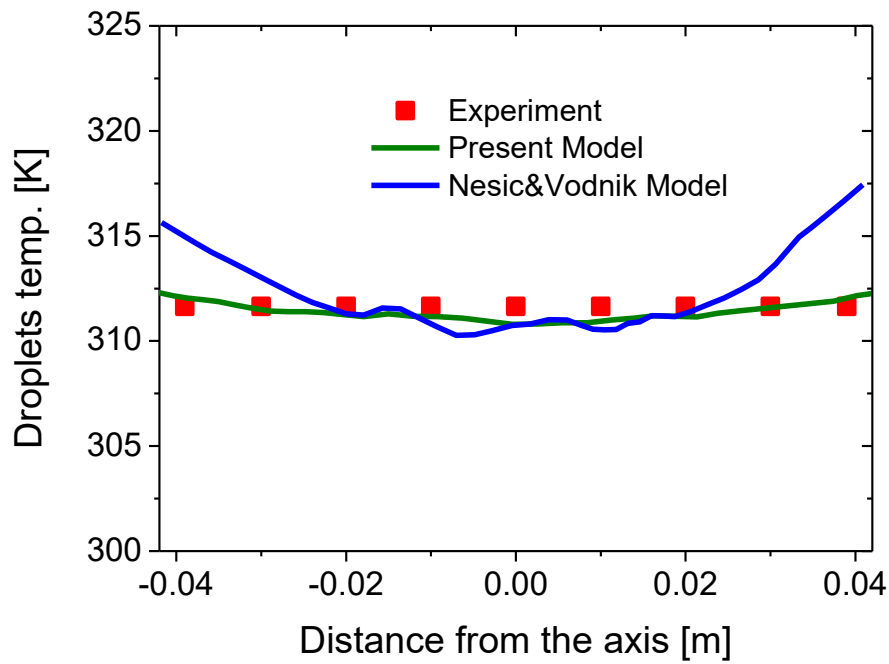


Fig. 6.19(a): Comparison of droplets temperature for different models at 0.2m from the beginning of calculation domain.

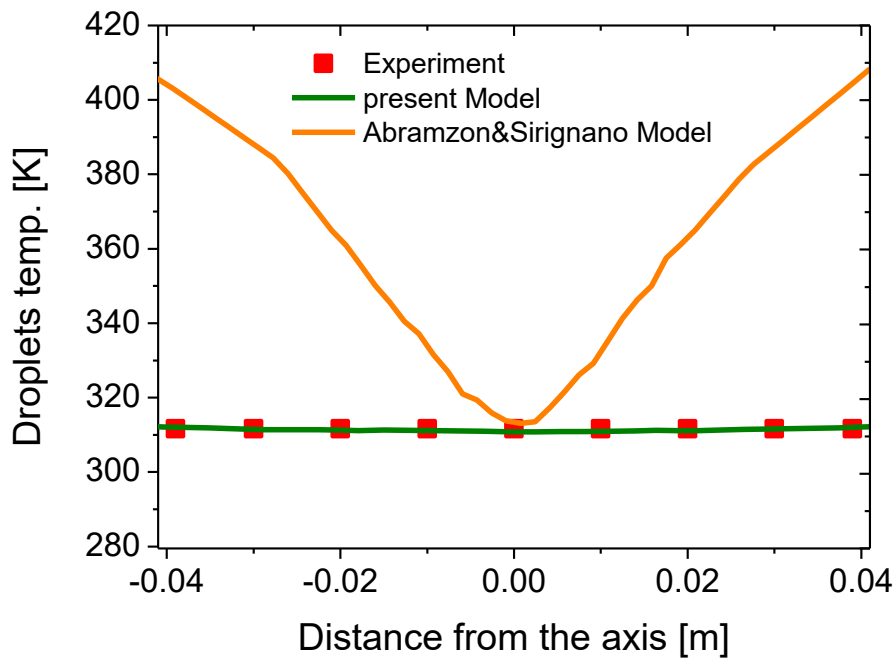


Fig. 6.19(b): Comparison of droplets temperature for different models at 0.2m from the beginning of calculation domain.

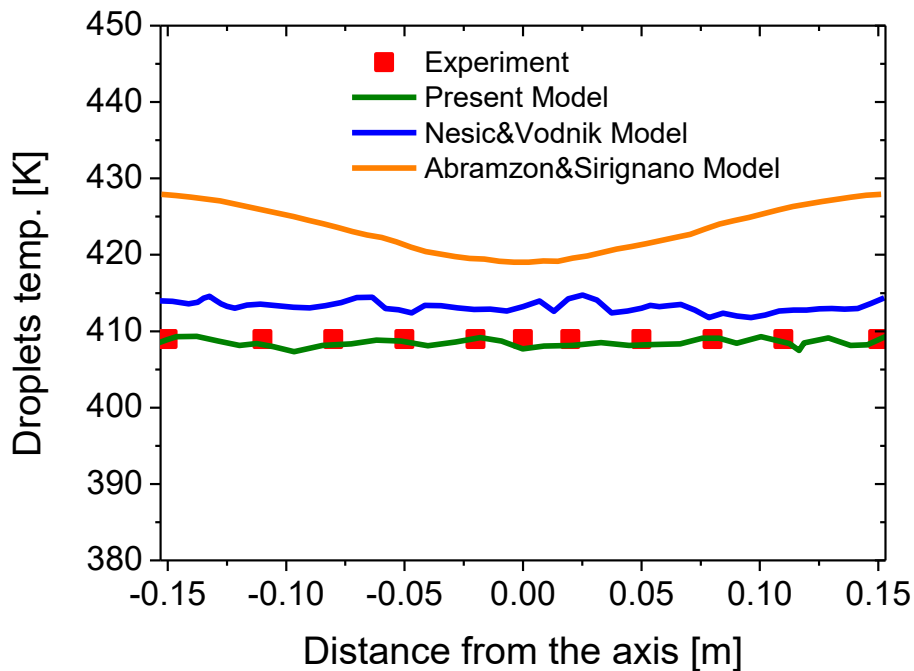


Fig. 6.19(c): Comparison of droplets temperature for different models at 1.25m from the beginning of calculation domain.

6.6 Summary of the chapter:

In order to evaluate the capability of the introduced drying model for the spray drying simulation in the large scale, this model was incorporated as a sub-model into the CFD calculation of a pilot-plant co-current spray dryer using the Euler-Lagrange approach.

In the simulation the interaction of the droplet phase and gas phase on each other was taken into account by using a 2-way coupled simulation in which the dispersion and modulation modelling were considered as well.

The experimental data required to determine the initial and boundary conditions and to validate the numerical predictions were provided by Professor Ireneusz Zbiciński at Technical university of Lodz in Poland.

The predicted results clearly showed the influence of jet produced by the pneumatic atomizer on the hydrodynamics of gas phase so that the gas velocity significantly increased in the vicinity of the nozzle because the drying gas was carried away by the injected droplets in this area. The effect of injected droplets was also noticeable in the contours of gas temperature and species concentration so that the concentration of water vapor in the drying gas increased in the areas of droplets evaporation but the air

temperature decreased in these areas due to the absorption of heat from the surrounding hot air by the droplets.

The predicted results for the droplet phase showed the continuous increase of the droplets temperature due to the heat transfer from the drying air to them (i.e. droplets) as well as the continuous increase of the droplets solid content due to the evaporation of water from the droplets.

The good agreements between the predicted results with the experimental measurements for the droplet phase velocity, temperature, solid content and size distribution in the different cross-sections of the dryer proved the ability and capability of the introduced drying model in order to be incorporated as a sub-model in the CFD simulation of spray dryers.

7 Conclusion

7.1 Conclusion

The main objective of this work was the developing of a reliable CFD model of spray drying process for describing the drying of suspension or solution droplets under the conditions relevant for the spray dryers and moreover, overcome some of the drawbacks recognized in the previous drying models existed in the literature.

The application of a drying model enables the consideration of mass- and heat exchange between the continuous and dispersed phase in the spray drying process, and additionally, the evaporation of solvent leads to the significant changes of material properties and hence will affect the collision behavior of drying particles (i.e. particle-particle collision, agglomeration and particle-wall collision). Due to these reasons, an appropriate drying model which is able to properly describe the heat and mass transfer between the droplets and drying gas is essential for the correct prediction of product characteristics by the modelling. Therefore, the main goal of the present work was the introducing of a more detailed droplet drying model which considers not only the rate of moisture loss, but also enables having a better understanding regarding the morphological evolution of the droplets throughout the drying process.

In comparison to the previously introduced models, in the present model, the diffusion equation for the solid phase within the droplet was solved in order to consider the concentration profiles inside the droplet. Moreover, the experiments proved that due to the growing concentration of solid content at the droplet surface during the constant drying rate period the temperature of droplet increases continuously in this period and therefore contrary to the previous models which supposed the droplet temperature to be constant in this period, the change of droplet temperature was considered in the present drying model by taking the heat balance equation into account during this period. Besides, by calculation of the crust thickness, it was possible to consider its role in the reduction of mass transfer rate in the present model, and additionally, it was supposed that both the internal and external heat transfer resistance, as well as both the internal and external mass transfer resistance control the drying process in the present model.

The successful applications of the developed model for simulation of three different systems of single droplets: colloidal silica, aqueous sodium sulphate and skimmed milk droplet proved the ability and capability of this model for estimation of the drying behavior of different single droplets throughout the drying process both in the constant and falling drying rate periods.

The colloidal silica was selected as a material which has a very porous and fragile crust that does not represent a considerable resistance for the heat and mass transfer. Due to this characteristic of colloidal silica the temperature levels and evaporation rates predicted by the developed drying model were very close to those of pure liquid droplets.

Sodium sulphate was selected as a material for those kinds of solutions which form an impermeable crust during the drying process. In these droplets a dense and relatively low porous structure (established during the falling rate period) generates a further resistance to the diffusion of water vapor. This characteristic of Sodium sulphate caused the predicted evaporation rates by the model to reduce significantly during the falling rate period of drying.

Skimmed milk was chosen as one of the most commonly spray dried biological materials. The behavior of skimmed milk droplets during the drying process was similar to the behavior of colloidal silica droplets. But, contrary to the fast rise in the temperature of colloidal silica droplets, in the temperature of skimmed milk droplets such a fast rise was not observed. The main reason of such a different behavior was the different values of crust thermal conductivity which these droplets (i.e. colloidal silica and skimmed milk) have.

Finally, after successful applications of the developed model for simulation of three different systems of single droplets, the developed drying model was implemented into the Euler-Lagrange approach for 2-way coupled simulation of a pilot-plant co-current spray dryer to evaluate the ability and capability of this model for prediction of the performance of these kinds of spray dryers and thus assess its applicability for the spray drying simulation in the large scale. The comparisons of the experimental measurements with the predicted results for this case proved that the ability of the developed drying model for approximation of the experimental results was completely satisfactory. As a

conclusion, the analysis of the results provided by the developed model and the good agreements which existed between the predicted results and experimental data for both the single droplet cases and the case of pilot-plant spray dryer confirmed the ability and potential of this drying model in order to be incorporated as a sub-model for the CFD simulation of the spray dryers.

7.2 Outlook

During the course of this work, the following research areas were identified to be further investigated. Some of the recommendations for the future works are listed below.

The developed drying model can be extended to account for the internal circulation, change of porosity, capillary force, as well as the consideration of different scenarios for predicting the final shape of particle as observed in the experiments. Consideration of these factors can further improve the capability and predictability of the model for estimation of the drying behavior of different droplets.

Furthermore, the lack of experimental data both concerning the physical parameters and the validation data for a wide range of droplets were one of the main problems during the course of this work. Some parameters such as the diffusion coefficients, density, heat capacity and viscosity of droplets are required for the accurate simulation of a drying system, and unfortunately, there are very few systems which are characterized in adequate detail. Therefore, more experimental works have to be done to determine the characteristics of different single droplets to enable the simulation of more drying systems.

Another problem regarding the experimental fields is the lack of sufficient validation data (e.g. for spray dryers). The only validation data existed in the literature are the droplet averaged temperature and mass histories and the lack of information about the change of droplet radius, moisture content etc. put a limitation on the validation of any developed drying model. Hence, future experimental works should focus on obtaining such information which can enable the better validation of drying models.

The new droplet drying model combined with the collision, agglomeration and breakup model might be used as sub-model in the CFD simulation of spray dryers to provide the detailed information about the dispersed phase, as well as a more realistic view of the drying process.

Hence, a 4-way coupled simulation of the spray drying towers can be done as an extension of this study in the future researches.

Nomenclature

C	Concentration	$\text{kg}_{\text{solid}} / \text{kg}_{\text{solution}}$
C_d	Drag coefficient	[-]
C_v	Heat capacity	$\text{J kg}^{-1} \text{K}^{-1}$
$C_{\varepsilon,3}^{k-\varepsilon}$	Constant model for the turbulence modulation of the k- ε model	
D_d	Initial diameter of droplet	m
D_{air}	Diffusion coefficient of vapor in air	$\text{m}^2 \text{s}^{-1}$
D_{cru}	Diffusion coefficient of crust	$\text{m}^2 \text{s}^{-1}$
E_a	Activation energy	J mol^{-1}
g	Gravitational acceleration	m s^{-2}
ΔH	Activation energy of diffusion	J mol^{-1}
h	air heat transfer coefficient	$\text{W m}^{-2} \text{K}^{-1}$
k_{co}	Thermal conductivity of droplet	$\text{W m}^{-1} \text{K}^{-1}$
k_{cru}	Thermal conductivity of crust	$\text{W m}^{-1} \text{K}^{-1}$
L	latent heat of evaporation	J kg^{-1}
m	mass of droplet	kg
Nu	Nusselt number	[-]
Pr	Prandtl number	[-]
R	Droplet radius	m
Re	Reynolds number	[-]
R_v	Radius of core–crust interface	m
R_{cri}	Critical radius (radius after shrinkage)	m
r	radial position	m
Sc	Schmidt number	[-]
Sh	Sherwood number	[-]
$S_\phi, S_{\phi,p}, S_{\phi,p,ev}$	Source terms	variable
T	Droplet temperature	K
T_g	Glass transition temperature	$^{\circ}\text{C}$
t	Time	s
u'	Fluctuation velocities	m s^{-1}
u, v, w	Velocity components	m s^{-1}
x, y, z	Cartesian Space Coordinates	m

X Mass concentration based on dry solid kg/kg dry solid

Greek letters:

α	Droplet thermal diffusivity	$\text{m}^2 \text{s}^{-1}$
ε	Turbulent dissipation rate	$\text{m}^2 \text{s}^{-3}$
k	Turbulent kinetic energy	$\text{m}^2 \text{s}^{-2}$
ϕ	The gas flow variable considered	variable
μ	Dynamic viscosity	Pa s
γ	Vapor concentration	kg m^{-3}
δ	Crust thickness	m
λ	Conductivity	$\text{W m}^{-1} \text{K}^{-1}$
ρ_{av}	Average density of droplet	kg m^{-3}
Γ	Effective diffusion coefficient of the general transport equation	variable
ω_0	Initial water mass fraction	$\text{kg}_{\text{water}}/\text{kg}_{\text{solution}}$
ω_b	Bound water mass fraction	$\text{kg}_{\text{water}}/\text{kg}_{\text{solution}}$
ω_A	Moisture content of droplet	$\text{kg}_{\text{water}}/\text{kg}_{\text{solution}}$
Ω	Angular velocity	m s^{-1}

Subscripts:

f	Fluid
i	index marker
p	Particle
s	Droplet surface
∞	Bulk air

References

Abramzon B., Sirignano W.A. (1989): *Droplet vaporization model for spray combustion calculations*. Int. J. Heat Mass Transfer 32, 1605-1618.

AL-Hafidh M. H., Ameen A. M. (2008): *Heat and mass transfer during air drying of fruits*. The Iraqi Journal For Mechanical And Material Engineering 8 (2), 110-126.

Ali M., Mahmud T., Heggs P.J., Ghadiri M., Gracia V.F., Bayly A., Djurdjevic D., Ahmadian H., de Juan L.M. (2013): *CFD Modelling of a Counter-Current Spray Drying Towe*. 8th International Conference on Multiphase Flow (ICMF), Korea

Anderson J.D. (1995): *Computational Fluid Dynamics: The Basics with Applications*. McGraw-Hill Education.

Azevedo J. L. T., Durst F., Pereira J. C. F. (1988): *Comparison of strongly implicit procedures for the solution of the fluid flow equations in finite difference form*. Appl. Math. Modelling 12, 51-62.

Bakker A (2002): *lecture 5 of applied computational fluid dynamics*. Fluent Inc.

Blei S. (2005): *On the Interaction of non-Uniform Particles during the Spray Drying Process: Experiments and modelling with the Euler-Lagrange Approach*. Ph.D. thesis, Martin-Luther University Halle-Wittenberg, Germany.

Blei S., Sommerfeld M. (2007): *CFD in Drying Technology – Spray-Dryer Simulation*, in Modern Drying Technology: Computational Tools at Different Scales, Volume 1 (eds E. Tsotsas and A. S. Mujumdar), Wiley-VCH Verlag GmbH & Co. KGaA, Weinheim, Germany.

Cebeci T., Shao P.J, Kafyeke F, Laurendeau E. (2005): *Computational Fluid Dynamics for Engineers*, Springer Berlin Heidelberg New York

Cheong, H. W. (1983): *The drying of small droplets of particulate slurries*. Ph.D. Thesis, University of Aston in Birmingham, UK.

Cheong H.W., Jeffreys G.V., Mumford C.J. (1986): *A receding interface model for the drying of slurry droplets*. AIChE Journal 32(8), 1334–1346.

Chen X.Q., Pereira J.C.F. (1996): *Computation of turbulence evaporating sprays with well-specified measurements: a sensitivity study on droplet properties*. Int. J. Heat Mass Transfer 39 (3), 441-454.

Chen X., Xie G. (1997): *Fingerprints of the drying behavior of particulate or thin layer food materials established using a reaction engineering model*. Food and Bio product Processing 75(4), 213-222.

Chen X. D., Farid M. M, Reid D., Fletcher A. (1999): Pearce, D.; Chen, N. X. *A new model for the drying of milk droplets for fast computation purposes*. CHEMECA99, Newcastle, Australia.

Crowe C.T., Sharma M.P., Stock D.E. (1977): *The Particle-Source-in-Cell (PSI-cell) model for gas-droplet flows*. In: Trans. ASME – J. Fluids Engng. 99, 325-332.

Crowe C.T., Sommerfeld M., Tsuji Y. (1998): *Multiphase flows with droplets and particles*. CRC Press LLC, Boca Raton, USA.

Crowe, C. T. (2000): *On models for turbulence modulation in fluid-particle flows*. Int. J. Multiphase Flow 26, 719-727.

Chrigui M. (2005): *Eulerian-Lagrangian Approach for Modeling and Simulations of Turbulent Reactive Multi-Phase Flows under Gas Turbine Combustor Conditions*. Ph.D. Thesis, Technical University of Darmstadt, Germany.

Dalmaz N. (2005): *Modeling and numerical analysis of single droplet drying*. M.Sc. Thesis, Thesis, Middle East Technical University, Turkey.

Date A.W. (2005): *Introduction to computational fluid dynamics*, Cambridge University Press.

Decker S. (2005): *Zur Berechnung von gerührten Suspensionen mit dem Euler-Lagrange-Verfahren*. Ph.D. thesis, Martin-Luther University Halle-Wittenberg, Germany.

Eckert E., Drake R. (1987): *Analysis of heat and mass transfer*. McGrawHills.

Farid M. (2003): *A new approach to modelling of single droplet drying*. Chemical Engineering Science 58, 2985-2993.

Ferziger J.H. , Peric M. (1999): "*Computational Methods for Fluid Dynamics*" (second edition). Springer Verlag, Berlin, Heidelberg

FLUENT™ User Guide (2001): *Computational Fluid Dynamics Software*. version 6.0, Fluent, New Hampshire.

Handscomb C. S. (2008): *Simulating droplet drying and particle formation in spray towers*. Ph.D. thesis, University of Cambridge, UK.

Harlow F. H., Welch, J. E. (1965), "*Numerical calculation of time-dependent viscous incompressible flow of fluid with free surface*", Phys. Fluids. 8, 2182

Katta S., Gauvin W.H. (1975): *Some Fundamental Aspects of spray drying*. AIChE 21 (1), 259-266.

Kohnen G., Rüger M., Sommerfeld M. (1994): *Convergence behavior for numerical calculations by the EULER/LAGRANGE Method for strongly coupled phases*. FED-Vol 185, Numerical Methods in Multiphases Flows ASME 1994.

Kohnen G. , Sommerfeld M. (1998): *Numerische Berechnung verdampfender Sprühnebel*. Chemische Technik 50 (5),225-234.

Lain S., Brüder D., Sommerfeld M. (2000): *numerical modeling of the hydrodynamics in a bubble column using the Euler-Lagrange approach.*“ Proc. On Int. Symp. On Multiphase Flow and Transport Phenomena, Antalya, Turkey.

Lain S. (2010): *On modeling and numerical computation of industrial disperse two phase flow with Euler-Lagrange approach* .Shaker Verlag Aachen.

Langrish T.A.G., Zbicinski I. (1994): *The effects of air inlet geometry and spray cone angle on the wall deposition rate in spray dryers*. Trans. I. Chem. 72 (A), 420-30.

Langrish T., Kockel T. (2001): *The assessment of a characteristic drying curve for milk powder for use in computational fluid dynamics modelling*. Chemical Engineering Journal 84(1), 69-74.

Launder B.E., Spalding D.B. (1974): *The numerical computation of turbulent flows*. Comp. Meth. Appl. Mech. Eng. 3, 269-289.

Leister H. J., Peric M. (1994): “*Vectorized strongly implicit solving procedure for seven-diagonal coefficient matrix*”. Int. J. Numer. Meth. Heat Fluid Flow 4,159-172

Li X. (2004): *CFD modeling of spray drying process*. Ph.D. thesis, Technical University of Lodz, Poland

Li X., Zbiciński I. (2005): *A Sensitivity Study on CFD Modeling of Co-current Spray Drying Process*. Drying Technology 23 (8), 1681-1691.

Liu Z., Zheng C., Hzhou L. (2002): *A joint model for turbulent spray evaporation/Combustion*. Proceedings of the Combustion Institute 29, 561-568.

Luikov A. V. (1975): *Systems of differential equations of heat and mass transfer in capillary-porous bodies*. Int. J. Heat and Mass Transfer 18, 1-14.

Magnaudet J.J.M. (1997): *The forces acting on bubbles and rigid particles*. In: ASME Fluids Engineering Division Summer Meeting, 1-9.

Marshall W.R., Seltzer E. (1950): *Principles of spray drying; part 1. Fundamental of spray dryer operation*. Chem. Eng, Prog. 46, 501-508

Masters K. (1991): *Spray Drying Handbook*. Longman Scientific & Technical, Harlow, England.

McComb W.D. (1990): *The physics of fluid turbulence*. Clarendon Press, Oxford University Press, Oxford.

Mei R. (1992): *An approximate expression for the shear lift force on a spherical particle at finite Reynolds number*. Int. Journal Multiphase Flow 18, 145-147.

Miesse C.C. (1957), in: Crowe C.T. (1980): *Modeling spray air contact in spray drying systems*, in: Mujumdar A.S.: *Advances in Drying vol. 1*, Hemisphere, New York, 63-99.

NASA Portal (2008); The NPARC Alliance CFD verification and validation:<http://www.grc.nasa.gov/WWW/wind/valid/tutorial/process.html#repeat>

Nesic S. (1989): *The evaporation of single droplets –experimental and modelling*. Drying 89, 386-393.

Nesic S., Vodnik J. (1991): *Kinetics of droplet evaporation*. Chemical Engineering Science 46 (2), 527–537.

NIS Muhammad. (2011): *COMPUTATIONAL FLUID DYNAMICS OF INDUSTRIAL SCALE SPRAY DRYER*, Master thesis, UNIVERSITI MALAYSIA PAHANG, Malaysia.

Oakley D.E., Bahu R.E., Reay D. (1988): *The aerodynamics of co current spray dryers*: in: M. Roques (Ed.), Proc. Sixth International Drying Symposium, Versailles, France.

Oakley D.E. (1994): *Scale-up of spray dryers with the aid of computational fluid dynamics*, Drying Technology 12, 217-233.

Oakley D.E. (2004): *Spray dryer modeling in theory and practice*. Drying Technology 22 (6), 1371-1402.

Parti M., Palancz B. (1974): *Mathematical model for spray drying*. Chemical Eng, Sci. Journal 29, 355-362.

Patankar S.V., Spalding D.B. (1972): *A calculation procedure for heat, mass and momentum transfer in three-dimensional parabolic flows*. Int. J. Heat and Mass Transfer 110, 1787-1806.

Patankar S. V. (1980): *Numerical heat transfer and fluid flow*. Hemisphere Publishing Corporation.

Peric M. (1985): *A finite volume method for the prediction of three-dimensional fluid flow in complex ducts*. Ph.D. thesis, University of London, UK.

Pope S.P. (2000): *Turbulent Flows*. Cambridge University Press, Cambridge, UK.

Prandtl L. (1945): *Über ein neues Formelsystem für die ausgebildete Turbulenz*. Nachr. Akad. Wiss. Göttingen, Math-Phys. K1, 6-19.

Ranz W. E., Marshall, W. R. (1952), *Evaporation from Drops, part 1*, Chem. Eng. Prog. 48 (3), 141-146

Roustapour O.R., Hosseinalipour M., Ghobadian B., Mohaghegh F., Maftoon Azad N. (2009): *A proposed numerical–experimental method for drying kinetics in a spray dryer*. Journal of Food Engineering 90, 20-26.

Sano Y., Keey R.B. (1982): *The drying of a spherical particle containing colloidal material into a hollow sphere*. Chem. Eng. Science 37 (6), 881-889.

Schäfer M. (2004): *Fastest-3D Manual*. Technical University of Darmstadt, Germany.

Schmidt E., Müller O. (1997): *Strömungskräfte auf Partikeln in Gasen*. VDI-Verlag GmbH, Düsseldorf, Germany.

Schiller L., Naumann A. (1933): *Über die grundlegenden Berechnungen bei der Schwerkraftaufbereitung*. In: Ver. Deut. Ing. 77, 318-320.

Sherwood T. K. (1929a): *The drying of solids I*. Industrial and Engineering Chemistry 21(1), 12–16.

Sherwood T. K. (1929b): *The drying of solids II*. Industrial and Engineering Chemistry 21(10), 976–980.

Simonin O. (1996): *Continuum Modeling of Dispersed Turbulent Two-phase Flows*. In VKI lectures: Combustion in Two-phase Flows, Jan 29-Feb. 2.

Sommerfeld M., Qiu H.H, Ruger M., Kohnen G., Muler D. (1993): *Spray evaporation in turbulent flow*. Proceedings of the 2nd Symposium on Energy Turbulence modeling and Measurements, Florence, Italy, 31, May-1 Jun, 935-945.

Sommerfeld M., Kohnen G., Rüger M. (1993): *Some open questions and inconsistencies of Lagrangian particle dispersion models*. In: Proceedings of the Ninth Symposium on Turbulent Shear Flows, Kyoto, Japan, paper no. 15-1.

Sommerfeld M. (1996): *Modellierung und numerische Berechnung von partikelbeladenen turbulenten Strömungen mit Hilfe des Euler/Lagrange-Verfahrens.* Shaker Verlag Aachen.

Sommerfeld M. (2001): *Validation of a stochastic Lagrangian modelling approach for inter-particle collisions in homogeneous isotropic turbulence.* Int. J. Multiphase Flow 27, 1829-1858.

Sommerfeld M. (2002): *Bewegung fester Partikel in Gasen und Flüssigkeiten.* VDI-Wärmeatlas, 9.Auflage, Lca1-Lca9.

Sommerfeld M., van Wachem B., Oliemans R. (2008): *Best Practice Guidelines for Computational Fluid Dynamics of Dispersed Multiphase Flows.* ERCOFTAC (European Research Community on Flow, Turbulence and Combustion. ISBN 978-91-633-3564-8.

Squires K.D., Eaton J.K. (1992): *On the modelling of particle-laden turbulent flows.* In: M. Sommerfeld (Editor): Proc. 6th Workshop on two-phase flow predictions. Erlangen, 220-229.

Stone H.L.(1968): *Iterative solution of implicit approximation of multidimensional partial differential equations.* J. Num. Anal. 5 (3), 530-557.

Stübing S. (2014): *Lagrangesche Berechnung von Agglomeratstrukturen am Beispiel eines Sprühtrockners.* Ph.D. Thesis, Martin Luther University Halle-Wittenberg, Germany.

Tu J., Yeoh G. H., Liu C. (2012): *Computational Fluid Dynamics: A Practical Approach.* Butterworth-Heinemann.

Verdurmen R.E.M., Menn P., Ritzert J., Blei S., Nhumaió G.C.S., Sonne Sørensen T., Gungsing M., Straatsma J., Verschueren M., Sibeijn M., Schulte G., Fritsching U., Bauckhage K., Tropea C., Sommerfeld M., Watkins A.P., Yule A.J., Schönfeldt H.

(2004): *Simulation of agglomeration in spray drying installations: the EDECAD project*. *Drying Technology* 22 (6), 1403-1461.

Versteeg H. K., Malalasekera W. (1995): *An introduction to computational fluid dynamics; the finite volume method*. Longman scientific & Technical, Longman Group.

Werner S.R.L (2005): *Air-suspension coating of dairy powders: A micro-level process approach*. Ph.D. Thesis, Massey University, New Zealand.

Werner S.R.L., Edmonds R.L., Jones J.R., Bronlund J.E, Paterson A.H.J. (2008): *Single droplet drying: Transition from the effective diffusion model to a modified receding interface model*. *Powder Technology* 179, 184–189.

Wijlhuizen A.E., Kerkhof P.A.J.M., Bruin S. (1979): *Theoretical study of the inactivation of phosphatase during spray drying of skim-milk*. *Chem. Eng. Science* 34, 651-660.

Yüzgeç U, Türker M, Becerikli Y.(2008): *Modelling Spatial Distributions of Moisture and Quality During Drying of Granular Baker's Yeast*. *The Canadian journal of chemical engineering* 86, 725-738

Zbicinski I., LI X. (2006): *Conditions for accurate CFD modeling of spray-drying process*. *Drying Technology* 24, 1109-1114.

Curriculum Vitae



Personal Data

Name Ali Darvan
Birthday 10.03.1984
Sex Male
Marital Status Married
Place of Birth Amol, Iran
Nationality Iranian
Address Zimmer 503, Mannheimer strasse 5, 04209 Leipzig
Tel: +49 1577 27 34 361
Email: ali_darvan.amiri@yahoo.com

Education

- 2003-2007 Kashan Islamic Azad University , Faculty of mechanical Engineering, BSc., design&solid Engineering
- 2007 -2010 Science and research university, tehran ,Iran, Faculty of mechanical Engineering, MSc. Heat and Fluid Engineering.
- 2012-Present Ph.D. Student at Martin Luther University Halle-Wittenberg, Germany.

Experience

- 2012-Present Martin-Luther-Universität Halle-Wittenberg, Halle, Germany
Position: Research Assistant (Wissenschaftlicher Mitarbeiter) at the chair for mechanical process engineering.
Head of the chair: Prof. Dr. –Ing habil. Martin Sommerfeld
Working on the project’’ CFD Simulation of Spray Drying process using a New Droplet Drying Kinetics ‘‘

Journal Publications

- M. Taeibi-Rahni, M. Ramezanizadeh, D.D. Ganji ,A. Darvan, E.Ghasemi, S.Soleimani, H.Bararnia, ‘‘Comparative study of Large eddy simulation of film cooling using, a dynamic global-coefficient subgrid-scale eddy-viscosity model with RANS and smagorinsky modeling ’’.*international communications in heat and mass transfer, Volume 38 (2011) 659-667.*

- M. Taeibi-Rahni, M. Ramezanizadeh, A. Darvan, D.D. Ganji, Soheil Soleimani, E.Ghasemi, H.Bararnia, “Large Eddy Simulations of Three Dimensional Turbulent Jet in Cross Flow using a Dynamic Sub-grid Scale Eddy Viscosity Model with a Global Model Coefficient”. *World Applied Science Journal* , 9(10): 1191-1200,2010.

- M. Alinia, D.D. Ganji, M. Gorji-Bandpy, Soheil Soleimani, E.Ghasemi, A.Darvan “ Two phase Natural Convection of SIO₂-Water Nanofluid in an Inclined Square Enclosure “ *Scientia Iranica B* (2014) 21(5), 1643-1654.

Conference paper

- A. Darvan and M. Sommerfeld, “Modelling and numerical analysis of the Drying stages During single droplet drying”. *International Drying Symposium (IDS 2014)* , 24-27th August 2014 , Lyon, France.

Conference Presentations

- A. Darvan and M. Sommerfeld, “A comparative study of numerical models for Eulerian- Lagrangian simulations of turbulent evaporating sprays and Solid-included droplets”. *FASTEST Workshop (9-10th of October, 2013) in technical university of Darmstadt, Darmstadt ,Germany.*

- A. Darvan and M. Sommerfeld “About Evaporation, Drying, Sublimation”. *Annual meeting of the sections Multiphase flows and Heat and mass transfer 24-25th march 2014, Fulda,Germany.*

- A. Darvan and M. Sommerfeld, “Atmospheric Sublimation Modelling”. *Annual Meeting SPP 1423, Process-Spray March 31, 2014 Halle (saale),Germany.*

- A. Darvan and M. Sommerfeld, “A new approach to modelling of single droplet drying”. *International Drying Symposium (IDS 2014)* , 24-27th August 2014 , Lyon, France.

- A. Darvan and M. Sommerfeld, “ Euler-Lagrange approach for simulation of spray dryers using FASTEST -Lag3D ”. *FASTEST Workshop (8-9th of October, 2015) in technical university of Darmstadt, Darmstadt ,Germany.*

- M. Sommerfeld and A. Darvan, “A NOVEL DROPLET DRYING MODEL APPLIED TO A LABORATORY SPRAY DRYER”. *9th International Conference on Multiphase Flow (ICMF), 22- 27 May, Firenze, Italy.*

Hiermit erkläre ich an Eides statt, dass ich, Ali Darvan, die vorliegende Dissertation entsprechend den in der Promotionsordnung des Zentrums für In-genieurwissenschaften der Martin-Luther-Universität Halle-Wittenberg festgelegten Regeln, ohne Mitwirkung Fremder und nur mit den angegebenen Hilfsmitteln angefertigt habe. Die Arbeit wurde bisher weder im Inland noch im Ausland in gleicher oder ähnlicher Form als Dissertation eingereicht und ist als Ganzes noch nicht veröffentlicht.

Halle (Saale), den 04.07.2016

Ali Darvan